Pattern Matching for Advanced Lithographic Technologies

Juliet Alison Rubinstein

Electrical Engineering and Computer Sciences
University of California at Berkeley

Technical Report No. UCB/EECS-2010-72
http://www.eecs.berkeley.edu/Pubs/TechRpts/2010/EECS-2010-72.html

May 13, 2010

Pattern Matching for Advanced Lithographic Technologies

by

Juliet Alison Rubinstein

A dissertation submitted in partial satisfaction of the

requirements for the degree of

Doctor of Philosophy

in

Engineering – Electrical Engineering and Computer Sciences

in the

Graduate Division

of the

University of California, Berkeley

Committee in charge:

Professor Andrew R. Neureuther, Chair
Professor Costas J. Spanos
Professor David A. Dornfeld

Spring 2010

The dissertation of Juliet Alison Rubinstein, titled Pattern Matching for Advanced Lithographic Technologies, is approved:

Chair _____ Date _____

_____ Date _____

_____ Date _____

University of California, Berkeley

Pattern Matching for Advanced Lithographic Technologies

Abstract

Pattern Matching for Advanced Lithographic Technologies

by

Juliet Alison Rubinstein

Doctor of Philosophy in Engineering – Electrical Engineering and Computer Sciences

University of California, Berkeley

Professor Andrew R. Neureuther, Chair

This dissertation extends fast-CAD kernel convolution methods for the identification of unintended effects in optical lithography, including OPC-induced sensitivities, high-NA and polarization vector effects. A more accurate through-focus physical model is incorporated, and the application of layout decomposition guidance for double patterning is demonstrated. All layout regions react differently to lithographic processes such as aberrations, and the vulnerabilities are non-intuitive and hard to capture with design rules. The pattern matcher is a fast tool, developed by Gennari and Neureuther, for quickly scanning layouts to find vulnerabilities to unintended effects of lithographic processes. Kernel convolutions are performed between Maximum Lateral Test Patterns (MLTPs) and mask layouts, and are over a factor of 10^4 times faster than rigorous simulation. Challenges faced in pattern matching extensions include MLTP derivation, edge movement prediction, defocus accuracy improvement, and integration of image effect estimation into real-time guidance for layout decomposition.

As motivation for why variability and yield are important, a study is presented in which a probabilistic distribution of transistor Critical Dimensions (CD) is generated given a focus-exposure joint distribution. An interpolation model is used to generate CD response surfaces, producing a fast method for the analysis of average CD variation for each transistor, the spread of individual variations, the OPC performance, the Across Chip Linewidth Variation (ACLV), and yield distribution. This study motivates the importance of understanding the variability in a layout; the remainder of the dissertation demonstrates how pattern matching can provide a fast approximation to variability due to lithographic effects.

MLTPs, derived as the inverse Fourier Transform of the Zernike polynomials, are the theoretically most sensitive patterns to lens aberrations. As well as being used as input to the pattern matcher, MLTPs can also be etched onto a mask to function as aberration monitors. However, MLTPs are inherently very costly and unfriendly for mask manufacturing, due to round edges and touching phases. Both a mask-friendly handmade pattern and an automated method of monitor modification are presented. The handmade pattern retains 68% of its sensitivity to defocus and orthogonality to other aberrations, and the automatically generated pattern passes all DRC checks with only minimal modifications.

Use of the pattern matcher on pre-OPC layouts admits the identification of problematic hot-spots earlier in the design flow. Several studies are presented on the effects of different

OPC algorithms on match factors. In most cases, match factors do not vary significantly between the pre-OPC layout and the post-OPC layout, and the pre-OPC match factor is a good indicator for the sensitivity of the post-OPC layout area. However, in some circumstances, especially when SRAFs are present, the pre- and post-OPC match factors can vary by a larger amount. It is shown that defocus and proximity sensitivities occur in different locations on a layout, and if OPC targets the best-case simulation, then it is possible for OPC to worsen sensitivities to aberrations. As a consequence, pattern matching should be used on post-OPC layouts to check for any created sensitivities.

Extensions of the pattern matcher are presented for high-NA and polarization vulnerabilities. This involves the generation of three to five match patterns for either on-axis or off-axis illumination, with a vulnerability score being calculated as a weighted sum of the match factors. The patterns are tested against simulation, and found to be good predictors of vulnerability to high-NA and polarization vector effects. High-NA and polarization vector effects are significant, causing intensity changes of 40% or 10% respectively for the on-axis case, and 8% for the off-axis case.

The accuracy of the pattern matcher is evaluated, and improved. A method for predicting edge movement through coma, rather than just change in intensity, takes the image slope into account and improves the R^2 from 0.73 to 0.95. A major contribution of this dissertation is the improvement of the pattern matching model for defocus. A quadratic model for defocus is presented, using both the Optical Path Difference (OPD) and OPD^2, rather than just the linear term. OPD^2 expands to yield two new patterns, Z_0 and Z_8, to be used in addition with Z_3 which is derived from the OPD term. Using the three match patterns, prediction of the change in intensity through focus improves from completely non-predictive to an R^2 value of 0.92. Results show that the Z_3 pattern and a combined Z_0 and Z_8 pattern predict change in intensity through defocus at line ends with an R^2 of 0.96, indicating that two match factors with algebraic weighting factors are likely possible. These results are of great importance, as defocus is not a small aberration, reaching typical values of nearly one Rayleigh unit, and the ability to find defocus-induced hot-spots is of practical interest.

Double patterning is identified as an emerging technique that benefits from the application of pattern matching. In double patterning, a layout is split into two masks, each mask being exposed separately, effectively doubling the pitch. A process flow is presented showing that pattern matching can add value both within the double patterning decomposition algorithm, and also on the post-decomposition layout. Pattern matching is tested on post-decomposition layouts, showing that in one particular case using complementary dipole illumination, the match factors for coma are increased significantly on the post-decomposition layout. In another case for annular illumination, introducing an extra split is shown to reduce the variability through coma, and reduces the match factor by 55%. Furthermore, when splitting an H-structure, a number of different splits are scanned by the pattern matcher, and the split with the lowest intensity change through defocus (which was two thirds smaller than the largest change) is correctly identified. These examples show that the pattern matcher is an appropriate tool for double patterning, that can quickly provide a measure of intensity change through defocus during the layout decomposition process.

Contents

List of Figures

List of Tables

Acknowledgments

The work presented in this thesis would not be possible without the help and support I have received from many sources. I would like to thank my advisor, Professor Andrew R. Neureuther, for his many technical discussion and his guidance, and also for introducing me to the many industrial partners who have offered insights and data sets for my work. I would like to thank the past and present members of Professor Neureuther's research group, who have explained many lithographic theory concepts to me over the years, and have acted as a sounding board for my work during the weekly research meetings. I would like to thank Frank Gennari, Scott Hafeman, Daniel Ceperley, Garth Robins, Jason Cain, Michael Lam, Wojtek Poppe, Greg McIntyre, Lynn Wang, Eric Chin, Chris Clifford and Marshal Miller. Frank Gennari in particular, as the author of the pattern matcher, has provided a platform for the follow on work from his original program. I would also like to acknowledge Professor Andrew Kahng and Hailong Yao for their collaborations on double patterning lithography.

I would like to acknowledge the industrial partners who have worked with me and provided me with data and feedback. I would like to thank Jongwook Kye and Yi Zou from AMD (now Global Foundries) for their collaborative effort and guidance on the gate CD distribution project. I would like to thank Eric Hendrickx from IMEC for his insights and layouts provided in double pattern lithography. I would like to thank the many members of the FLCC and IMPACT grants who spoke to me during the poster workshops, and offered ideas and feedback on my work.

I would like to thank the many wonderful friends, the 'chums', I've made at Berkeley, who have provided support and who have enriched my experience at Berkeley during our weekly dinners and games nights. I would like to thank my family, most of all my parents for their support and phone-calls from afar, and especially my husband Ben who has encouraged me and supported me throughout my PhD. And I would like to thank my son Lachlan, for the precious little while that he shared with us.

This work was funded by the Feature Level Compensation and Control Grant (FLCC), a UC Discovery project, the IMPACT grant which replaced the FLCC grant, by SRC grant 1443, and by the Intel Foundation Fellowship.

Chapter 1

Introduction

1.1 Motivation

The ability to control yield and variation is vital in order to keep integrated circuit design and production costs at a workable level. A circuit layout will pass through a large variety of filters, checks and modifications before being taped out to a mask. Many of these steps are extremely time consuming, taking up to several days for just one simulation, and the layout will make many iterations through each of the different phases, passing back further up in the flow to try again after a problem is discovered. A method for providing approximate, but fast evaluation of sensitivities of a layout to lithographic effects, which affect variability and yield, would help reduce the number of iterations through the flow, saving time and money. The pattern matcher is such a tool that can do this.

The pattern matcher was written by F. Gennari (Gennari and Neureuther, 2004), and is a very fast tool for finding areas on a layout that have a high geometric similarity to a given input pattern. A set of input patterns has been designed by G. Robins (Robins et al., 2002) that can work with the pattern matcher, allowing it to quickly find layout hot spots for the Zernike aberrations. This thesis aims to extend this work, allowing it to work for newer and more advanced technologies, and also to examine its accuracy and improve it where possible. Additionally, new applications to the pattern matcher are investigated.

As a motivating example for why the ability to characterize and control sources of variation is important, Chapter 3 covers and in depth study in the production of a probabilistic distribution for the Critical Dimension (CD) of transistor gate lengths across a whole chip. The analysis in this chapter allows the designers to identify the high variation transistors, the low yield transistors, the spread of variation of transistors, the goodness of the biasing and Optical Proximity Correction (OPC) and other characteristics of the design. This work was completed during a summer internship at AMD, and highlights the importance to industry of characterizing and controlling variability and yield.

1.2 Problem

Advanced optical lithography uses a variety of resolution enhancement techniques that optimize the illumination and mask types even among the various layers in a given IC manufacturing process flow. The derived benefits are highly feature type and size dependent. The designers must be very careful that no feature type or size appears that would be adversely affected. In fact these worst case pattern scenarios are 2-D in nature and involve surrounding layout features. Thus, even with a large set of design rules, it is difficult for designers to avoid these scenarios.

There are several categories of issues that needed to be addressed for the pattern matcher to be used in current technologies, and to extend the use of the pattern matcher for emerging applications. These can be loosely grouped into several categories: mask issues, such as application to different types of masks and OPC issues; advanced image issues, such as pattern matching under polarization and high numerical aperture; the accuracy of the pattern matcher, and its use for not only odd aberrations such as coma, but also even aberrations such as defocus; and the application of pattern matching to double patterning.

1.3 Mask Issues

Mask issues are addressed in Chapter 4. The mask is the physical plate to which the layout is etched, and which light is aimed through to expose the layout pattern into the photoresist on the wafer. The manufacturability of the mask, the phase and configuration of the mask, the post-design modifications made through OPC are all issues that are relevant to the use of the pattern matcher.

The patterns that are used with the pattern matcher, known as Maximum Lateral Test Patterns (MLTPs) are the inverse Fourier transform of the Zernike polynomials. They represent the theoretically most sensitive patterns to the aberrations. Thus, when a layout is scanned for similar layout configurations to the MLTPs, the layout locations with the highest similarity or match factor to the patterns will be more sensitive to the aberration, and will vary the most from their design intent when the aberration is present in the system. As well as their use in the pattern matcher environment, the MLTPs can be etched onto a mask and used to monitor the amount of aberration in the system. However, the MLTPs are not inherently mask friendly, and are very expensive to manufacture in their original form.

An automated flow is devised to transform the MLTPs to become more mask friendly by moving vertices that violate Design Rule Checks (DRC), and is shown to successfully transform the patterns to become more mask friendly. Additionally, hand made monitors that resemble the original patterns are analyzed for their retained sensitivity to the aberration both through pattern matching with the original pattern, and through simulation, and are found to retain 68% of the sensitivity to the aberration.

The type of mask is another mask related lithography issue that the pattern matcher is affected by. A binary mask is a mask that has a dark background with openings for the features. An alternating phase-shift mask is another type of mask, but instead of a dark

background, a phase shifted 180° background with 6% transmission is used. The pattern matcher can function correctly for this type of mask, as long as the background layer is created and given the appropriate phase and transmission weightings.

Optical Proximity Correction is applied to a layout immediately prior to being written to the mask. The layout is fragmented, and each of the fragmented edges are moved in small increments until the simulated image matches the drawn layout within a very small tolerance. Thus, the edge movement error is minimized. The pattern matcher is most effective when it is applied prior to OPC, that way any sensitivities that are found can be treated prior to the lengthy simulation and OPC cycles. Pattern matcher is 10^4 to 10^5 times faster than OPC, and OPC takes processor days as opposed to the processor minutes of pattern matching, so using the pattern matcher earlier in the design flow is desired.

In order for pattern matching to be applied to pre-OPC layouts, it needs to be understood how OPC affects the match factors. A number of studies were completed in this thesis showing examples that do and don't affect OPC, and it was found overall that the pre-OPC match factors were good indicators of post-OPC match factors, but that there were still some situations, such as when SRAFs happen to be placed to bump up or down a match factor, where the match factor and thus sensitivity of the layout is changed by a considerable amount by the OPC process.

1.4 Advanced Image Issues

Polarization and high Numerical Aperture (NA) are two types of imaging issues that are good candidates for extensions for pattern matching. In collaboration with G. McIntyre (McIntyre et al., 2005; Holwill et al., 2006), a set of patterns were devised to predict sensitivities of a layout to polarization and NA vector effects and were tested using the pattern matcher. This work is covered in Chapter 5. In this case, three to five patterns were required rather than the usual one pattern, and the results showed a good correlation between predicted vulnerability and actual simulated vulnerability. A layout location with a high vulnerability to these effects would be most misrepresented by a scalar imaging model, and would be most vulnerable to an illumination that is slightly different to that which was programmed.

1.5 Accuracy of the Pattern Matcher

Chapter 6 covers the accuracy of the pattern matcher. The pattern matcher is not as accurate as rigorous simulation, but is orders of magnitude faster, so there is a trade-off between speed and accuracy. Pattern matching makes an excellent candidate for use as a first-cut approximation to simulation, to catch unacceptable sensitivities to lithographic effects and correct them before they travel down the pipeline to be simulated rigorously, only to be sent back to the designers. Although the pattern matcher is not designed to be as accurate as rigorous simulation, it is important to know just how accurate it is, and to improve the accuracy wherever possible.

The test patterns that are used with the pattern matcher are designed to give match factors that are linearly proportional to the change in intensity due to the aberration at the match location. Work in this thesis extends this result to predict the edge movement through the aberration by taking the image slope into account. The ability to use the pattern matcher with the current test patterns resulted in very poor results for even aberrations such as defocus. A new, quadratic model is introduced, which along with some other technical improvements, allows the pattern matcher to predict the change in intensity through focus with high confidence and an R^2 value of 0.92 between the predicted and simulated results. This result is of high importance, as defocus is not a small aberration that is present in today's lithographic processes, and the ability to find hot spots caused by defocus sensitivities is of high relevance.

1.6 Pattern Matching applied to Double Patterning

Double patterning lithography is a new technology whereby a layout is split into two masks to be exposed sequentially, rather than just the one. This allows the effective doubling of pitch. One of the challenges for double patterning is the decision on how to split the layout into two masks. It would be convenient if each of the polygons in the layout could be assigned to either the first mask or the second mask, but in reality the polygons need to be split amongst the two masks, with an overlap margin at the split to ensure that pinching does not occur. The decision of where exactly to split the polygon, and how much overlap to include is an ongoing challenge with largely heuristic algorithms.

In Chapter 7, the effectiveness of pattern matching as an application to double patterning is examined. Pattern matching can be used to check a double patterning layout split for sensitivities to aberrations before it is passed onto OPC and simulation. This can save valuable iterations and catch problems earlier up in the design flow. In one example, a new split is made to reduce the match factor to coma by 55%. The pattern matcher is also examined as a method to examine splits during the decomposition process, rather than post-decomposition. Pattern matching can quickly measure the sensitivity to defocus of a split polygon end, and if the line end has an unacceptably high vulnerability, then the split can be moved slightly. This could be a method to reduce variability and improve yield through focus, and to save OPC and simulation cycles. A flow is designed to fit into an existing double patterning decomposition algorithm by creating a grid of possible splits for assessment by the pattern matcher.

1.7 Major Contributions of this Thesis

The major contributions of this thesis are the extensions to the pattern matcher through the design of better models and patterns, through the testing and improvement of accuracy and through the identification of applications for effective use of the pattern matcher. The simulation experiments outlined in this thesis have improved the confidence of the pattern matcher in its ability to be used as a first-cut method for identification of sensitivities in a

layout to lithographic processes. Pattern matching has been extended for high-NA, polarization, off-axis illumination, edge movement prediction and defocus sensitivity identification. These extensions are all vital if the pattern matcher is to be relevant for today's technology.

Additionally, patterns have been modified for mask manufacturing, which allows them to be extended as physical monitors for the lithographic system. OPC effects have been studied, and features which affect the sensitivity of a layout to aberrations have been identified. The fact that proximity and defocus effects occur in distinct locations has highlighted the fact that it is possible for OPC to increase or decrease a layout location's sensitivity to an aberration such as defocus, and that care must be taken to check for these sensitivities. Pattern matching has been shown to be a good, fast approximation to quickly check for sensitivities to a variety of aberrations.

Chapter 2

Background

2.1 Maximum Lateral Test Patterns

Lenses used in optical lithography ideally produce a perfectly spherical wavefront traveling from the lens to the image plane. However, in reality there are aberrations present in the system, and the wavefront deviates from a perfect sphere. This deviation can be represented as the Optical Path Difference (OPD) using the Zernike polynomials. The Zernike polynomials use polar coordinates, are invariant under rotation and are orthogonal. The presence of an aberration in a lithographic lens system results in imperfect imaging of the layout onto the wafer. However, some layout patterns will be more affected by the aberration than others.

Robins et al. (2003) devised that the inverse Fourier transform of the Zernike polynomials gives the theoretically most sensitive patterns to the aberrations. These 2D patterns, if placed on a wafer, collect a proportional amount of spillover light into their center depending on the amount of defocus present. Following from this, if a layout geometry has a very similar pattern to that of the inverse Fourier transform of a Zernike, then one could theorize that the layout geometry will also have a high sensitivity to the aberration. These patterns, taken as the inverse Fourier transform of the Zernike polynomials are known as Maximum Lateral Test Patterns (MLTPs).

2.1.1 Pattern and Probe Monitors

Robins ran a series of experiments on how to place the MLTPs on a mask, so that the resulting exposure to a wafer would be informative of the amount of aberration present in the system. The patterns are discretized by rounding the continuous phases to the closest of either one hundred and eighty degrees or zero degrees. Robins made modifications to the MLTPs to allow them to collect the spillover. A central probe was placed in the monitors, with a ninety degree probe being used for the even aberrations and a zero degree probe used for the odd aberrations. The spillover for the even aberrations, such as defocus, is imaginary, so the spillover is additive with the ninety degree probe. This central probe does not print by itself, but as the level of aberration is increased, a probe of increasing size is

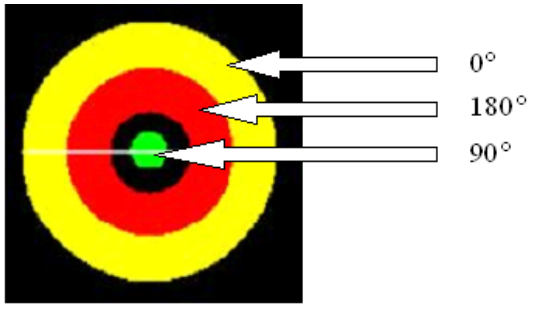

Figure 2.1: Two ring defocus pattern and probe monitor. Black represents chrome, yellow represents 0° phase, green represents 90° phase and red represents 180° phase.

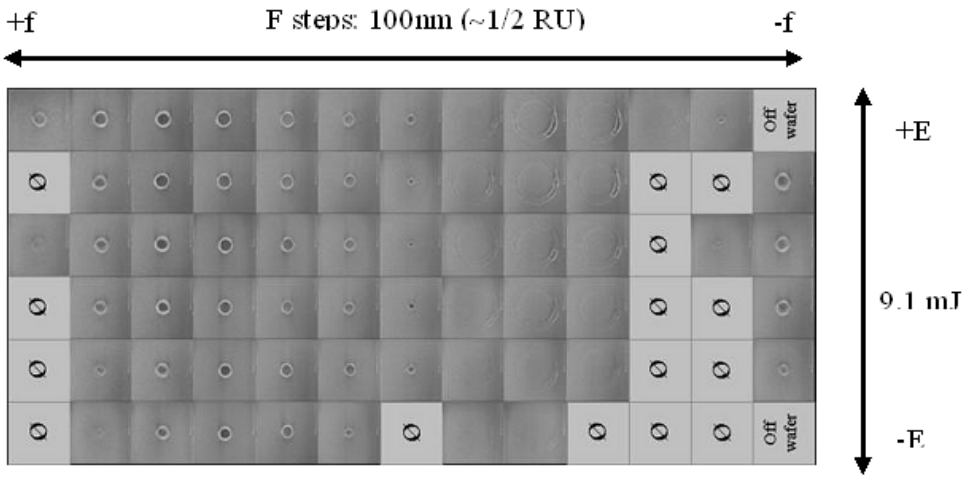

Figure 2.2: A focus exposure matrix for the two ring defocus pattern and probe monitor.

printed in the photoresist. This probe can then be examined using an SEM. A diagram of a defocus monitor is shown in Figure 2.1.

To demonstrate the application of these monitors, a result from Robins et al. (2003) is reproduced in Figure 2.2. This focus exposure matrix shows the emergence and enlargement of the printed probe as the amount of defocus is increased. This shows that these monitors are in fact sensitive to defocus, and also that an SEM can be used to measure the amount of defocus using the photoresist image. Electrical version of the aberration monitors have also been designed (Holwill and Neureuther, 2006; Rubinstein and Neureuther, 2007).

2.2 The Pattern Matcher

The pattern matcher is a fast tool developed by Gennari (2004) which quickly scans a layout for locations with a high geometric similarity to a given input pattern. When the

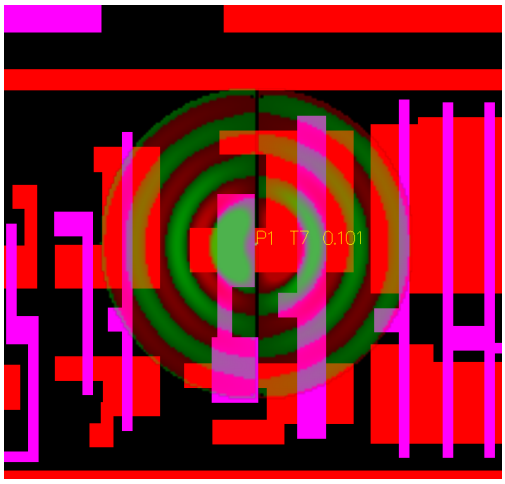

Figure 2.3: An example of a layout snippet with the coma MLTP overlaid at a high match location.

input pattern is a MLTP, the pattern matcher can be used to very quickly find areas of a layout that are sensitive to a lens aberration.

The largest design on which the pattern matcher was run was a critical layer of a post-OPC full chip layout. This 5.6GB hierarchical layout contained over a hundred million rectangles and polygons. The match factor for this pattern-matching run was computed at the corners of the layout for two 128 by 128 pattern orientations, taking 1.3GB of memory and running for 17 minutes on a single 2.8GHz processor. The non-OPC version of this layout took 11 minutes to process.

The tool has been run on a 5.6GB hierarchical full chip, post-OPC layout in a time of 17 minutes (with 11 minutes for the non-OPC layout), and is orders of magnitude faster than full simulation (Gennari, 2004). A screenshot of the pattern matcher is shown in Figure 2.3, with the layout in the background and a MLTP for coma in the foreground. The pattern matcher performs a 2-D convolution between the input MLTP and the layout at the match location, and a match factor is returned according to Equation 1. A match factor is a number between -1 and +1 that represents the degree of similarity between the pattern and the layout at that position. The match factor is normalized so that a value of +1 is an exact match, and a value of -1 is an exact opposite match. The number of layers to match with, their phases and their weights can all be specified within the pattern matcher framework.

$$MF = \sum_{i=0}^{ysize-1} \sum_{j=0}^{xsize-1} (pattern[i][j] \times layout\_matrix[i][j]) \tag{2.1}$$

The pattern matcher flow is shown in Figure 2.4. The inputs to the pattern matcher are a layout file in GDS format and a pattern file, which is a text file of complex numbers representing the magnitude and phase at each pixel of the MLTP. The outputs of the pattern matcher are the match locations with the highest matches, the match factors corresponding

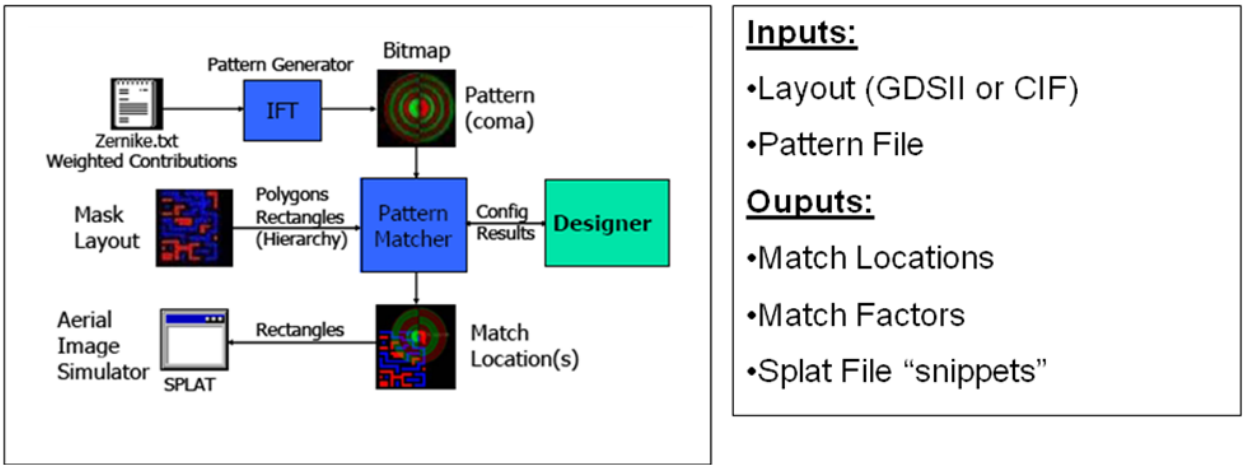

Figure 2.4: Pattern matcher process flow (Gennari, 2004).

to those locations, and SPLAT file snippets, which are the small layout segments which surround the match locations (Lee et al., 1995).

The pattern matcher is not intended to replace simulation, but instead gives a much faster, but approximate estimation of the change in intensity at a layout location in the presence of an aberration. The pattern matcher can be used as a pre-screening tool to find the areas which are most sensitive to a particular effect, and then simulation tools may be used on only those snippets, thus saving designers a lot of time and pre-warning them of problematic areas. The fast speed of the pattern matcher is due to many factors, such as the pre-integration of patterns, which reduces the number of pixels that must be computed against the layout. There is the selection of only select locations of interest to match against on a layout, such as corners or line ends. The layout is input into memory in a fast way, using partitioning, to maximize speed. Polygons are split into rectangles, and filtering is applied to the possible number of match locations to produce an exponential speed up over the case where every pixel was matched against. All of these speed-ups contribute to the very fast speed of the pattern matcher.

2.2.1 Through-Focus Effects and Pattern Matching

The through-focus behavior of various feature types and feature-to-feature layout interactions in dense patterns fundamentally limit the process window for optical projection printing. Two-dimensional features such as contacts and line ends suffer the most severe effects and the higher sensitivity of the critical dimension of isolated lines compared to line arrays is well known. Design rule restrictions can help filter out the use of highly focus sensitive scenarios such as forbidden pitches but identifying interactions among 2-D features is challenging in DRC. Once a layout is generated, OPC can help extend through-focus performance generally by increasing image quality and specifically by adding non-printing features such as SRAFs. There remains, however, a need for physically based through-focus models to anticipate problematic issues during the initial circuit design and to improve the efficiency

with which post layout OPC computes multiple focus behavior for pre-compensation. Additionally, the ability to provide through-focus feedback during double patterning decomposition would allow the identification among optional split locations of those splits which yield the lowest through-focus variability.

Historically, through-focus effects have been well characterized, considered in design rules, mitigated in OPC, and examined with approximate fast-CAD Pattern Matching techniques. The focus dose latitude such as the E-D trees of Bern Lin (Lin, 1994) are often used to determine the starting set points for biases and expected process window. The relative quality of features versus pitch are commonly used to identify and set placement constraints in design rules. The image simulation engines of OPC are often used to consider several additional out-of-focus points and simulation of the laser bandwidth on focus is also recommended (Lalovic et al., 2008). Perturbation based fast-CAD techniques, that is, Pattern Matching considered focus among other aberration terms (Gennari and Neureuther, 2004; Robins and Neureuther, 2004), and later illumination, high-NA, and polarization (McIntyre et al., 2005; Holwill et al., 2006). These approximate methods employ continuous layout convolution kernels in contrast to the discrete on-off rectangle overlaps that have become associated with Pattern Matching today. The upside potential for these fast-CAD approximate methods is enormous for finding edge placement errors (Rubinstein and Neureuther, 2008), Ring Oscillator variations (Wang et al., 2008) and interconnect delay variation (Chin et al., 2007). The bottleneck, however, has been that while most aberrations are small (Strehl Ratio > 0.97), defocus is not a small aberration (Strehl ≈ 0.9) and the perturbation based formulation must be revisited.

2.3 Polarization and High-NA Pattern Generation

It is well documented in lithography that the electric field component oriented radially in the pupil, or the TM component, will suffer a loss of contrast due to high-NA vector effects (Adam and Maurer, 2004; Smith and Cashmore, 2002). A set of MLTPs, derived by McIntyre et al. (2005), can be used by the pattern matcher to predict vulnerabilities to these vector effects.

The specific equations for the five MLTPs that are generated for the high-NA vector effects are outlined in McIntyre et al. (2005), and this section will give a high level overview of the derivation of these patterns. A graphical representation of the pattern generation is shown in Figure 2.5 and Figure 2.6.

For high-NA systems, the high angle of incidence means that the TM component of the pupil will be partially radiated normal to the wafer. That is, there will be an introduced z component to the electric field, when it is desirable to only have an x and y component. This z component can interfere destructively in locations where the x and y components interfere constructively. It is this z component that the MLTPs are created to find sensitivities to.

It turns out that the z component is proportional to the spatial derivatives of the low-NA components, and that the patterns can be generated by taking the partial derivatives of the electric field profile due to a coherent source (the Airy pattern). For extensions to off-axis and aberrated illumination systems, the partial derivative is taken of the pupil convolved

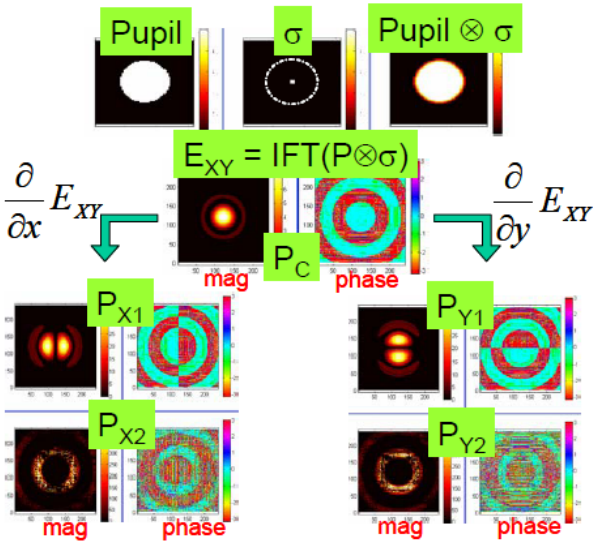

Figure 2.5: Visual representation of equations 3-5 for coherent illumination, resulting in four complex components of high-NA, z-component proximity effect. P_X2 and P_Y2 are assumed numerical noise.

with the source. This method produces five patterns, two of which are numerical noise and can be ignored for the on-axis case. The vulnerability score for both high-NA and polarization vector effects are calculated as a weighted sum of the patterns.

2.4 Double Patterning Lithography

Double Patterning (DP) is the process where a layout is split into two layouts, and each layout is exposed sequentially, with a processing step in between. This allows the critical pitch to be increased by a factor of two, thus allowing the k1 factor to also be increased by two. This technology is seen as a bridging step until Extreme Ultraviolet Lithography (EUV) is ready for production. There are extra costs involved in DP, such as the decreased wafer throughput and the increase in mask costs. Another cost that must be paid is the development of software to evenly split a layout into two masks, making appropriate split choices where polygons cannot be assigned to only one mask.

When a polygon must be split, the decision must be made exactly where to make the split, and how much overlap to include between the two layers. There is generally a fair amount of leeway in where to make the split. Often the actual split location is chosen heuristically, and this is where the pattern matcher can add value to this process. The pattern matcher can be used during the double patterning decomposition algorithm at the point where a split decision must be made. The pattern matcher, being much faster than rigorous simulation, can be used to evaluate the split decision for sensitivity to defocus, thus allowing the avoidance of any splits that would reduce the yield unsatisfactorily through focus.

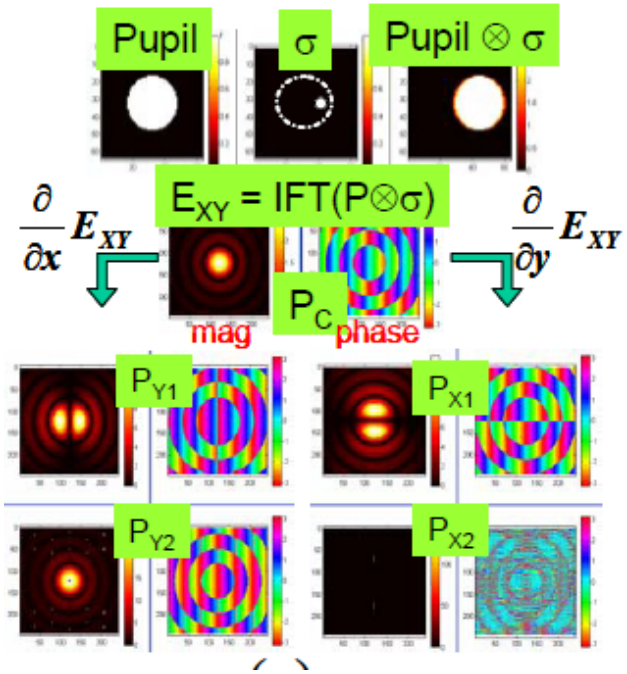

Figure 2.6: Derivation of MLTPs for off-axis illumination. MLTPs can derived for various optical conditions.

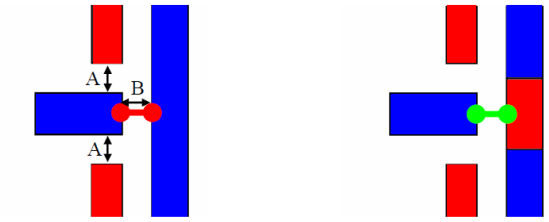

Figure 2.7: An example of a polygon that must be split, from Chiou et al. (2008). The figure on the left has a conflict still to be resolved, and the figure on the left shows a split that has resolved the conflict.

Chapter 3

Statistical Analysis of Gate CD Variation for Yield Optimization

This chapter presents a new method for analysis of variation and yield across the whole chip. This method takes into account the stochastic distribution of the input process parameters such as focus and exposure, and performs simulations of the design at the extreme points of the process window. Using a robust model to extrapolate the points within the process window, a full distribution of CDs is produced for each gate, which then is analyzed to provide information about both the individual gate and the variation across the chip.

This work was done as part of my internship at AMD, in consultation with Jongwook Kye and Yi Zou, and appeared in a publication (Holwill et al., 2007). This work provided an opportunity to investigate current industry areas that helps motivate the in-depth investigations in later chapters. This chapter serves as a motivation that yield is a very important topic in lithography, and that there are many ways to analyze and simulate layouts in order to try to characterize their variation through the process window and their yield. This chapter presents one such analysis in which distributions of CDs are produced and analyzed, and the rest of this thesis looks at how pattern matching can be used to characterize variation through the process window.

3.1 Introduction

While simulations of layout contours are available for given input conditions, and CDs can be simulated across chip for these given input conditions, it would be more useful to obtain a distribution of CDs so that the yield could more accurately be predicted. Current OPC tools modify the circuit layout so that it meets product requirements under given process conditions (Toublan et al., 2005), but that is no longer sufficient and a process is required to help mitigate yield losses. In this chapter, a novel method for calculation of the Gate CD distribution across the whole chip is presented. This is particularly important for analysis of across chip linewidth variation and yield. The process takes into account the fact that input parameters are not static, but have a probabilistic distribution in order to generate a CD distribution.

An advantageous aspect of the presented analysis is that only a small number of simulation data points are required, and thus the analysis can be applied to a full chip. Simulations are performed through focus and exposure, but only simulations at the extreme points of the process window, in additional to nominal values are required. CD values across the full range of six sigma are then extrapolated using a focus-exposure model. Although this analysis can be applied to any design features, this chapter concentrates on the gate layer, and CD measurements are recorded across the device.

A full stochastic distribution is generated for each transistor in the same way as described by Mack and Byers (2003). Given a distribution for the process parameters, and also the gate CD response to each combination of these parameters, the overall gate CD distribution is produced. This chapter explores the analysis that is made possible by generating the distributions for all of the transistors across the chip, rather than for one individual transistor. In particular, we look at the distributions of individual transistor variation and yield. A desirable transistor variation distribution would have a small mean and a tight spread. Additionally, having the actual distribution for transistor yield, rather than an average figure such as Across Chip Linewidth Variation (ACLV), the sections of the design that give a low yield or high variation can be targeted. One way that hot spots can be identified is with a graphical user interface in the Calibre simulator, Calibre RVE (Mentor Graphics, 2010), which produces a histogram of the results and zooms in on transistors in each bin. This analysis allows us to evaluate our OPC for bias, optimize process parameters, and optimize design style. Since the CD response curve to focus and exposure is non-linear, optimization of OPC and input parameters can be non-intuitive, so this method of analysis can provide additional insight.

This chapter develops a method for identifying low yield and high variation gates in a layout, and for measuring both the variation across chip and the distribution of transistor variations, while only requiring a small number of simulation points across the process window for each transistor.

Section 3.2 describes the methodology for the generation of the CD distribution, Section 3.3 describes the process flow, Section 3.4 describes how the data is analyzed, and Section 3.5 is the summary.

3.2 Methodology for CD Distribution Generation

The general methodology for generating the CD distribution is extended from the work described by Charrier et al. (1997). Let us start by explaining the methodology when given only one input parameter. Without loss of generality, let us assume that this parameter is defocus. In traditional simulations, a single input value is given for focus. A through focus simulation for CD of a feature can be simulated with any lithographic simulator such as SPLAT, Prolith or Calibre. Then, for this single focus value, the corresponding CD value can be found by looking up the corresponding data point on the through focus simulation curve. This methodology differs from the traditional approach in that instead of a single input value for focus, a probabilistic distribution of values is given. Now, there is not a single simulated CD value to look up in the through focus CD simulation curve, but rather a distribution of

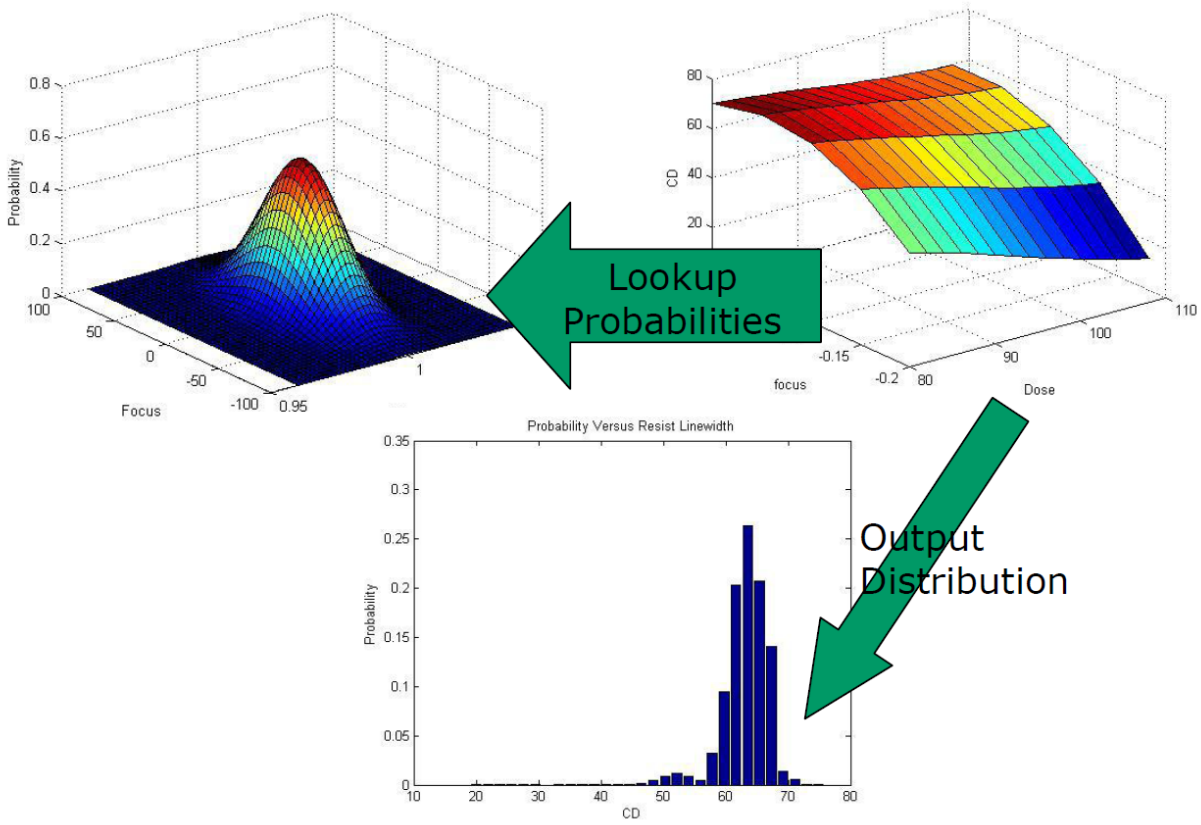

Figure 3.1: The methodology used to generate the CD distribution for the case of two Gaussian input parameters, focus and exposure.

CD values. For each point on the through-focus curve, there is a corresponding probability for that input focus value, and thus a corresponding probability for that CD value. For this project, it is assumed that the input values are Gaussian, but any distribution could be used with the same methodology. To extend this method to two dimensions, for example focus and exposure, the two probability distributions for focus and exposure can be multiplied, since it is assumed that as input parameters they are independent. The CD response curve is now a CD response surface, which depends on both focus and dose. For each point on the surface, the corresponding probability for that input parameter combination is looked up in the input probability distribution, and this gives the probability for that CD. If there are multiple points on the surface with the same CD, the probabilities are summed for each of these points to give the overall probability for that CD. Throughout this project, the two input parameters are focus and exposure.

Figure 3.1 explains graphically the process of looking up the probabilities for each CD to generate a CD distribution. Although focus and exposure have been used to demonstrate this example, any input parameters at all could be used, such as chuck flatness, partial coherence or illumination imbalance.

This project differs from the work of Charrier et al. (1997) in that it is designed for the

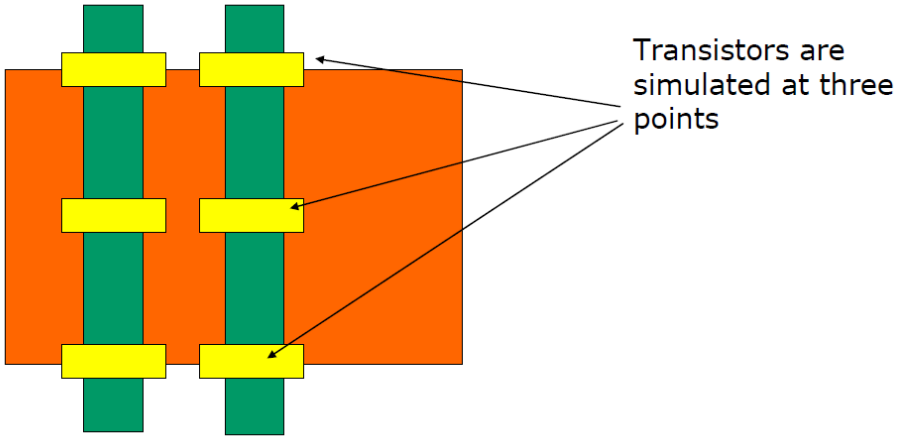

Figure 3.2: The gate lengths are simulated at these three points where the poly overlaps with the active.

whole chip, rather than a single feature. This is achieved by approximating the CD response curves, which is discussed in Section 3.2.1. Additionally, the gates across the whole chip are sampled at three points along the gate. See Figure 3.2 for the location of these sampling points. The reason that the three points are used is that the sampling points at the top and the bottom will be subject to line end shortening, and the point in the middle may be subject to other reasons for CD change such as neighboring feature interaction.

3.2.1 Approximations used in Simulation

We are interested in the CD response curve for values of the process parameters within their values of $+3\sigma$ and -3σ, where σ is the standard deviation of the input distribution. Values outside this range would not be useful because the input values will be within this range for over 99% of the time, by definition of standard deviation. Simulating the full CD response surface across for all of the process parameter values within $+3\sigma$ and -3σ would be too time consuming to apply to a full chip. So, instead of simulating the CD across all of the process parameter values, the CD is simulated for the input parameter nominal values, the -3σ values and the $+3\sigma$ values. Then a robust model is used to extrapolate the data points between these values, across the whole process window. This is shown in Figure 3.3. A number of different polynomial models were experimented with, and any can be used within this framework. Through trial and error, it was found that a good polynomial fit was found with fifth degree the formula shown in Equation (3.1). The fit was made using multiple regression, which minimizes the error for the curve fitting the data points. An example is shown with the real simulated data overlaid with the extrapolated data in Figure 3.4.

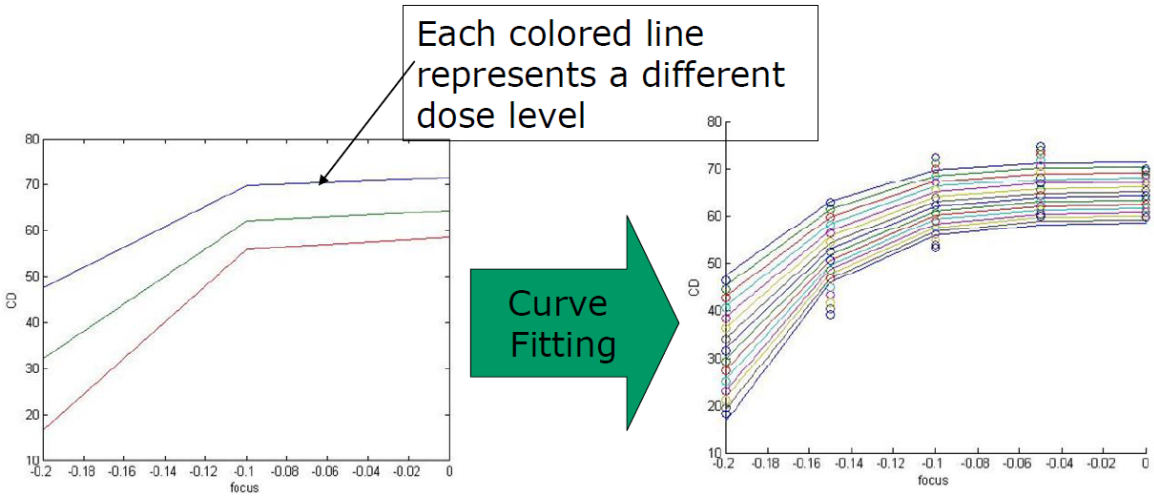

Figure 3.3: Extrapolation of the CD simulation data from 9 data points to 75 data points.

$$\begin{aligned} CD &= a_{00} + a_{01}F + +a_{10}E + a_{11}FE + a_{02}F^2 + a_{20}E^2 \\ &\quad +a_{03}F^3 + a_{30}E^3 + a_{05}F^5 + a_{50}E^5 \end{aligned} \tag{3.1}$$

Another robust model that can be used is that of Mack and Byers (2003). Mack found that rather than using a polynomial model as was traditionally done, focus-exposure curves are better fitted with the function shown in Equation (3.2). Here E_s is the exposure to dose, E is the input exposure value, F is the input focus value, and M and N determine the degree of the equation. In the particular simulations that were run for this work, similar results ensued from both of these models.

$$CD = \sum_{m=0}^{M}\sum_{n=0}^{N} a_{nm}\left(1 - \frac{E_s}{E}\right)^n F^m \tag{3.2}$$

3.3 Process Flow

For this project, Mentors Calibre was used to simulate the CD values at the 9 process window points for each layout simulation point. The overall process flow can be seen in Figure 3.5. The Calibre Simulation section of the flow consists of TCL and TVF scripts which generate any necessary optical models, and begin the simulations for the given process conditions and outputs RDB files, which are text files containing the simulation data, as well as GDS layout files which contain the simulated contours. The RDB files are then fed into the Matlab (Mathworks, 2010) analyzer. The flow for the Matlab analyzer is shown in Figure 3.6.

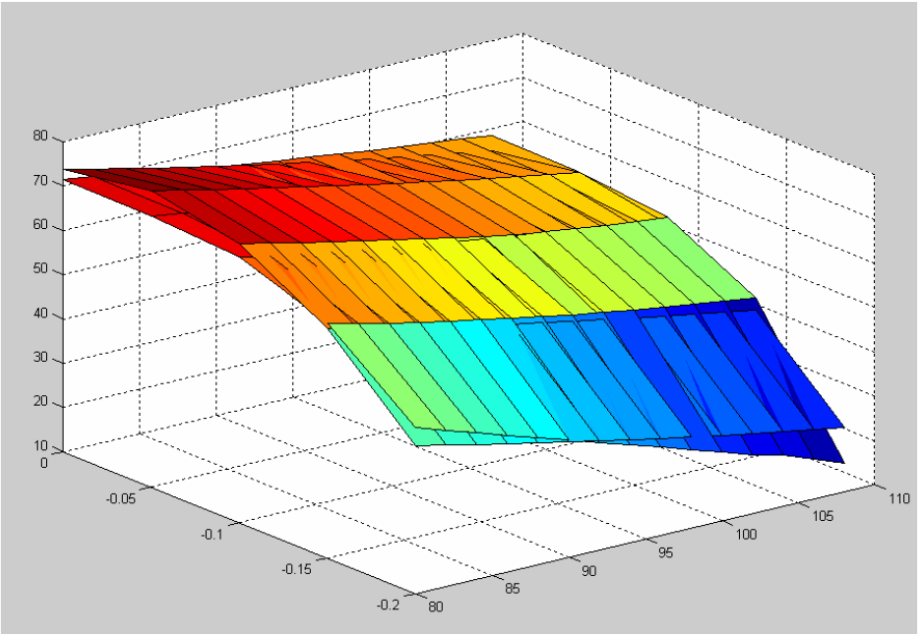

Figure 3.4: Simulated data overlaid with extrapolated data across the process window for focus and exposure.

The Matlab Analyzer takes as its input the text-based RDB file, and a configuration file which provides information on the process window and input parameter distributions. A model of best fit is applied to the data, and then the extrapolated points are generated. With these extrapolated points, a full CD response surface has been generated. For each point on the response curve, the probability of that combination of focus and exposure is referenced in the probability matrix, and then when all of the points have been processed, a probability distribution for that layout location has been generated. The expectation, standard deviation, and yield are recorded to a file, and then the process is repeated for the next layout location until all have been processed.

The Matlab program outputs the data both as a tab delimited text file and also as an RDB file. The text file can be imported into any statistical analysis program, such as JMP (JMP, 2010) or a tool such as R (R Development Core Team, 2009) or Matlab. Then the distributions of expectations, standard deviations and yields can be analyzed. The yield is calculated by giving a range of CDs that are acceptable, and returning the probability that the CD lies within that range. The RDB output file can be read back into Calibre and locations of high variation or low yield can be visualized graphically. The analysis methods used are covered in further detail in Section 3.4.

3.4 Analysis of Data

The data that is produced are parameters of the CD distribution for each layout location, in particular the expectation μ_i, standard deviation σ_i and yields for each layout location i.

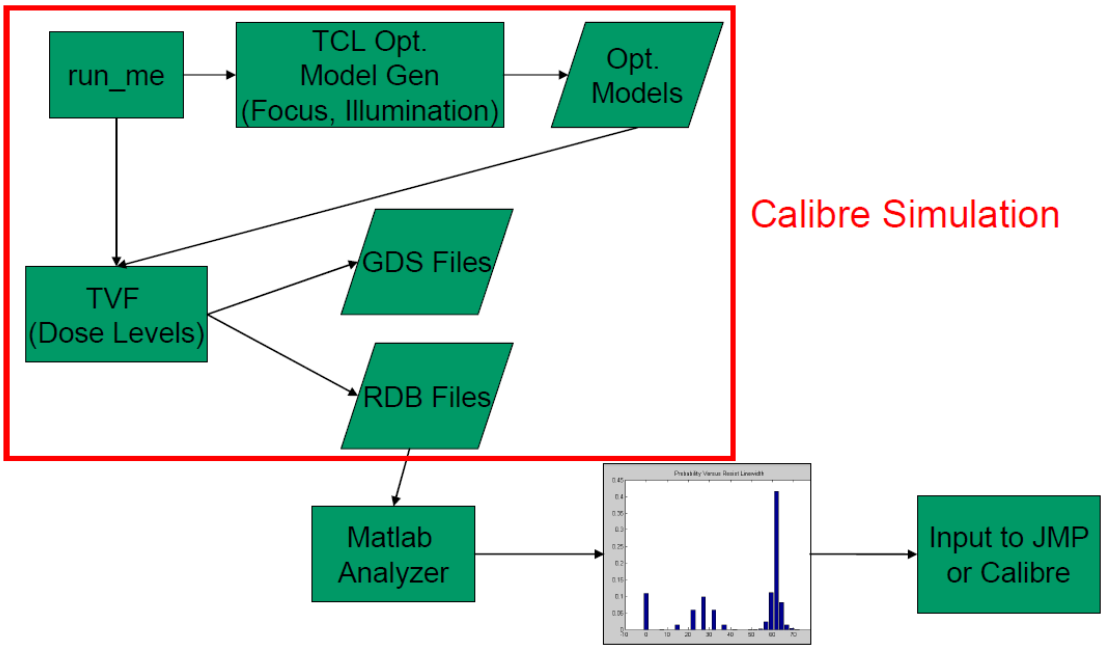

Figure 3.5: Overall process flow for the CD Distribution Generation.

One aim of the analysis is to incorporate these individual parameters into predictors of the performance of the chip as a whole.

One whole-chip layout statistic that can be deduced is the average standard deviation $\overline{\sigma} = \frac{1}{N}\sum_i \sigma_i$. This statistic tells us the average variation for each transistor. If this measurement is high, then this means that on average all of the gates are experiencing large variation, and it is not just a few that are having trouble.

The standard deviation of the σ_i, given by the formula $\sqrt{\frac{1}{N}\sum_i (\sigma_i - \overline{\sigma})^2}$ is an indicator of the spread of variation across the chip. If this measurement is low, then this indicates that most of the gates are experiencing the amount of variation given by $\overline{\sigma}$. If this is high, then this tells us that there may some transistors that are experiencing very little variation, and some that are experiencing a large amount of variation. By importing the output RDB file into Calibre RVE, gates with high CD variation can be zoomed in upon and visually inspected. This is shown in Figure 7.

The average of the expectations $\overline{\mu} = \frac{1}{N}\sum_i \mu_i$ predicts whether there is any bias in the OPC algorithm. If this value is not within the target range, then the OPC algorithm needs to be modified to correct this bias.

The standard deviation of the expectations $\sqrt{\frac{1}{N}\sum_i (\mu_i - \overline{\mu})^2}$ corresponds to the traditional Across Chip Linewidth Variation (ACLV). This is the amount that the expected CD varies across the chip. If this parameter is high, then it is very likely that when the wafer is imaged, a large spread of CDs will be observed.

The yield statistics are useful for highlighting the high yield and low yield transistors. This can be achieved using Calibre RVE as shown in Figure 3.7.

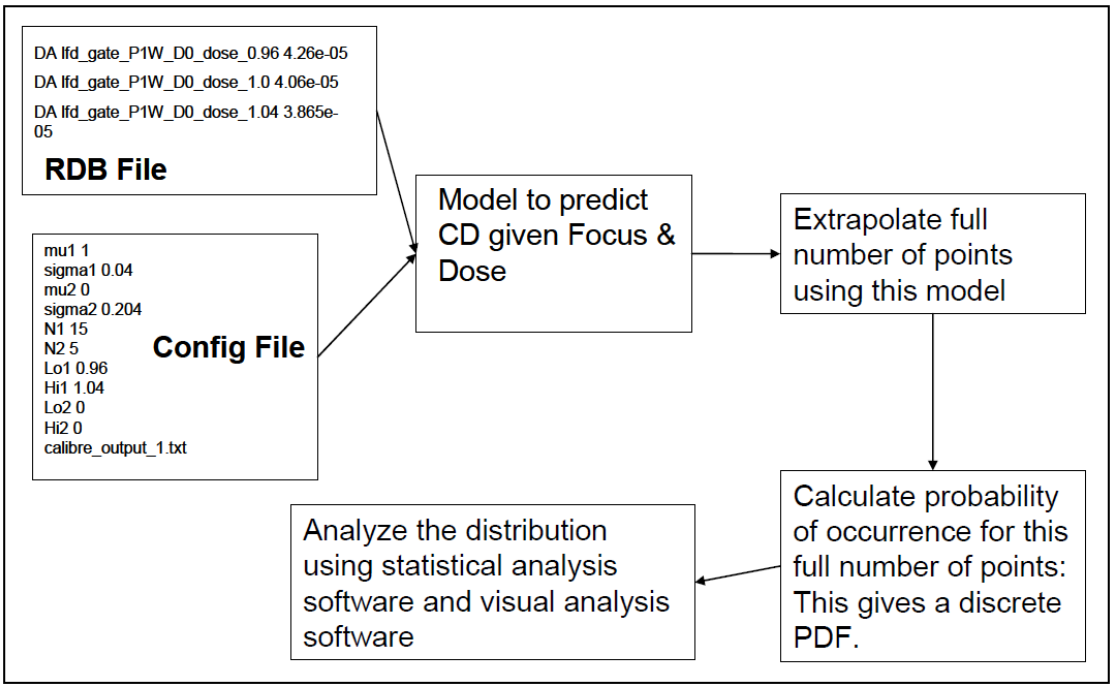

Figure 3.6: Overall process flow for the CD Distribution Generation.

3.4.1 Use of Data to Form an Optimization Feedback Loop

An optimization loop can be formed around the data to improve the yield, minimize the variation across chip, minimize the average variation or minimize the spread of variation. The way this is done is to form a loop around the experiment and plot the value of the optimization parameter for each loop iteration. For each iteration of the loop, an input parameter or setting is varied. This could be exposure, illumination conditions, gate length, or any other number of input parameters.

3.4.2 Comparison with Experimental Data

In order to give a rough estimation that the process described in this chapter is accurate, it was compared with experimental data. The experimental data had a 3σ value between 2.6 and 2.9, and our program output a 3σ value of 2.81. This does not verify the correctness of the program, but rather gives some confidence that the values are in the correct range. Further experiments would be required to fully test the accuracy of this project.

3.5 Summary

A method for producing CD distributions for each of the transistors in a layout is presented. This method takes into account the probabilistic distributions of the input parameters, and using the process response curve a CD distribution curve is generated. This

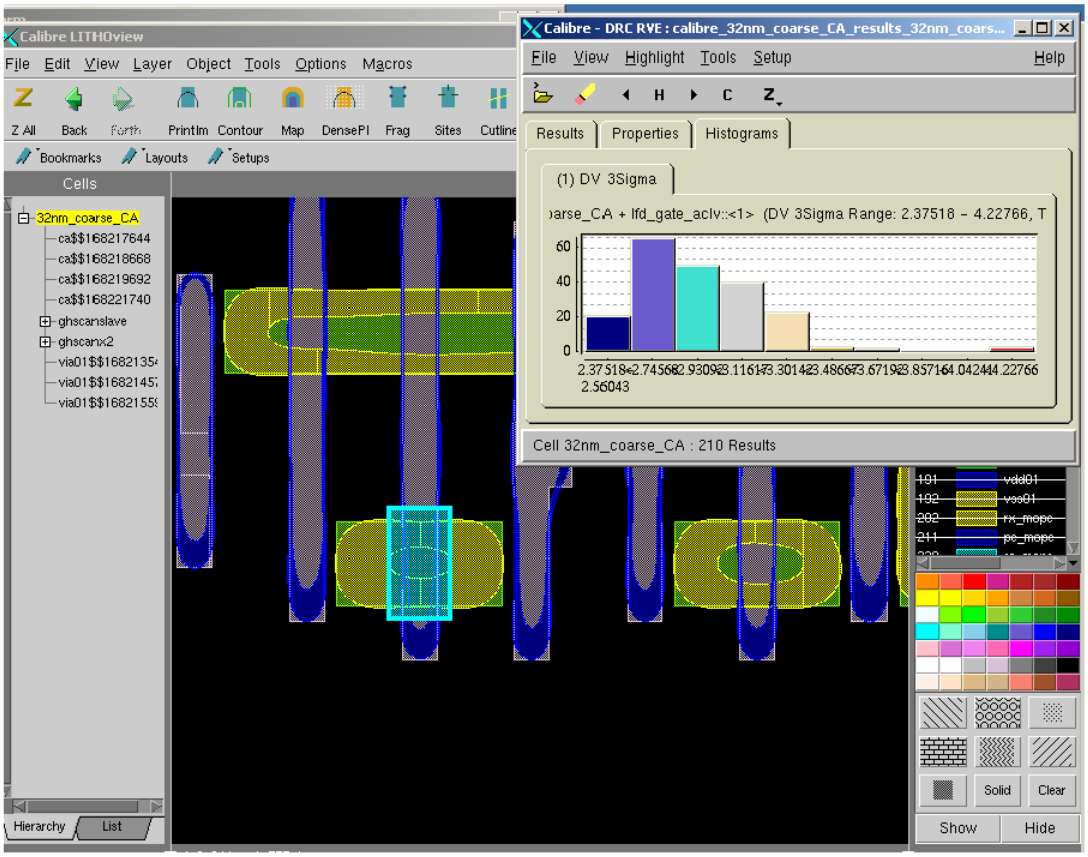

Figure 3.7: This is the RVE interface in Calibre that visualizes the information from the output RDB file. Here, the GDS file with both the layout and its contours is shown, and the standard deviation measurements have been imported from an RDB file. A histogram is produced for the distribution of standard deviations, and by double clicking on a histogram bar, the layout locations which are from a bin of interest are highlighted and can be inspected.

process response curve is generated not with full simulation, but rather with simulation at a few points in the process window, and then uses a model to extrapolate between these points.

A number of useful metrics are produced and their meanings analyzed in this work. These metrics provide insight into the amount of OPC bias, the ACLV and the spread of transistor variation. This project provides both a visual method for zooming in on the problematic gates, and a method for analyzing the output metrics with a statistical analysis program. This method can be used to either evaluate the current layout and process parameters, or to optimize input conditions or the layout to improve yield and lower variation.

Chapter 4

Mask Issues

4.1 Introduction

This chapter looks at mask issues for lithography and how pattern matching and the Maximum Lateral Test Patterns (MLTPs) are affected by these mask issues. The first issue that is examined is that of mask friendliness of the MLTPs when they are written on a mask for use as a monitor. MLTPs, taken as the inverse Fourier Transform of the Zernike polynomials, while very sensitive to the aberrations from which they are derived, tend not to be very manufacturable when placed on a mask as a physical monitor. In particular, they have round edges which translate to many small edges. Section 4.2 will cover an analysis of an automatic process in which to remove Design Rule Check (DRC) violations, and will discuss the aberration sensitivity of both handmade and automatically generated patterns.

Another mask issue that affects the pattern matcher is that of masks which are intended as attenuated phase shift masks. The addition of an 180° phase layer with a weighting of 0.25 allows the pattern matcher to be effectively used for this type of mask. No additional runtime penalty is incurred apart from the initial generation of this layer.

Lastly, Optical Proximity Correction (OPC) is a technique used extensively in current technologies. It involves the fragmentation of a layout into smaller lengths, followed by a feedback loop in which each of the edges are shifted slightly and simulated, until the image on the wafer is satisfactorily close to the drawn intent, and the edge placement errors are minimized. The pattern matcher is typically used on drawn layouts in design before OPC is applied just prior to mask writing, and the studies in this chapter analyze the effect that OPC has on match factors that were run on a pre-OPC layout, and looks at cases in which OPC can change the match factor and thus the sensitivity of a layout location to an aberration.

4.2 Adaptation of Patterns for DRC Requirements

This section considers modifications of the Pattern-and-Probe monitors to make them suitable for inclusion within a circuit design as drop in monitors for the lithography process. Nonidealities such as lens aberrations can be monitored using patterns derived from the

Zernike polynomials. However, the non-Manhattan geometries produced by this theoretical method are not mask friendly, and in fact took many hours to manufacture in their first attempt. This section presents modifications to original aberration monitors to allow them to pass DRC checks and thus be more mask-friendly. The principles expressed in the original aberration monitors can be integrated into more traditional circuit layouts to create more processing acceptable patterns, with the example shown in this paper retaining 68% of it sensitivity and no decrease in orthogonality.

Characterization of aspects of lithography systems such as lens aberrations is of great importance as critical dimensions continue to shrink. One characterization tool for lens aberration monitors is to examine photoresist images with an SEM that are printed using sensitive patterns (Kirk, 2000). One such version of sensitive patterns are the pattern and probe monitors (Robins et al., 2002). The SEM image produced by these patterns varies depending on the amount of lens aberration, producing large changes in the photoresist image. However, their original geometric form requires a great amount of expense to be written to a mask, due to the rounded edges. These edges require conversion into jaggered Manhattan geometries. Additionally, if this jaggering process is done prior to being sent to the mask manufacturer, there is the possibility that the edge segments may be too short. These theoretical patterns also have additional problems such as diagonal distances that may violate DRC and touching opposite phases that may violate DRC. Therefore, patterns that pass DRC and do not have these problems would be more mask friendly.

The exact modification to the pattern depends highly upon the method used to produce it. In this Section 4.2.3.2, an automatic method for removal of DRC-failed vertices is investigated, and in Section 4.2.3.1, a hand-made modification that is much more mask friendly than the original pattern is looked at.

In Section 2.1.1, a theoretical background is given on the original pattern and probe monitors. Section 4.2.1 covers the role of DRC checks for mask manufacturability. Section 4.2.2 covers the application of these patterns to model calibration, Section 4.2.3 looks at the possible methods for modification to the patterns, and Section 4.2.4 looks at sensitivity analysis of such patterns. Section 4.5 is the conclusion.

4.2.1 Mask Making and DRC Checks

One measure of how difficult a pattern is to manufacture on a mask is whether or not it passes DRC checks. Although there are more tests that a layout may be put through before being printed onto a mask, a mask that fails DRC is unlikely to be mask manufacturing friendly. For this reason, a selection of DRC checks are used for this project to improve the manufacturability of the mask. Depending on where the mask is being manufactured, design rules can be imported into the program and used in place of the checks currently being used. This makes the process versatile for any manufacturer.

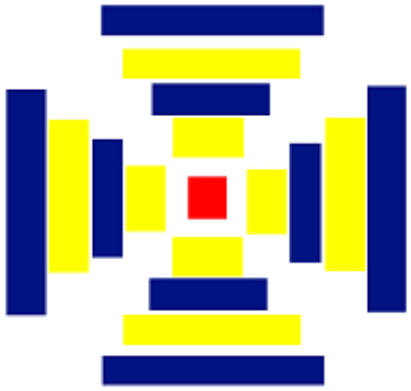

Figure 4.1: A handmade defocus sensitive pattern that is mask friendly.

4.2.2 Pattern and Probe Monitors for Model Calibration

Many structures are used for calibration of optical models. These structures are imaged in photoresist using the optical process to be modeled, and then the SEM images are used to calibrate the model. With the shrinkage of CDs, variability has become much more of an issue for power and performance, and accurate simulation across the process window is very important.

The patterns used for calibration are generally lines, line ends, contacts, holes, H-structures and other such structures that can be frequently found in real layouts. Highly sensitive patterns across the process window, such as those presented in this chapter, might be a good addition to the current set of patterns. This would give the model robustness in the presence of small amounts of aberration, and may give more simulation results for across process window measurements. This has not been tested, but would be a worthy investigation for future research.

4.2.3 Methods of Pattern Generation

The method of DRC-friendly pattern generation determines the types of patterns that are derived. In all cases, the original pattern is morphed into a new pattern that is more mask friendly than the original. In the case of the hand made pattern, rectangles were drawn in replacement of the original circles, overlapping as closely as possible the original layout. In the case of the automated layout, an automatic process was used as is described in Section 4.2.3.2.

4.2.3.1 Hand Made Pattern Generation

In order to see more variety in the kinds of patterns produced, a hand made example was generated which has no round edges, no short edges, and passes the DRC checks that were put in place for this project. However, it still retains the basic shape of the original pattern. The resulting pattern in shown in Figure 4.1.

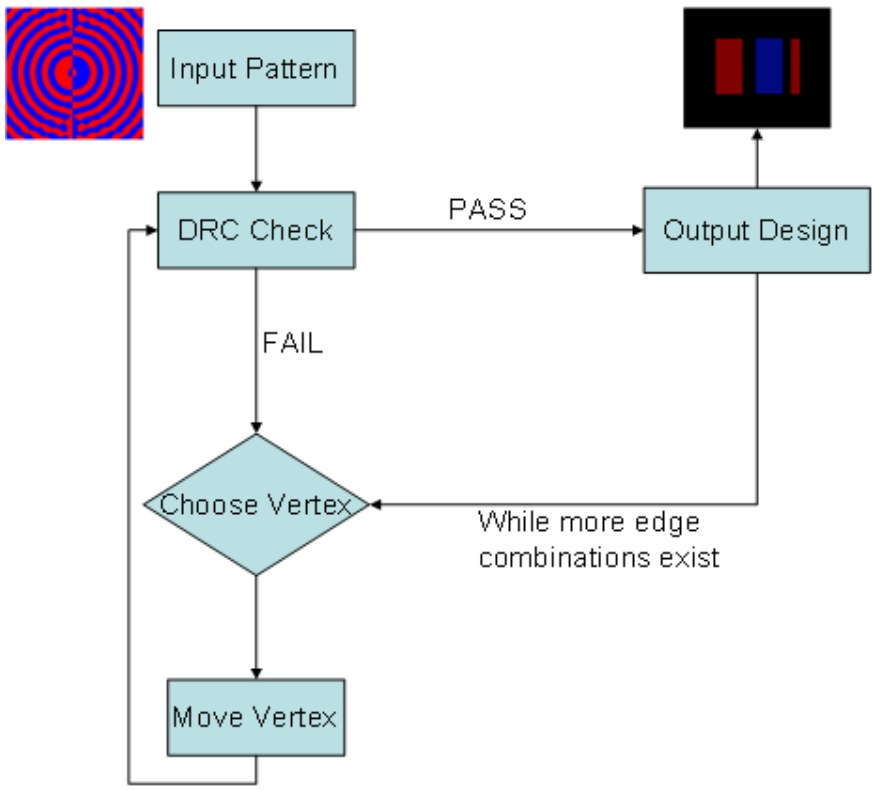

Figure 4.2: Automatic process flow used for generation of modified patterns that pass DRC checks.

4.2.3.2 Automatic Pattern Generation

The handmade layout from Section 4.2.3.1 gives a good starting point, but for automatic generation of layouts dependent upon particular layout requirements, an automatic process is shown. For this project, the process shown in Figure 4.2 is used.

The original pattern is input to a DRC check, and the list of vertices that it fails on are returned in a text format. A vertex is chosen, and this vertex is moved. The modified layout it saved, and the layout is checked for DRC again. Since the layout pattern is very small, each iteration runs very fast, in just a matter of seconds.

When a vertex is selected for moving, there are a number of places where it could be moved while keeping the layout Manhattan. Assuming that the layout is Manhattan to start with, this allows the removal of DRC failure points without the introduction of non-Manhattan rule violations. The vertex movement selections are shown in Figure 4.3. A vertex that causes a DRC violation is connected to at least one edge that is causing a violation, so removal of an adjacent edge is one way to remove a violation. This is done by replacing the x-coordinates position with that of its predecessor (or successor) and the y-coordinates with that of its successor (or predecessor). Alternatively, to explore a larger variety of different patterns, the vertex can be moved an arbitrary distance, and then the predecessor and successor to the vertex must be modified appropriately to keep the layout

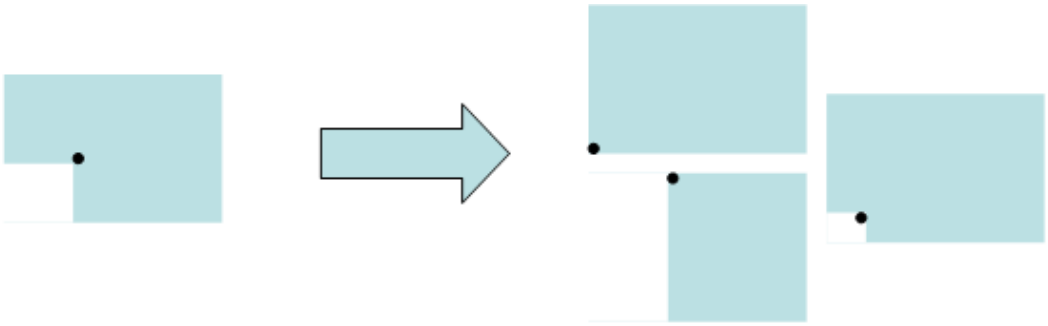

Figure 4.3: A vertex that does not pass DRC checks is selected on the left. It can move completely down or completely up to remove the edges it was connected to, or move partway between these two positions to a new point, creating new edges.

of Manhattan geometry. The first option of removing an edge adjacent to the vertex is explored in this project, and the method of moving the vertex an arbitrary amount would be an interesting experiment for future research.

The goal function for this process is not only that the pattern passes DRC, but also that it remains sensitive to the aberration for which it is a monitor. In order to quickly check the sensitivity of the pattern, it can be matched against the original pattern using the Pattern Matcher. See Figure 4.4 for the process flow used in judging the sensitivity of the patterns. The higher the match factor for the modified pattern matched against the original pattern, the higher the similarity between the two patterns, and the higher the probability of the modified pattern having a good sensitivity to the aberration.

One important factor to note is that the probe size plays a large role in the actual, simulated sensitivity. In order to compare the modified patterns in a fair manner, the probe area is kept equal for all modified patterns. This allows us to concentrate on the features that are actually changing the sensitivity of the pattern, rather than using optimizations of the probe size.

Given this goal function, there are a number of options available for searching for new patterns. One is to randomly move vertices, removing edges, until the DRC checks are passed. This is the method that has been used for this project. An example modification to a layout pattern is shown in Figure 4.5.

The method described here is a version of hill climbing. With each iteration, the number of DRC checks that fail is reduced, and thus the goal function is increased. Other methods that could be used for generation of modified patterns are simulated annealing or genetic algorithms. Simulated annealing would involve moving some vertices in such a way as to temporarily increase the number of DRC checks that fail, in case the pattern is stuck in a locally optimal geometry rather than a globally optimal geometry. Another method to investigate could be genetic algorithms, by which a set of patterns is maintained through a sequence of generations. From generation to generations, patterns which pass more DRC checks and retain sensitivity are selected to be retained, and retained patterns are combined in some way to search for new patterns.

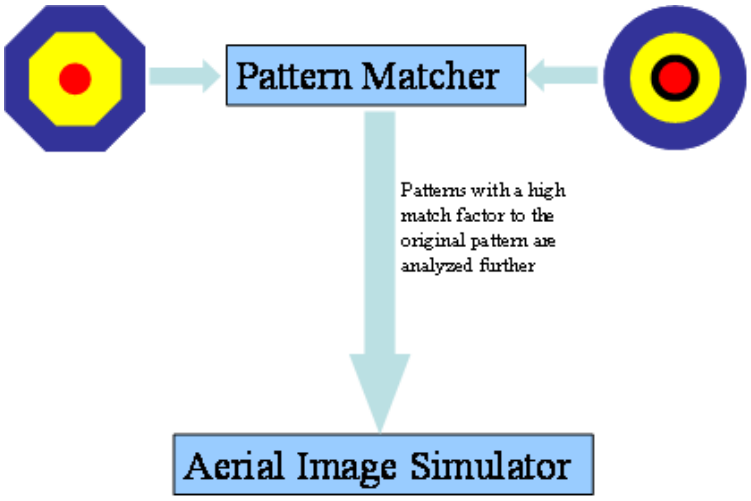

Figure 4.4: A method for testing the sensitivity of the patterns involves using the pattern matcher to judge their similarity to the original pattern. An aerial image simulator, such as SPLAT, can be used to measure the actual sensitivity with more accuracy.

	Original Pattern	**Modified Pattern**
Intensity Difference with Focus	0.59	0.4
Match Factor with Focus Monitor	0.421	0.268
Match Factor with Spherical	0.224	0.142

Table 4.1: Sensitivity and Orthogonality of the modified pattern as compared to the original pattern.

4.2.4 Sensitivity and Orthogonality Analysis

The hand made pattern of Figure 4.1 was tested for sensitivity to defocus. First it was tested using the Pattern Matcher. These matchings are shown in Figure 4.6. The Pattern Matcher returned a match factor close to 0.421 for the original pattern, and a match factor of 0.268 for the modified pattern. This represents a 64% retention of match factor for the modified pattern. These results are shown in Table 4.1.

In order to gain a more accurate estimation of sensitivity to defocus, the modified pattern and original pattern were both simulated using the SPLAT aerial image simulator built into Mentors Calibre. For the original pattern, the intensity difference with 0.04λ RMS Defocus is 0.59. For the modified pattern, the intensity difference with Intensity difference with 0.04λ RMS Defocus is 0.4. This represents a 68% retention of intensity change with defocus for the modified pattern.

In addition to sensitivity to defocus, it is important for the pattern to remain orthogonal to other aberrations. This allows the monitor to remain uncoupled from other effects. The defocus monitor is most similar to the spherical pattern, in that they are both rotationally symmetric even functions, as opposed to odd functions such as coma. With edges being removed and added, it is conceivable that a modified pattern might lose its orthogonality

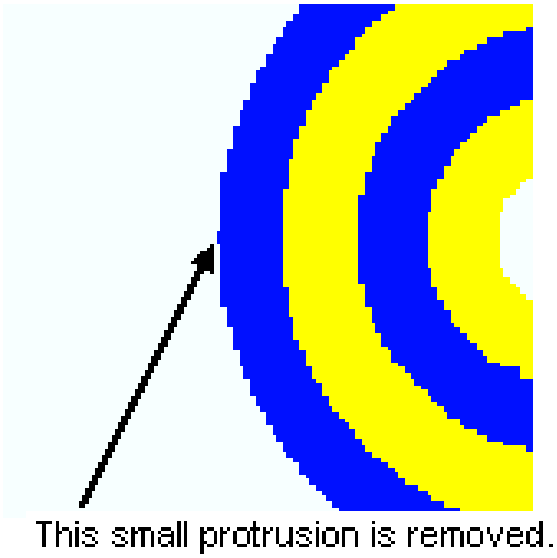

Figure 4.5: A small protrusion was successfully removed using the process flow described in Figure 4. This small jog is difficult for mask makers to manufacture, and is removed automatically.

to the other aberration monitors. The handmade pattern was matched using the pattern matcher against the spherical pattern, and its match factor dropped by 47%. This is the same amount that the original pattern dropped by, so this indicates that it is still orthogonal by an acceptable amount.

Thus, the handmade pattern is both still very sensitive to defocus, and is orthogonal to the other lens aberrations. It uses only large rectangles, with no difficult features to print. This makes it a good modification to the original focus monitor.

4.3 Extension for Attenuated Phase Shift Masks

Another mask issue that the pattern matcher must be able to perform under is masks of varying phase shifts. The Pattern Matcher is designed to accept a layer allocation from the user, which each layer given a phase and a weight. Attenuated phase shift masks have a background intensity of 6% at a phase of 180°. For pattern matching to be used with attenuated masks, the background must be recognized by the pattern matcher as its own 180° layer. This additional background 180° layer must be created to be used in computing the match factor, and it must be weighted at a transmission of $\sqrt{0.06} \approx 0.25$. This layer can be generated using the Boolean layers function of a standard layout tool such as Cadence or Calibre Work Bench, and the layer weight can be set as an input to the pattern matcher.

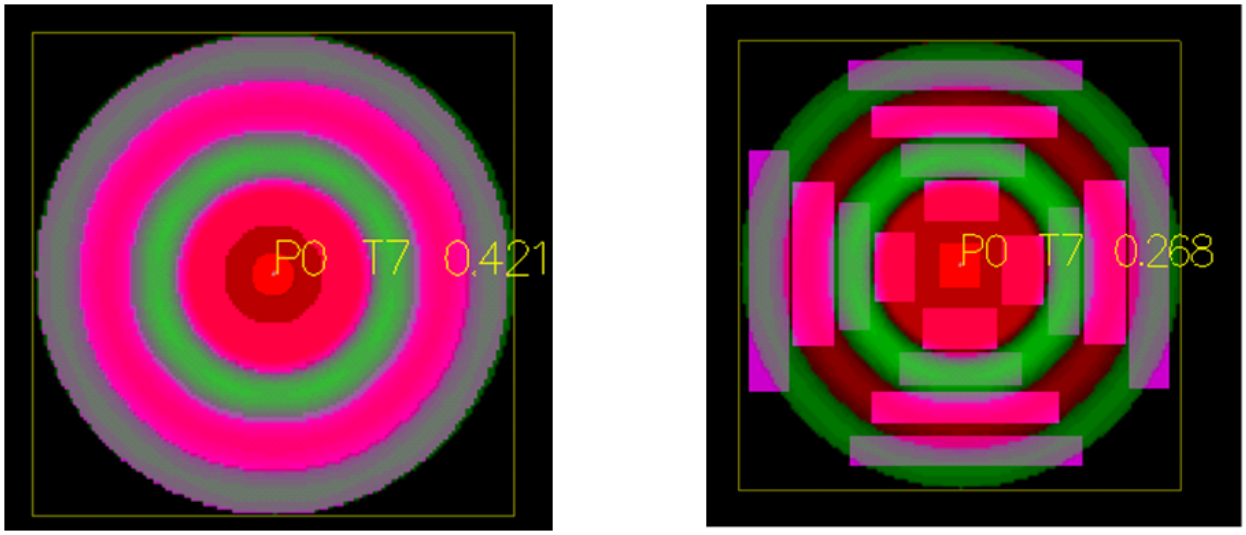

Figure 4.6: The Pattern Matcher as applied to the original and modified patterns.

To test the pattern matcher with an attenuated phase shift mask, a layout was transformed to include the background layer, and the pattern matcher was applied to the phase shift layout with the coma target from Figure 4.7. The resulting layout snippets at the points of maximal match factors were simulated with the SPLAT aerial image simulator, and the intensity differences between the simulation with no aberration and with a coma of 0.02λ RMS were recorded. The plot of the results is shown in 4.8.

The results suggest a strong correlation between match factor and intensity change, suggesting that a high match factor will be indicative of a potential printing problem in the presence of coma for a phase shift mask. However, there is some spread on the plot, and one possible reason for this could be that some simulation cutlines may not be optimally placed to run perpendicular to layout drawn edges. Additionally, pattern matching is not as accurate as simulation, and the pattern could be someone sensitive to coma, but there could still be a small spread of intensity changes that are produced for a given match factor.

The results seen here for coma are very encouraging that the fast-CAD pattern matching technique can be used to quickly find problematic areas of a layout. Specifically, the large changes in the change in ΔI in Figure 4.8 can be found through the large match values on the horizontal axis that can be calculated 10^4 to 10^5 times faster than the aerial image simulation of ΔI. As is shown in Chapter 6 as well as many other examples throughout this thesis, for focus and dose and for every feature size, type and surrounding region has a different response to an optical system change and no one point in Figure 4.8 is representative of all layouts.

For further details on how Matlab factors for alternating masks and binary masks as well as their complements are interrelated see the paper by Wang et al. (2009).

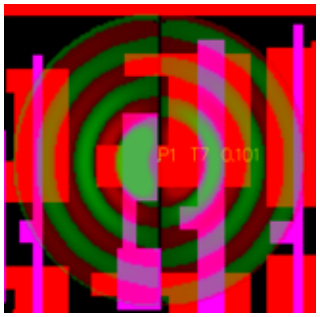

Figure 4.7: The coma Maximum Lateral Test Pattern shown overlaid with a layout.

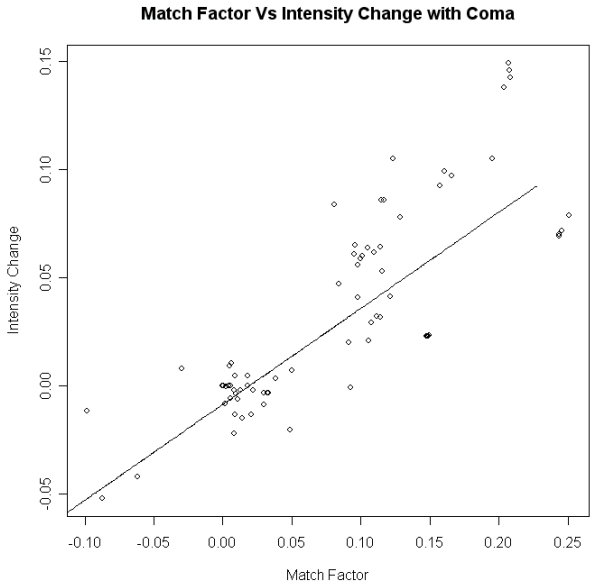

Figure 4.8: Match factors versus change in intensity through coma for an attenuated phase shift mask.

4.4 Pattern Matching for OPC Treated Layouts

Optical Proximity Correction (OPC) Treatments are a method for modifying a layout to give smaller Edge Placement Errors. The layout is fragmented and small edges are shifted, and the layout is simulated over a number of iterations to produce a layout which will print closer to the design intent than the original layout. OPC treated layouts thus have a different mask layout to the drawn layout and to the pattern that is expected on wafer. This section shows that pattern matching is valid on layouts that have been treated with OPC, and can be used to track the sensitivity of the layout to residual effects as different treatments are applied to it. For the pattern matching to be most effective, the locations of the match factors should be taken on the design intent, not on the OPC features such as serifs, but the actual match factors should be computed on the post-OPC layout. This

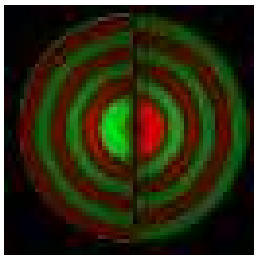

Figure 4.9: The coma maximum lateral test pattern.

is for both accuracy and decrease in runtime. The accuracy would be increased slightly by this because, assuming that the OPC is successful, then the image that will be printed in the resist will actually be the design intent, and it is these edges that are important and should be monitored with the pattern matcher. Also, the number of edges in a post OPC layout may be much larger than the number of edges on the design intent. One of the aspects that makes the pattern matcher so efficient is that not every pixel is tested for its match factor—only edges or corners and edges, as specified by the user, are selected as match locations. Thus, the pattern matcher could have a much slower runtime on post OPC layouts if locations are chosen from the post OPC layout. Further aspects of runtime speedup for the match factor are detailed by Gennari (2004).

However, as an approximation to this algorithm, for the simulations in this section the post OPC layout has been used to specify the match locations. This should only affect the accuracy a small amount, and small layouts were used so that runtime was acceptable.

Two OPC treatments were run on an adder circuit in an attenuated phase shift layout from a short loop electrical test of gates. The OPC treatments differed in the number of fragmentation, ripples, size of edges and number of iterations used, and no SRAFs were used in either of the treatments. A layout feature is shown in Figure 4.10 after being treated with each of the OPC algorithms.

The pattern matcher was run on these two post OPC layouts, as well as the design intent, matching against the coma pattern from Figure 4.9. The layout match locations were simulated with SPLAT and the intensity change with 0.02λ RMS is plotted in Figure 4.11. What is found here is that in most cases, the difference in match factor is either zero or very minimal. The reason for this is that the two OPC treatments only change the edges by very small amounts, so the sensitivity to aberrations should not change significantly. What we can conclude from this test is that varying the parameters of similar OPC algorithms is unlikely to alter the layouts sensitivity to aberrations. However, this is not always going to be the case for every OPC algorithm, and OPC does not address the change in a layout over the process window. If OPC were to attempt to track changes in sensitivity to the process window, then many lengthy aerial image simulations would be required. Instead, the pattern matcher could be used for this purpose by quickly screening changes made by OPC algorithms for sensitivity to residual effects.

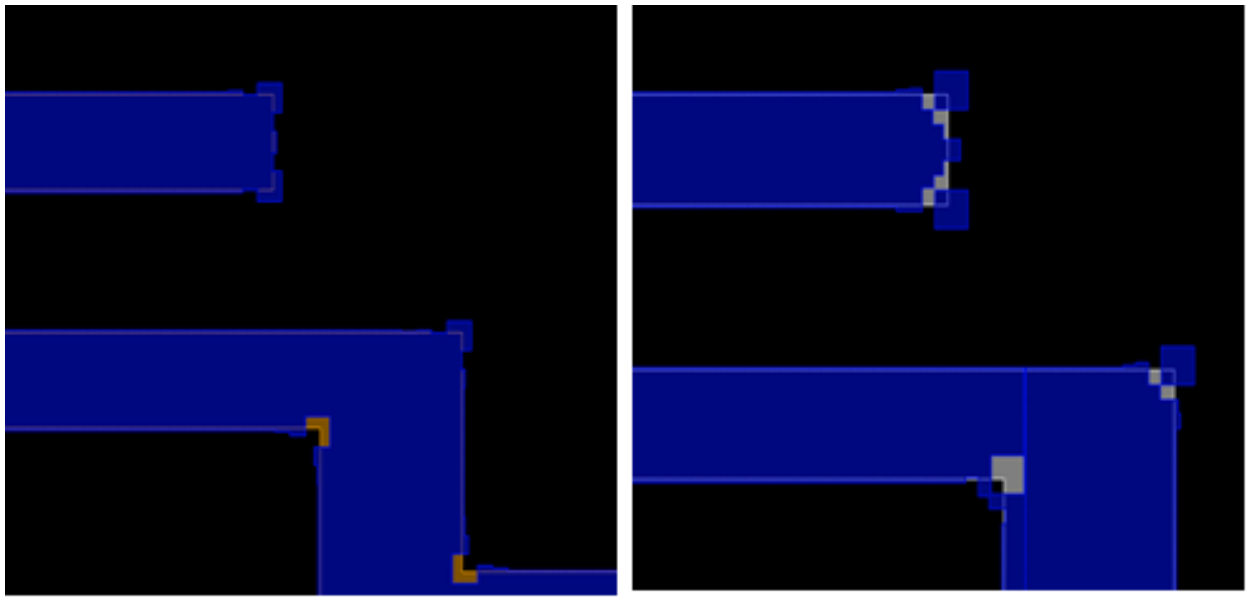

Figure 4.10: Layout features under the two OPC treatments—'mild' OPC with smaller and fewer edges and ripples, and 'aggressive' OPC with more edges, larger edges and more iterations.

4.4.1 Application of the Pattern Matcher to Pre-OPC Layouts

The pattern matcher is much faster than simulation and OPC, so if it can be applied to pre-OPC layouts then this may reduce the number of times a layout must go through OPC by finding and correcting sensitivities to aberrations prior to this phase. To test the validity of applying the pattern matcher to a pre-OPC layout, the pattern matcher was run with coma on a set of coordinates for a pre-OPC layout, and was then run on a post-OPC layout at the same coordinates. The pre-OPC versus the post-OPC matches are plotted in Figure 4.12. The line of best fit goes almost through $y = x$, which shows that on average the post-OPC matches correlate well with pre-OPC matches. The R^2 factor is 0.78, and the reason for this to be somewhat low is that in some cases OPC causes the match factor to go up or down, indicating that sensitivities to coma are being increased or decreased. Similar results to those shown in Figure 4.12 were found with the nominal illumination conditions, and with the focus pattern.

The pre and post OPC match factors are shown overlaid on the same graph in Figure 4.13. It can be seen that in some cases the match factor decreases with the application of OPC, and in some cases the match factor increases. This means that OPC does not always correct for aberration sensitivities. One particular case where the match factor has increased significantly is shown in Figure 4.13. The reason for the increase in match can be seen here with the amount of light overlapping with the green (0 degree) region of the coma pattern being increased and the amount of light overlapping with the red (180 degree) region of the coma pattern being decreased. This shows exactly how OPC can increase or decrease the match factor at a specific location, and shows that running the pattern matcher on both

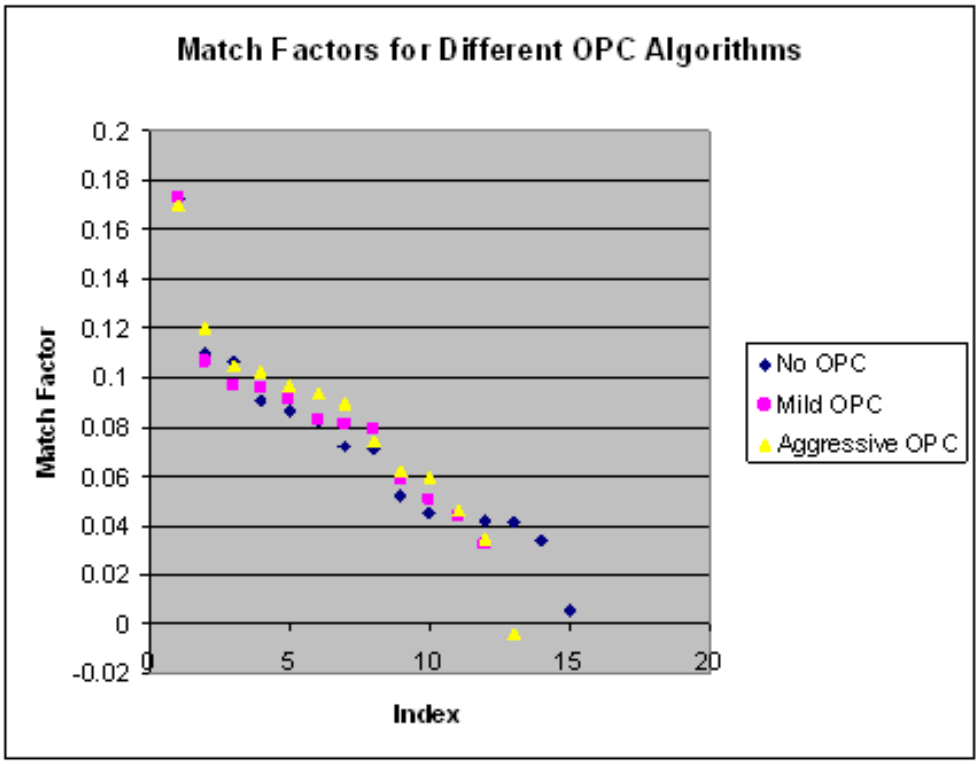

Figure 4.11: Match factors obtained for the design intent, and post OPC layouts with mild and aggressive OPC.

pre and post OPC layouts is useful as a first pass for finding sensitivities to aberrations.

Additionally, Sub Resolution Assist Features (SRAFs) appear to be playing a role in the match factors of the post-OPC layout. An SRAF is a thin feature that does not itself print, yet its presence assists in producing a better quality image on the wafer. The SRAFs are added as an OPC feature. These would also affect the sensitivity of the layout to focus, so it is relevant that they change the match factor of the layout. These are perhaps one of the larger factors in producing a different post-OPC match factor to that of the pre-OPC match factor, and this must be taken into consideration if it is known ahead of time that SRAFs will be used in the OPC recipe.

4.4.2 Proximity and Focus Effect Locations – A Consideration for OPC Treated Layouts

The pattern matcher was run with both a Z_3 and a Z_0 pattern on a 0.4λRMS feature attached perpendicularly to a larger feature, as shown in the pattern matcher output in Figure 4.14. The Z_0 pattern is used to find areas that are susceptible to necking, and the focus pattern is used to find locations which have a high variability under defocus. The results show that the highest matches are in distinct locations, with the Z_0 pattern matching 108nm (about one feature size) from the edge of the larger feature, but with the defocus

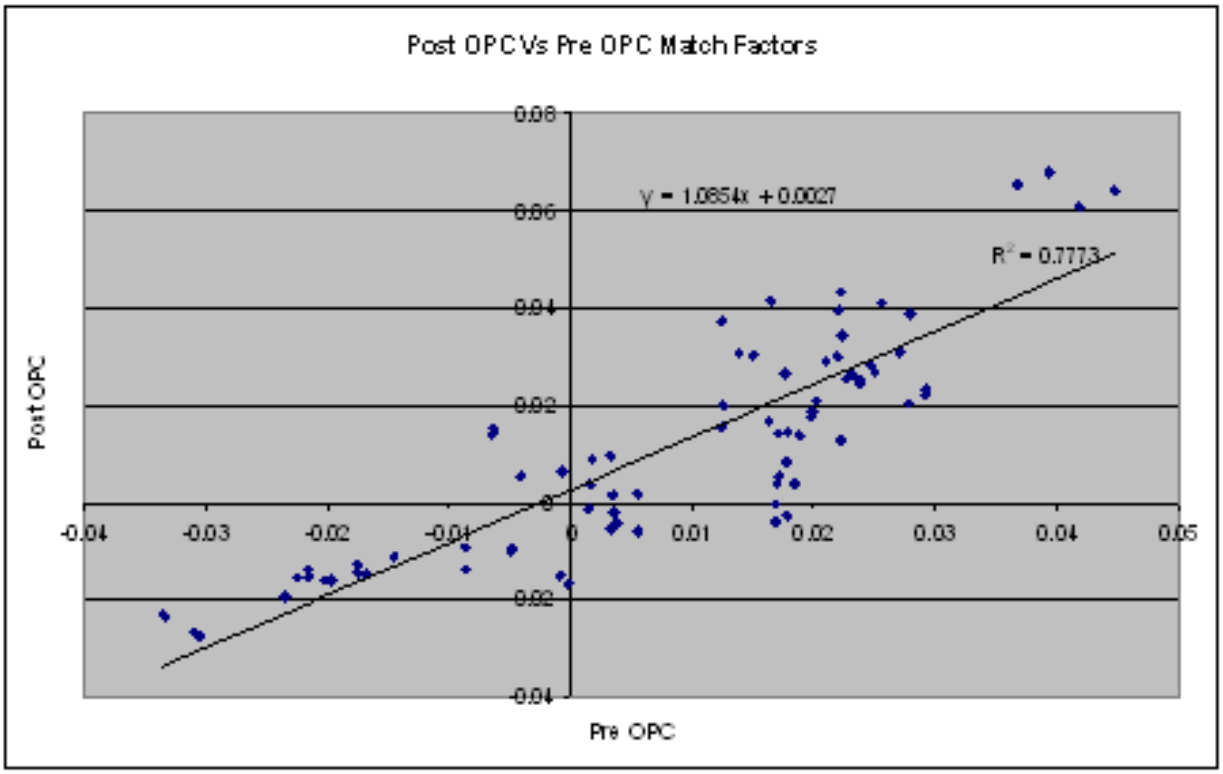

Figure 4.12: Post-OPC matches plotted against pre-OPC matches at the same coordinates with the coma pattern. Darkfield chrome with openings and 0.5-0.9 Annular illumination with NA=1.2 simulation conditions are used.

pattern matching almost at the corner of the feature. This shows that the area that is most sensitive to necking and the area that is most sensitive to defocus are distinct locations, and if OPC is run to correct for one of these conditions, then the other condition will not necessarily also be corrected.

The pattern matcher results are backed up with an aerial image simulation shown in Figure 4.15. Necking can be seen at the match location for Z_0 and an increased gap between the focus contours can be seen at the match location for defocus.

4.5 Summary and Discussion

Mask issues that affect pattern matching and the patterns that it uses have been addressed in this chapter. OPC is a mask issue that is important to pattern matching, because pattern matching is generally run on pre-OPC layouts and it is important to know whether this produces relevant match factors. The morphing of Maximum Lateral Test Patterns to a more mask friendly version is an important topic, because in their original form they are too expensive for tool makers to construct, and with the help of an automatic flow and the pattern matcher, such mask friendly version can be found. Alternating phase shift masks

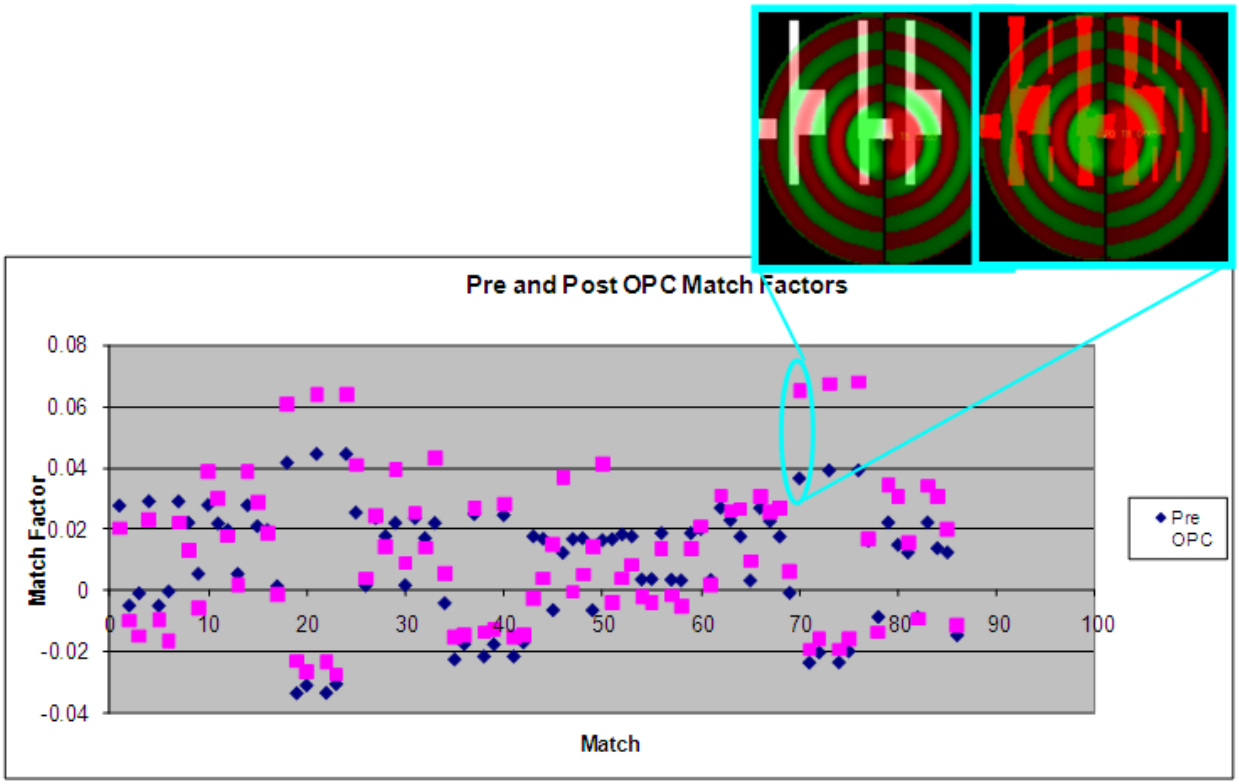

Figure 4.13: Pre and Post OPC match factors for specific locations on a layout with the coma pattern. Darkfield chrome with openings and 0.5-0.9 Annular illumination with NA=1.2 simulation conditions are used.

are also important for pattern matching to be effective with, because many masks in the current technology nodes utilize such a style.

A need for mask friendly aberration monitors has been addressed. The original patterns, while highly sensitive to the aberrations that they were designed for, were not mask manufacturing friendly and there was no automatic way to have the patterns modified. A method for automatic generation of modified patterns is presented, which has been tested with a DRC rule deck. The automatic process successfully moved vertices to allow the pattern to pass DRC, by moving only a minimal set of vertices a minimal amount. This resulted in patterns that were not significantly different to the original pattern, but passed the given DRC checks. A hand made modified pattern, with more significant modifications, was also investigated. The handmade pattern retained 68% of its sensitivity to defocus, and remained orthogonal to the spherical aberration. This shows a trade off between sensitivity and mask making friendliness. In this case, the pattern is much more mask friendly, as it consists of only seventeen larger rectangles, as opposed to a detailed pattern with many hundreds of vertices. The pattern matcher was shown to be useful in the process of the design and verification of sensitive patterns which are mask friendly. In future work, as more varieties of patterns are investigated, it is possible that more circuit-like patterns can be found which will allow automatic SEM readings of the photoresist images. These patterns many also

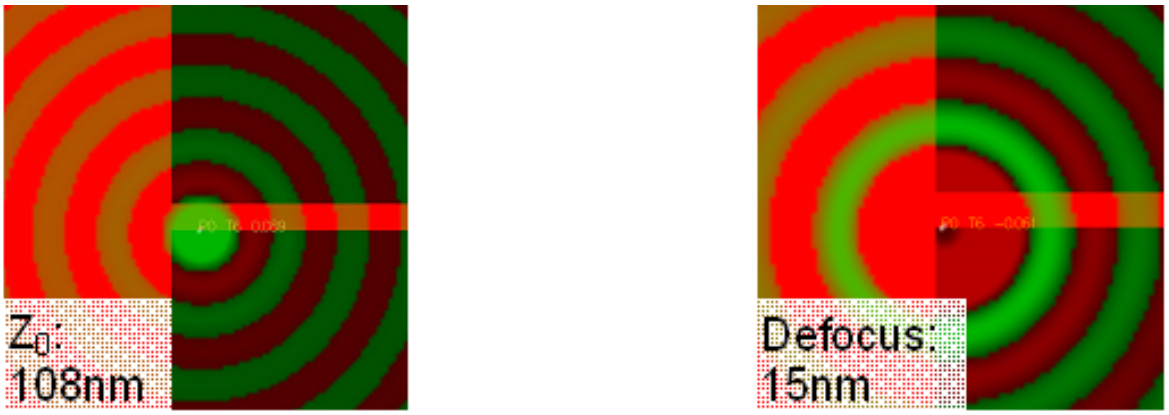

Figure 4.14: Match locations for the Z_0 function and the Defocus function on a 0.45λRMS sized feature. Case B simulation conditions are used.

make good candidates for structures for model calibration.

The pattern matcher was shown to be effective for use in predicting aberration hot spots for phase shift masks, by utilizing a created layer at 180° with a weighting of 0.25. With these input parameters, the pattern matcher required no further modification for use with phase shift masks.

The pattern matcher was tested on both pre-OPC and post-OPC layouts. Different OPC algorithms were compared for sensitivity to coma using the pattern matcher, and in this case were found to not differ significantly for most data points. It was found that SRAFs in particular played a large factor in producing a change in post-OPC match factors. Pre-OPC and post-OPC match factors were compared for a layout, and while the overall trend showed that the match factors were roughly equivalent with $R^2 = 0.78$, the match factors were pre- and post-OPC match factors varied more significantly were investigated. The pattern matcher thus appears to provide useful guidance to the designer prior to a standard OPC treatment.

Pattern matching has shown that proximity effects and focus effects are distinct, motivating the need for pattern matching, due to the fact that an OPC that corrects for one may not correct for the other. Pattern matching can thus be used to check for areas of a layout that are sensitive to focus if OPC is performed under ideal focus conditions. Additionally, the use of the pattern matcher of pre-OPC layouts was validated as a method for predicting post-OPC sensitivities, and specific cases were shown where OPC had caused a sensitivity from a pre-OPC layout to become higher.

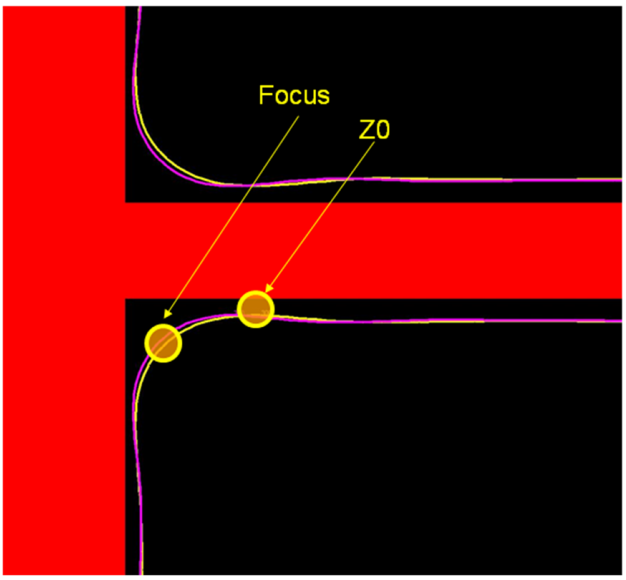

Figure 4.15: Aerial image simulation with contours for 0 defocus and 0.04λRMS (0.94 Strehl Ratio). Case B simulation conditions are used.

Chapter 5

Extensions for Advanced Image Issues in Lithography

5.1 Introduction

Polarization has quickly become an important issue in optical lithography for semiconductor manufacturing (Adam and Maurer, 2004; Smith and Cashmore, 2002). The rapid adoption of NA above 0.75 and immersion lithography and hypernumerical aperture (NA) projection printing systems requires the vector nature of light to not be neglected. Much attention has been paid to developing and understanding lithography tools with polarization control (Nishinaga et al., 2004; Rubingh et al., 2005). This chapter focuses on the use of pattern matching for high-NA and polarization vulnerabilities, both in the case for on-axis illumination and off-axis illumination. This work on polarization of high-NA was a team effort with G. McIntyre (McIntyre et al., 2005; Holwill et al., 2006). McIntyre worked on the theoretical aspects of designing the required patterns, and the author worked on the technical issues required for pattern matching and simulation.

5.2 Theoretical Background

For high-NA vector effects, the set of five Maximum Lateral Test Patterns (MLTPs), as derived in more detail in the Background Section 2.3, are theoretically the most sensitive patterns and can be used for scanning a layout for sensitivities. Pattern matching can be used to quickly find areas in an integrated circuit layout that are geometrically similar to these MLTPs. A high match factor suggests that the location in the layout will be vulnerable to high-NA vector effects. Weighed combinations of three (on-axis case) to five (off-axis case) match factors are used to determine vulnerability scores for one of two related applications. Either locations are scored identifying the amount of discrepancy between using scalar and vector imaging models (Vulnerability to high-NA) or they are scored according to how severely they are impacted by perturbations to the designed illumination polarization state (Vulnerability to polarization). This can serve as an efficient means to communicate in

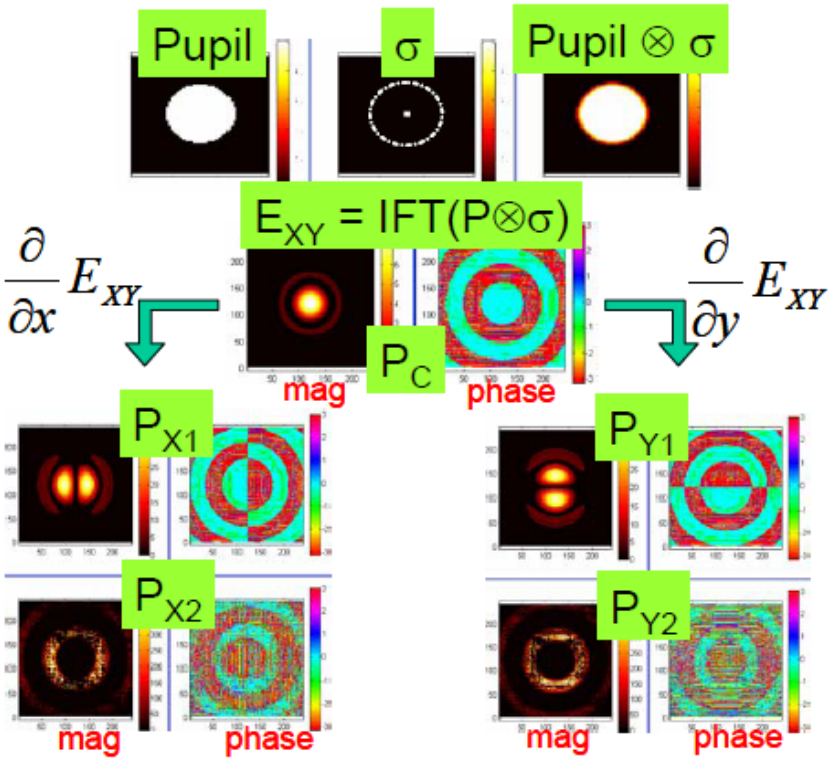

Figure 5.1: Visual representation of equations 3-5 for coherent illumination, resulting in four complex components of high-NA, z-component proximity effect. P_X2 and P_Y2 are assumed numerical noise for explained reasons.

advance to designers the potential impacts of effects that are difficult to describe, even with the use of advanced design rules.

5.3 High-NA and Polarization Pattern Matching Examples for On-Axis Illumination

This section describes two simulated examples showing the validity of vulnerability predictions for high-NA (V_NA) and also perturbation to illumination polarization state (V_Pol). These examples use on-axis coherent illumination and alternating phase shift masks. However, Section 5.4 shows that this technique is extendible to off-axis illumination schemes.

For the on-axis case, the five MLTPs used for high-NA and polarization patterns are derived using the flow shown in Figure 2.5, reproduced here for convenience in Figure 5.1. The five patterns, P_{X1}, P_{X2}, P_{Y1}, P_{Y2}, and P_C can be visualized here. For the on-axis case, P_{X2} and P_{Y2} are considered numerical noise and are not needed, so only three patterns are needed for the on-axis case.

To illustrate the vulnerability to high-NA technique, Figure 5.2 shows a set of alternating PSM and binary layout clips that were fabricated to show a large range of match factors.

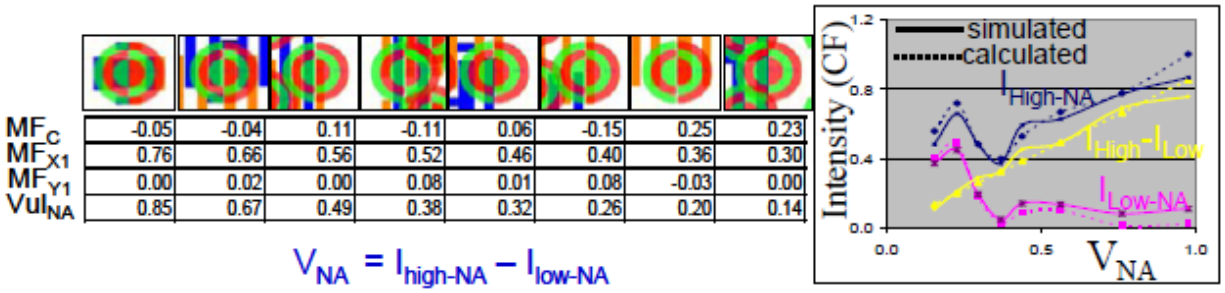

Figure 5.2: Simulated examples confirming vulnerability predictions to high-NA. Vulnerability scores are good indicators of intensity change at match location.

These match factors are plugged into Equation (5.1), derived by McIntyre et al. (2005) to give the intensity with high NA ($I_{P,High-NA}$), the intensity at low NA ($I_{P,High-NA}$), and the vulnerability to NA (V_{NA}). Equation (5.1) is explained in more detail in Section 2.3.

$$\begin{aligned} V_{NA} &= I_{P,High-NA} - I_{P,Low-NA} \\ &= [\{E_{0X} \cdot MF_{X1} \cdot E_{X1,max}\hat{z} - MF_{X2} \cdot E_{X2,max}\} \\ &= +\{E_{0Y}\,(iMF_{Y1,max}\hat{z} - MF_{Y2} \cdot E_{Y2,max}\hat{y})\}] \end{aligned} \tag{5.1}$$

The match factor results and calculated V_{NA} scores for each layout clip are listed in Figure 5.2. The corresponding plot shows good correlation between the calculated and simulated values of $I_{High-NA}$ and I_{Low-NA}. Additionally, the V_{NA} score is linearly proportional to intensity change with a slope of about 80% of the clear field per V_{NA}, and the average intensity change due to this effect is around 40% of the clear field. Thus, this technique proves an efficient method to determine, for example, areas that will be the most misrepresented by a scalar imaging model. Additionally, areas can be found that are likely to have the greatest difficulty in scaling to use in a higher numerical aperture tool.

The second example, illustrated in Figure 5.3, uses a slightly different set of fabricated layout clips to show prediction of a layouts vulnerability to perturbation in the illumination polarization state. The same five MLTPs required for pattern matching for high-NA effects are used for pattern matching for polarization effects. In this case, the vulnerability to polarization is found by $V_{Pol} = \frac{\partial I_P}{\partial E_{0X}}$, where these identities are explained in further in Section 2.3.

The corresponding plot shows a potential practical use for this technique. Here, it is assumed that these layout clips were intended to be used with 100% y-polarized light. However, the illumination design is not perfect resulting in, for this example, 10% unwanted xpolarized light. A nearly-linear correlation exists (with a slope of about 77% ICF/V_{pol}) between the V_{Pol} scores and the actual (simulated) change in intensity at those locations for this perturbation to the illumination polarization. This indicates that this technique is a good means to quickly screen layouts for areas that are susceptible to this potential process variation. Simulation, on the other hand, would require simulating the entire layout twice (once for each polarization condition) and comparing the results. This would be a much

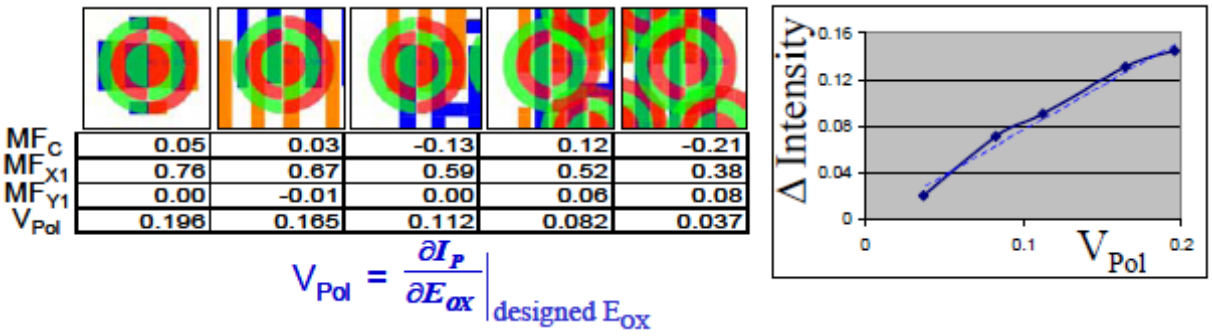

Figure 5.3: Simulated examples confirming vulnerability predictions to polarization. Vulnerability scores are good indicators of intensity change at match location.

more time consuming process. Also note that if a 10% variation is reasonable for control of the illumination polarization state, then image intensity for some layouts can change up to about 10% of the clear field. For both of these examples, prediction is accurate with simulation by better than 90%.

5.4 High-NA and Polarization Pattern Matching Examples for Off-Axis Illumination

The examples so far in this chapter have focused on coherent illumination, where the patterns are derived for a single illumination frequency. However, pattern matching for other illumination schemes are feasible, as outlined in Section 2.3. For example, dipole illumination can be represented by two sets of patterns from opposing source locations. Generally, this technique is suited for illumination schemes accurately represented by a few single illumination frequencies. This section will show examples for pattern matching for High-NA and Polarization for a single off-axis monopole.

The MLTPs for off-axis patterns are derived in a similar way to the on-axis patterns, but now instead of taking the inverse Fourier transform of an aberrated pupil function, the pupil function is first convolved with an off-axis illumination ray. The effect of this convolution is to incorporate a linear phase progression into the patterns which corresponds to the off-axis illumination frequency of interest. The resulting patterns are thus the maximal lateral test patterns for a particular aberration for the given off-axis illumination frequency.

The five polarization and high-NA patterns, for the off-axis case, are derived as in Figure 2.6, repeated here as Figure 5.4 for convenience. The inverse Fourier transform of an unaberrated pupil function convolved with an off-axis illumination ray results in the point spread function multiplied by a linear phase progression. The spatial derivatives of this pattern in both the x- and y-directions result in multiple polarization-dependent proximity effect functions. For example, in Figure 5.4, the pattern labeled P_{Y1} represents the proximity effect of off-axis y-polarized light that is coupled into the normal component due to high-NA effects. As discussed by McIntyre et al. (2005), the normal component is proportional to the

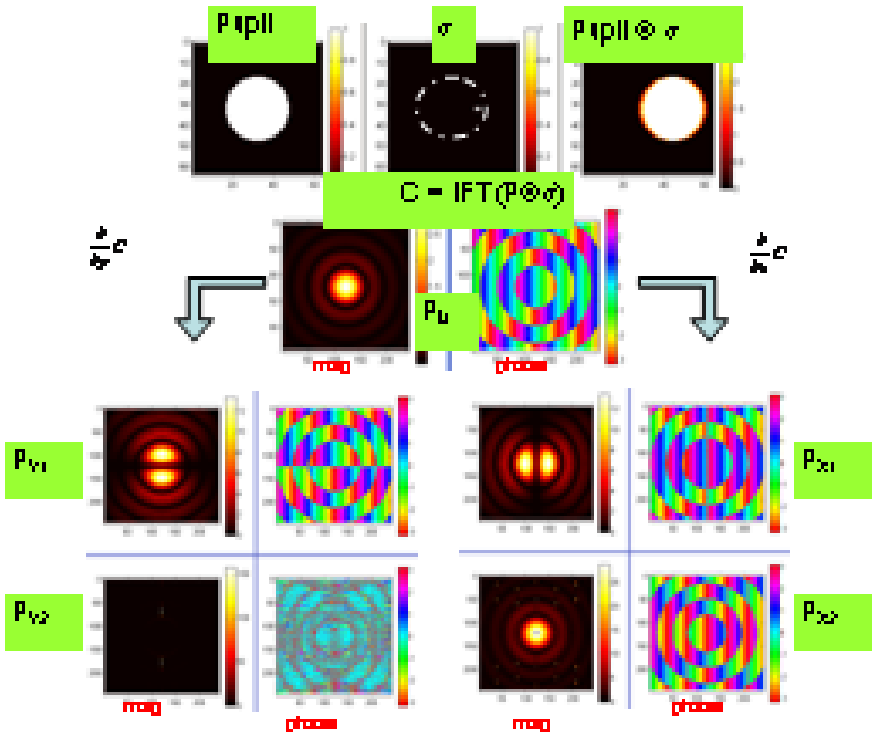

Figure 5.4: Pattern generation process for off-axis polarization and high-NA patterns. The inverse Fourier transform of an unaberrated pupil convolved with an off-axis illumination ray is taken, and then the derivative with respect to x and y are taken. There are two patterns resulting from the derivative because P_U is complex, so the complex chain rule is applied to give two patterns.

spatial derivative of the fields oriented in the wafer plane. The x-polarization component is slightly more complicated, where the derivative with respect to x of this complex function results in two orthogonal patterns (a direct application of the chain rule).

The MLTPs for off-axis illumination no longer have constant valued step function phases, but instead have a linear phase progression corresponding to the illumination spatial frequency used. When binary or phase shift mask layouts are matched against these patterns, the maximum attainable match factor is significantly reduced because the phase of the pattern differs from the phase of the layout in many of the locations, due to the phase ripple in the pattern. This is because the phase is continuous for the patters being used.

As with the on axis case for polarization and high-NA outlined in Section 5.3, the match factor of one pattern alone is not sufficient for predicting the sensitivity of a layout to polarization and high-NA under off-axis illumination. Instead, multiple patterns must be matched at each match location, and a vulnerability score must be calculated. The difference between the off-axis case and the on-axis case is that complex match factors are now returned by the pattern matcher. However the vulnerability score will always be real because of the multiplication of the complex match factors by their conjugate, similar to the manner in which intensity is determined from complex electric fields. The process for

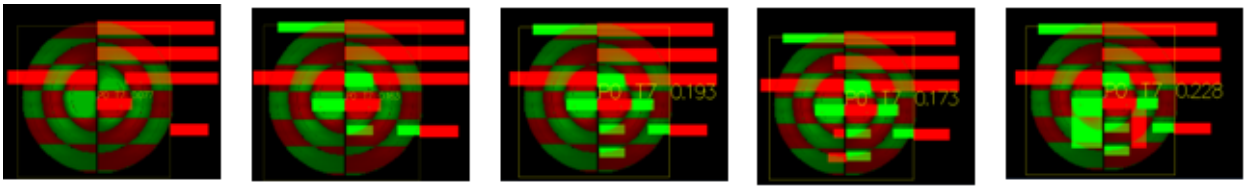

Figure 5.5: The handmade patters used for matching in the off-axis polarization and high-NA simulations.

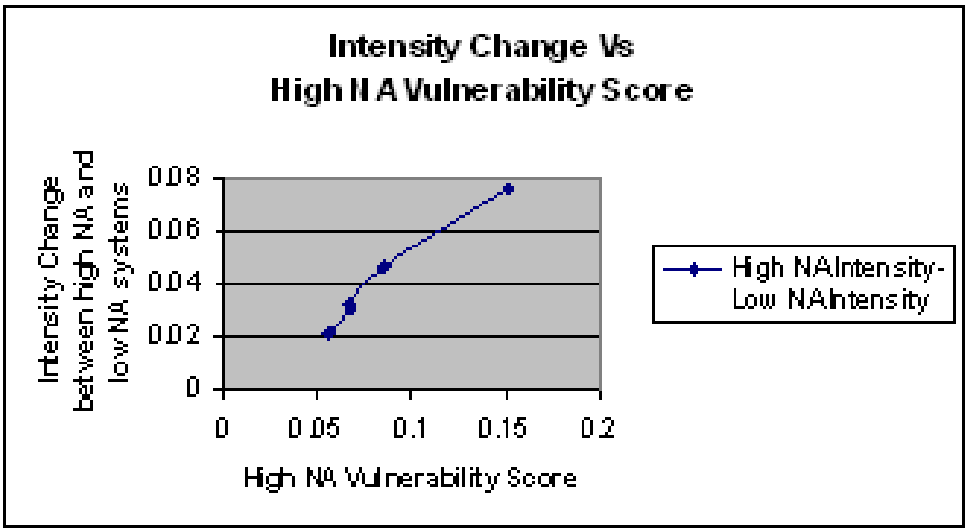

Figure 5.6: High-NA simulation results for the layouts in Figure 5.5.

generation of the off-axis high-NA and polarization patterns and the vulnerability score calculations is shown by McIntyre et al. (2005).

The vulnerability of layouts under off-axis illumination to polarization and high-NA effects was tested for accuracy in this paper. Five layouts were handmade to give a variety of match factors for the off-axis polarization and high-NA patterns. These layouts are shown, overlaid with one of the off-axis patterns, in Figure 5.5.

The vulnerability to high-NA of each of these layouts was calculated using the pattern matcher, and the layouts were simulated with Mentor Calibre Work Bench (Mentor Graphics, 2010) under both high-NA and low-NA illumination. The resulting intensity change under the differing illumination is plotted against the vulnerability score in Figure 5.6. The plot shows a linear trend, suggesting that the vulnerability score is predictive of layout sensitivity to high-NA effects.

The vulnerability of the layouts to polarization was also calculated with the pattern matcher, and the layouts were simulated with polarized and unpolarized light. The resulting intensity change under the differing illumination is plotted against the polarization vulnerability score in Figure 5.7. Again, the plot shows a linear trend, suggesting that that polarization vulnerability score is predictive of layout sensitivity to polarization effects.

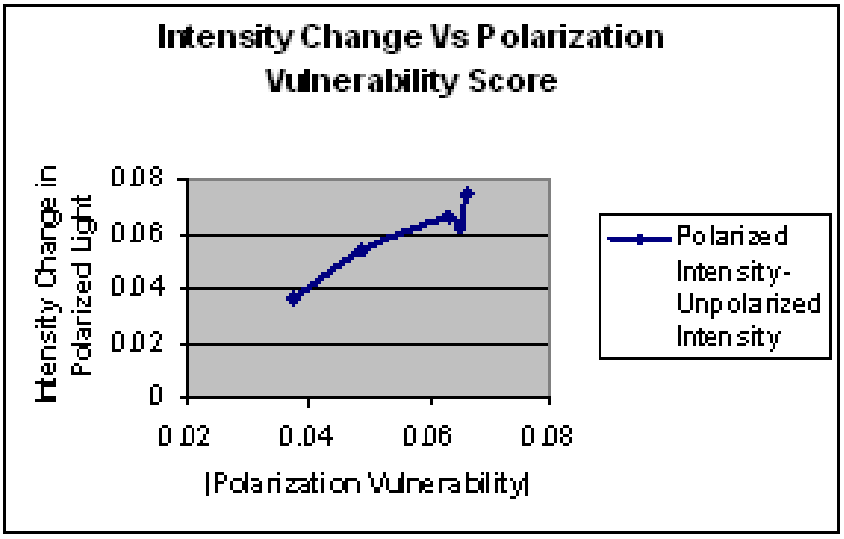

Figure 5.7: Polarization Simulation results for the layouts in Figure 5.5.

It can be noted that this technique can be somewhat similar to a simulator using the sum of coherent systems (SOCS) approximation (Cobb et al., 1996). SOCS essentially decomposes an optical system into an orthogonal, and thus incoherent, set of appropriately weighted eigenfunctions. This technique is similar in nature, however the aim is to use the minimum number of functions (MLTPs) to extract vulnerability to a particular effect. In practice, these two techniques would complement each other, for each might have a use at different stages in the design cycle. For example the pattern matching approach might be an efficient means to communicate to designers in advance the potential impacts of effects that are difficult to describe, even when using advanced design rules.

5.5 Discussion

A technique to quickly screen integrated circuit design layouts for regions most vulnerable to high-NA and polarization vector effects has been presented. These effects are important, even in simple layouts, and can cause intensity changes of about 40% or 10%, respectively, for the on-axis case and about 8% for the off-axis case. A set of maximum lateral test patterns (MLTPs) which are theoretically the most sensitive patterns to high-NA and polarization effects are used. Three patterns are required for the on-axis case, and five for the off-axis case. Pattern matching is then used with these patterns to find areas in the layout that are geometrically similar to the MLTPs. A quantitative vulnerability score is determined by a weighted combination of the three to five resulting match factors. The vulnerability scores have been shown to be linearly proportional to intensity change. Examples have been shown for both on-axis coherent illumination and also off-axis illumination. In each of these examples, vulnerability score was shown to be a good indicator for the expected change in intensity to either high-NA or polarization effects.

Chapter 6

Accuracy of the Pattern Matcher

6.1 Introduction

The pattern matcher is a very fast tool, much faster than simulation, used to give an estimate for the sensitivity of a particular layout location to a given effect, such as defocus or coma. While the pattern matcher isn't intended to compete with simulation in terms of accuracy of its prediction, it is important to know just how accurate it is, and to improve the accuracy where possible, in order to make the trade-off between speed and accuracy worthwhile.

In this chapter, the accuracy of the coma pattern is examined, and its accuracy for coma with edge placement rather than change in intensity is improved. Next, the accuracy for the pattern matcher through focus is examined, and improved with the use of a quadratic model. Several other technical issues, along with the new model, are used to give a large improvement in accuracy.

6.2 Accuracy of the Coma Pattern

The match factor for coma has been shown to be predictive of the change in intensity and thus electric field (Gennari, 2004). This section aims to extend the use of the pattern matcher for not only predicting a change in intensity, but also the edge movement that it produces.

The pattern matcher was run on a small logic layout using the coma Maximum Lateral Test Pattern (MLTP), and a range of match factors were returned. The resulting layout snippets corresponding to the match factors were then simulated rigorously in SPLAT and cross sections of their aerial images were returned. Edges were estimated at 0.4 of the clear field, and simulations were taken both with no coma present and with 0.04λRMS coma, which is a Strehl ratio of 0.94. The simulation parameters were: a darkfield chrome mask with openings, $\sigma = 0.3, NA = 0.85$. The edge movement between simulations with and without coma is shown in Figure 6.1. A clear linear trend between match factor and the amount of edge movement can be seen, with R^2=0.73. While this is high enough for the

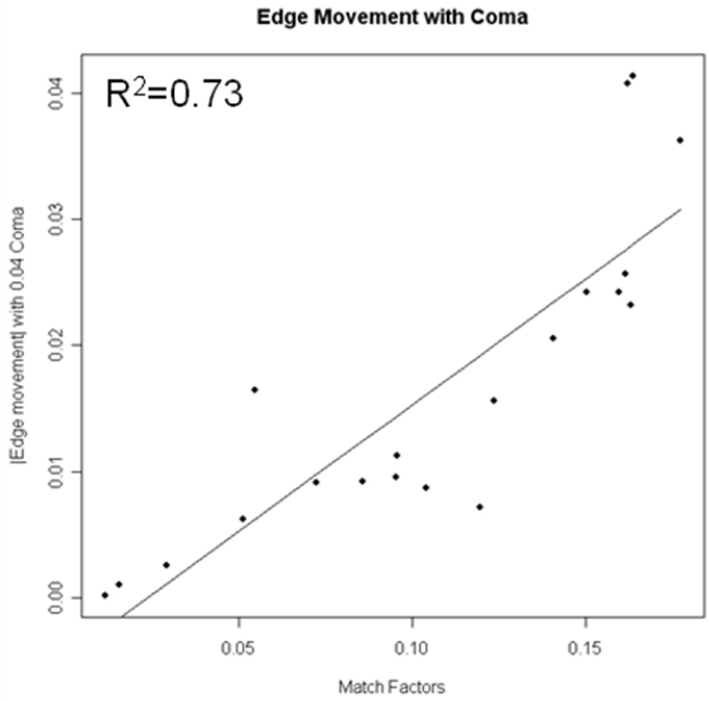

Figure 6.1: Amount of edge movement with coma versus match factor. The image slope is not taken into consideration..

match factors to be somewhat predictive of edge movement, the accuracy can be increased by taking the image slope into account.

According to the Equation (6.1) it is known that edge movement depends not only on the intensity change but also image slope. Since the amount of light that spills into the centre of the MLTPs depends on the amount of aberration present, it would be expected that the intensity change can be predicted with the pattern matcher. However, by calculating not only the match factor but also the image slope at the match location, a much tighter correlation can be gained, with a higher confidence in predicting edge movement. This is shown in Figure 6.2, where edge movement is plotted against Match Factors/Slope. In this case, the pattern matcher is used much more effectively in predicting the edge movement, and R^2=0.95 for the linear model through the data. Note that full simulation is required only across cutlines of the points of interest returned by the match factor, and this simulation is required only with the no-coma condition. Full simulation across chip both with and without coma is avoided, and the total running time is still extremely fast.

$$\Delta Length \quad = \quad \frac{\Delta Intensity}{Slope} \tag{6.1}$$

It can be seen in Figure 6.2 that an outlier exists in the top right quadrant, as indicated by the arrow and the snippet. The snippet here shows that match location on the layout and

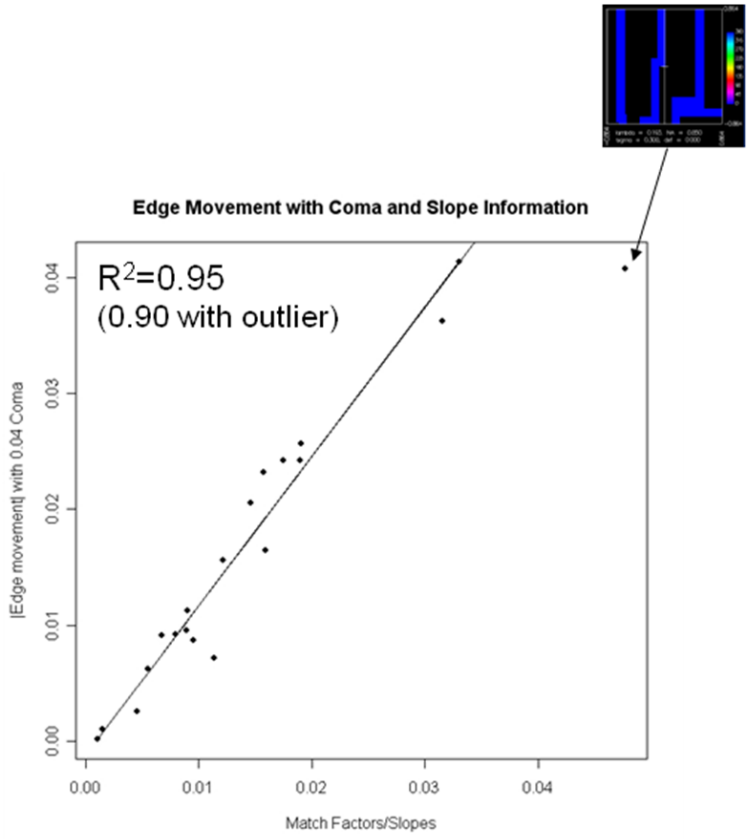

Figure 6.2: Amount of edge movement with coma versus Mach Factors divided by Slopes.

the surrounding layout to that match location. The cutline can be seen in the center of the snippet running vertically. The cause of this outlier is likely the fact that the match location is on a corner, and the cutline runs along the edge of the feature and not perpendicular to the expected simulation contours, invalidating the image slope calculation. This is an artifact of the software used to produce the snippet and the fact that the image slope is not a good predictor when the cutline is taken in this way. For future accuracy, a different model for placing the cutlines or using the image log slope along feature-edge cutlines would need to be used if the corner match factors are to be analyzed with the pattern matcher.

6.3 Accuracy of the Focus Pattern

Finding an accurate model for the focus pattern has proven more difficult than the coma pattern. The pattern and probe monitors for defocus, as described in Section 2.1.1, have a central 90 degree probe to catch imaginary spillover light. Actual layouts do not have the 90 degree phase shift regions for interferometric detection. A benefit is that defocus only creates a quadratic variation through focus, nonetheless focus sensitivity of layouts remains as can be seen when the center is restored by a 180 degree region. In Figure 6.3, the 90

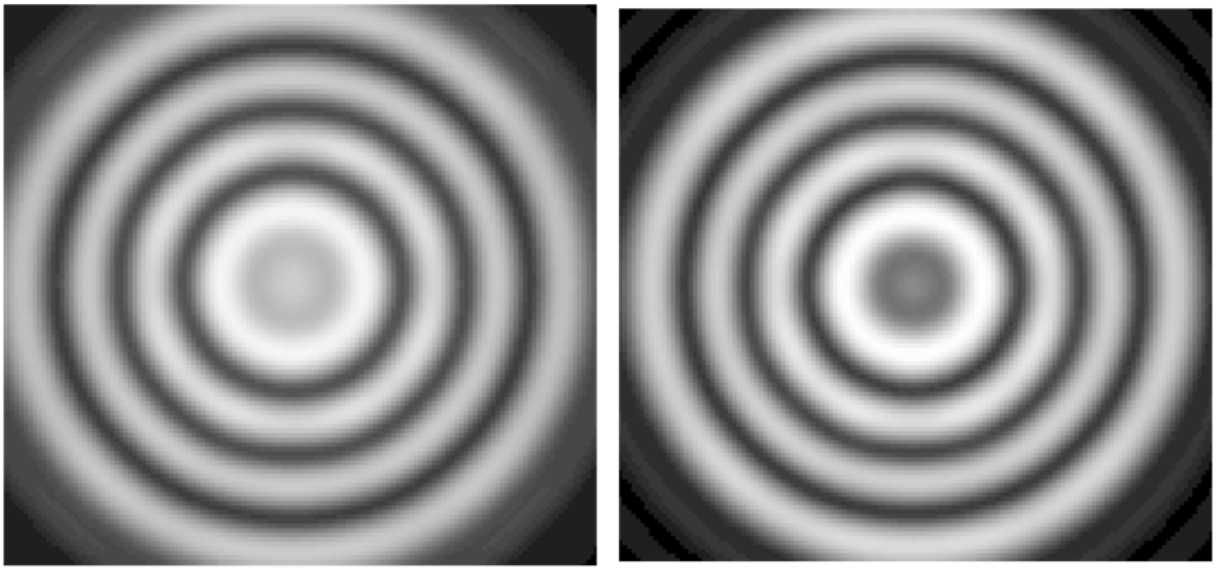

Figure 6.3: Aerial image simulations of focus patterns containing a 180 degree center probe. An increase in spillover light into the center of the focus pattern is seen in the simulation containing defocus, as opposed to the simulation containing no defocus. The simulation parameters were: a darkfield chrome with openings, $\sigma = 0.3$ and $NA = 0.85$.

degree probes from the original focus patterns have been replaced with 180 degree probes and then simulated both with no defocus and with 0.04λ RMS defocus (Strehl ratio 0.94). The amount of light spillover into the central probe is much higher for the simulation under defocus, which indicates that there is still definitely a sensitivity to focus with this pattern, and thus it should be able to be used in some way to predict defocus sensitivity.

When a similar experiment to that which was run with coma in Section 6.2 is run with defocus to try to correlate match factor with change in intensity, a very loose plot is seen with no obvious correlation between change in intensity and match factor, as shown in Figure 6.4. The same type of illumination that was used for the coma test was used (a darkfield chrome mask with openings, $\sigma = 0.3, NA = 0.85$). One reason for the lack of correlation may be that without the 90 degree probe, the expected relationship between match factor and change in intensity is no longer linear, making calibration of the model more difficult. Another reason for the model to differ is that focus is not a small aberration, and so when the electric field is approximated using a Taylor series expansion as in Equation (6.2), it may not be sufficient to include only the constant and the $jOPD$ term. For the design of the original monitors, only these low order terms were used, and thus the patterns consist of the Fourier transform of the Optical Path Difference (OPD).

As will be shown in Section 6.3.1, in order to improve the model for the focus pattern, it becomes necessary to also include the OPD^2 term. Here OPD is Z_3 and when OPD is squared is expanded consists of the Zernike Z_0 and Z_8 terms as shown in Equation (6.3). It will be shown that these can be incorporated into the pattern matching process by matching

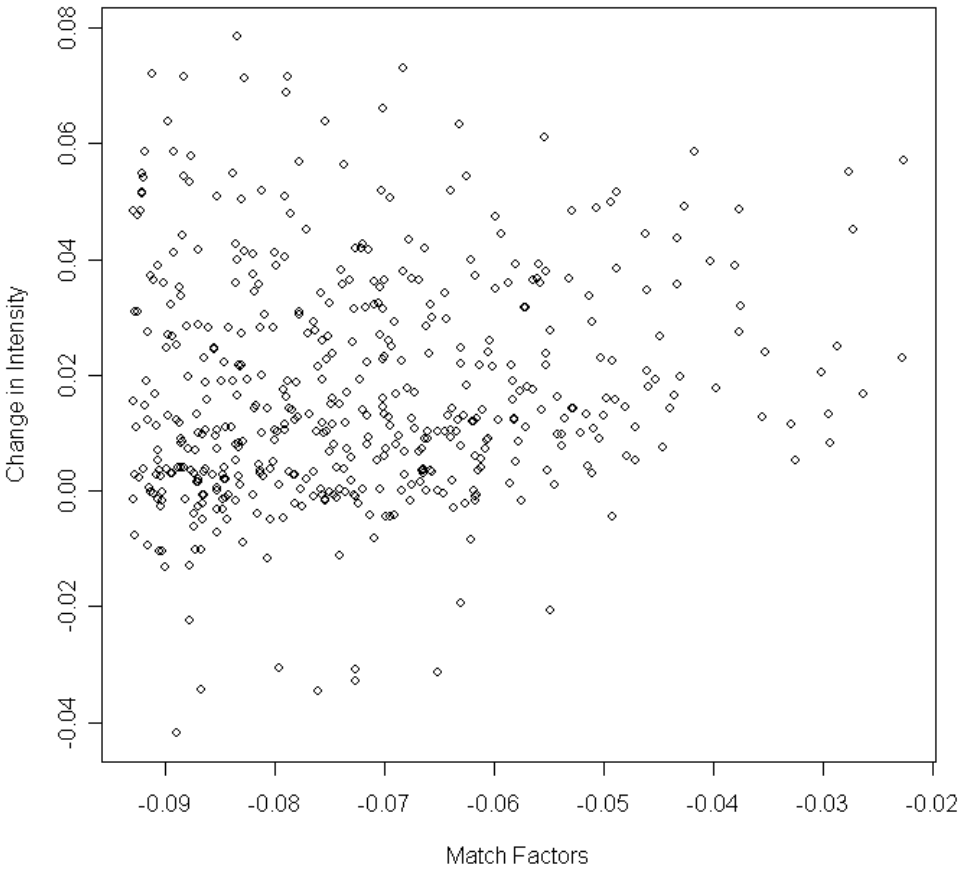

Figure 6.4: Intensity change versus the Z_3 match factor for the defocus pattern. No clear correlation is seen using this model. 0.06λRMS defocus is used.

each location with not only the Z_3 defocus term, but also with a weighted matching of the Z_0 and Z_8 terms.

$$\begin{aligned} E(x_{ow}) &\approx \int_{pupil} \left[1 - jOPD - \frac{OPD^2}{2} + ...\right] e^{\overline{k}\cdot\overline{x}_{ow}} r d\phi dr \qquad (6.2) \\ OPD &= 2\rho^2 - 1 \\ &= Z_3 \\ OPD^2 &= \left(2\rho^2 - 1\right)^2 \\ &= \frac{1}{3}(Z_0) + \frac{2}{3}(Z_8) \qquad (6.3) \end{aligned}$$

Note that $jOPD$ and $\frac{OPD^2}{2}$ together make the change in electric field due to defocus a complex quantity, and this will need to be accounted for in computing the Intensity, $I = EE^\star$. We also know that $\frac{OPD^2}{2}$ is a significant term for defocus modeling, because for 1 Rayleigh Unit defocus, $OPD = \frac{\pi}{2}$ and therefore the ratio of $\frac{OPD^2/2}{OPD} = \frac{OPD}{2} = \frac{\pi}{4}$, so the

OPD^2 term is 0.78 as large as OPD.

6.3.1 Through-Focus Model Formal Derivation

This through-focus model is an extension of Robins' model (Robins et al., 2002). Robins' derivation starts by giving the electric point spread function. Here the image plane with coordinates are (x', y'), the source location coordinates are (x, y) and the pupil coordinates are (ρ, θ). The Optical Path Difference (OPD) is represented by $\Phi(\rho, \theta)$, and k is the constant $2\pi/\lambda$.

$$E_{image}(x', y', x, y) = \frac{1}{\pi} \iint_{pupil} E_{diff}(\rho, \theta) e^{\frac{jk}{f_3}[\rho cos(\theta)(x'-x)+\rho sin(\theta)(y'-y)]} e^{jk\Phi(\rho,\theta)} \rho d\rho d\theta$$

Approximating the exponential term for the OPD with the Taylor series expansion, the original model includes the constant term and the linear term.

$$\begin{aligned} E_{image}(x', y', x, y) &= \frac{1}{\pi} \left[\iint_{pupil} E_{diff}(\rho, \theta) e^{\frac{jk}{f_3}[\rho cos(\theta)(x'-x)+\rho sin(\theta)(y'-y)]} \rho d\rho d\theta \right] \\ &\quad + \frac{1}{\pi} \left[jk \iint_{pupil} E_{diff}(\rho, \theta) e^{\frac{jk}{f_3}[\rho cos(\theta)(x'-x)+\rho sin(\theta)(y'-y)]} \Phi(\rho, \theta) \rho d\rho d\theta \right] \end{aligned}$$

In our new extended through-focus model, a quadratic term is also included in the Taylor series expansion.

$$\begin{aligned} E_{image}(x', y', x, y) &= \frac{1}{\pi} \left[\iint_{pupil} E_{diff}(\rho, \theta) e^{\frac{jk}{f_3}[\rho cos(\theta)(x'-x)+\rho sin(\theta)(y'-y)]} \rho d\rho d\theta \right] \\ &\quad + \frac{1}{\pi} \left[jk \iint_{pupil} E_{diff}(\rho, \theta) e^{\frac{jk}{f_3}[\rho cos(\theta)(x'-x)+\rho sin(\theta)(y'-y)]} \Phi(\rho, \theta) \rho d\rho d\theta \right] \\ &\quad - \frac{1}{\pi} \left[\frac{k^2}{2} \iint_{pupil} E_{diff}(\rho, \theta) e^{\frac{jk}{f_3}[\rho cos(\theta)(x'-x)+\rho sin(\theta)(y'-y)]} \Phi^2(\rho, \theta) \rho d\rho d\theta \right] \end{aligned}$$

If we apply this electric field to the mask, where the observation point x,y is the point of interest, and sweep over the mask pixels surrounding the observation point, we obtain the following.

$$
\begin{aligned}
E_{image}(x',y') &= \sum_{x_i,y_i}\left[\frac{1}{\pi}\iint\limits_{pupil} E_{diff}(\rho,\theta)e^{\frac{jk}{f_3}[\rho cos(\theta)(x'-x_i)+\rho sin(\theta)(y'-y_i)]}\rho d\rho d\theta\right] \\
&\quad+\sum_{x_i,y_i}\left[\frac{1}{\pi}jk\iint\limits_{pupil} E_{diff}(\rho,\theta)e^{\frac{jk}{f_3}[\rho cos(\theta)(x'-x_i)+\rho sin(\theta)(y'-y_i)]}\Phi(\rho,\theta)\rho d\rho d\theta\right] \\
&\quad-\sum_{x_i,y_i}\left[\frac{k^2}{2\pi}\iint\limits_{pupil} E_{diff}(\rho,\theta)e^{\frac{jk}{f_3}[\rho cos(\theta)(x'-x_i)+\rho sin(\theta)(y'-y_i)]}\Phi^2(\rho,\theta)\rho d\rho d\theta\right]
\end{aligned}
$$

This sum can be interpreted as the sum over a function centered at (x', y'). It can be related to the point spread function for the electric field by introducing $\theta' = \theta + \pi$. This transformation has a physical interpretation of changing from a summation of multiple point spread functions surrounding pixels in the neighborhood of the observation point to the convolution of the rotated point spread function centered at the reference point. This transformation is applied below.

$$
\begin{aligned}
E_{image}(x',y') &= \sum_{x,y_i}\left[\frac{1}{\pi}\iint\limits_{pupil} E_{diff}(\rho,\theta)e^{\frac{jk}{f_3}[\rho cos(\theta')x'+\rho sin(\theta')y']}\rho d\rho d\theta\right] \\
&\quad+\sum_{x,y_i}\left[\frac{1}{\pi}jk\iint\limits_{pupil} E_{diff}(\rho,\theta)e^{\frac{jk}{f_3}[\rho cos(\theta')x'+\rho sin(\theta')y']}\Phi(\rho,\theta)\rho d\rho d\theta\right] \\
&\quad-\sum_{x_i,y_i}\left[\frac{k^2}{2\pi}\iint\limits_{pupil} E_{diff}(\rho,\theta)e^{\frac{jk}{f_3}[\rho cos(\theta')x'+\rho sin(\theta')y']}\Phi^2(\rho,\theta)\rho d\rho d\theta\right]
\end{aligned}
$$

In general one has to match with the rotated point spread electric field for each term. Since both of the OPD induced defocus patterns are rotationally symmetric, this rotation by π has no effect. We can take $E_{diff}(\rho,\theta) = 1$ and then the Fourier Transform of Φ is the Maximum Lateral Test Pattern (MLTP) for that aberration.

$$
\begin{aligned}
E_{image}(x',y') &= \sum_{x,y_i}\left[\frac{1}{\pi}\iint\limits_{pupil} e^{\frac{jk}{f_3}[\rho cos(\theta)x'+\rho sin(\theta)y']}\rho d\rho d\theta\right] \\
&\quad+\sum_{x,y_i}\left[\frac{1}{\pi}jk\cdot MLTP(Z_3)\right]-\sum_{x_i,y_i}\left[\frac{1}{\pi}\cdot\frac{k^2}{2}\cdot MLTP(Z_3^2)\right]
\end{aligned}
$$

This summation over the pixels is now just the pattern match factor (MF) for the MLTP.

$$
\begin{aligned}
E_{image}(x',y') &= \sum_{x,y_i}\left[\frac{1}{\pi}\iint\limits_{pupil} e^{\frac{jk}{f_3}[\rho cos(\theta)x'+\rho sin(\theta)y']}\rho d\rho d\theta\right] \\
&\quad +\frac{1}{\pi}jk\cdot MF(Z_3)-\frac{k^2}{2\pi}MF(Z_3^2)
\end{aligned}
$$

We can make a simplification to ${Z_3}^2$ by expanding its Zernike polynomial definition.

$$
\begin{aligned}
Z_3 &= \left(2\rho^2-1\right) \\
{Z_3}^2 &= \left(2\rho^2-1\right)^2 \\
&= 4\rho^4-4\rho^2+1 \\
&= \frac{2}{3}Z_8+\frac{1}{3}Z_0 \qquad (6.4)
\end{aligned}
$$

Now substituting this definition for ${Z_3}^2$ and taking the intensity, $I = EE^*$ we obtain a formula for the intensity at a point (x', y').

$$
\begin{aligned}
& I \\
= \;& EE^* \\
= \;& \frac{1}{\pi}\left[\sum_{x_i,y_i}\iint\limits_{pupil} e^{\frac{jk}{f_3}[\rho cos(\theta)x'+\rho sin(\theta)y']}\rho d\rho d\theta-\frac{k^2}{2}\left(\frac{2}{3}MF(Z_8)+\frac{1}{3}MF(Z_3)\right)+jk\cdot MF(Z_3)\right] \\
& \times\frac{1}{\pi}\left[\sum_{x_i,y_i}\iint\limits_{pupil} e^{\frac{jk}{f_3}[\rho cos(\theta)x'+\rho sin(\theta)y']}\rho d\rho d\theta\right. \\
& \qquad\qquad \left.-\frac{k^2}{2}\left(\frac{2}{3}MF(Z_8)+\frac{1}{3}MF(Z_3)\right)-jk\cdot MF(Z_3)\right] \\
= \;& \frac{1}{\pi^2}\left[\left(\sum_{x_i,y_i}\iint\limits_{pupil} e^{\frac{jk}{f_3}[\rho cos(\theta)x'+\rho sin(\theta)y']}\rho d\rho d\theta-\frac{k^2}{2}\left(\frac{2}{3}MF(Z_8)+\frac{1}{3}MF(Z_3)\right)\right)^2\right. \\
& \left.+\left(k\cdot MF(Z_3)\right)^2\right]
\end{aligned}
$$

We can use the approximation that for small values of x, $(1-x)^2 \approx 1-2x$. We now have the theory derivation which relates the intensity at a point to the Z_3, Z_0 and Z_8 terms.

$$
I \simeq \frac{1}{\pi^2}\left[\sum_{x_i,y_i}\iint\limits_{pupil} e^{\frac{jk}{f_3}[\rho cos(\theta)x'+\rho sin(\theta)y']}\rho d\rho d\theta-k^2\left(\frac{2}{3}MF(Z_8)+\frac{1}{3}MF(Z_0)\right)+k^2\cdot MF(Z_3)^2\right]
$$

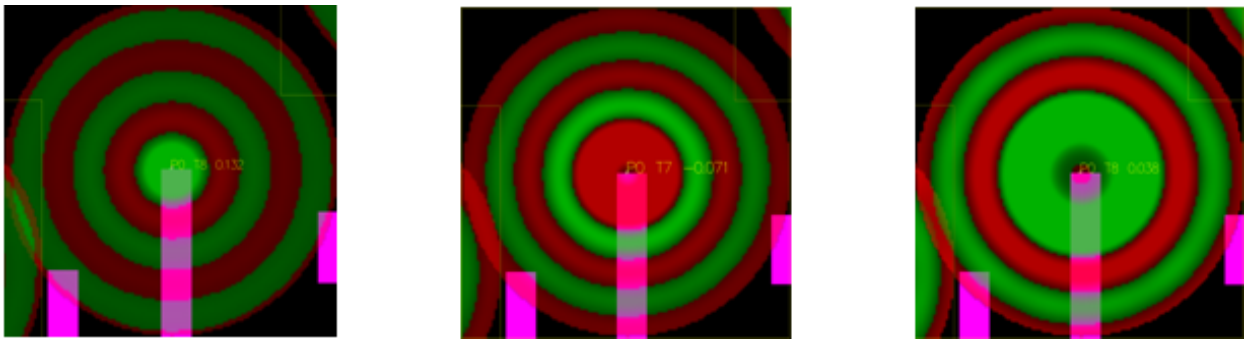

Figure 6.5: From left to right, the Z_0, Z_3 and Z_8 MLTPs.

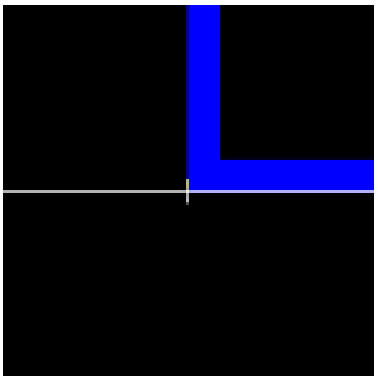

Figure 6.6: This cutline would be improved by making a 45 degree angle with the corner, rather than being placed horizontally.

Thus instead of just matching with Z_3 to find the sensitivity to defocus, we now match with Z_3 and take the square of this result, and we also match with Z_0 and Z_8.

6.3.2 Accuracy of Intensity Prediction for Defocus

The process for using pattern matching according to the new extended quadratic through-focus model requires match factors for Z_0, Z_3 and Z_8. Images of these three patterns are shown in Figure 6.5. One way to achieve the required match factors is to first scan the layout using the Z_3 pattern, and then to match Z_0 and Z_8 and the locations which returned the highest match factors for Z_3.

SPLAT files are produced by the pattern matcher at each match location, with a cutline automatically added through the point of interest. These SPLAT files are simulated with best focus and with a certain amount of defocus (0.06λRMS for this project), and the difference between the two cutlines at the point of interest gives the change in intensity. There were two improvements made on addition to the use of multiple match factors, one to the screening of the cutlines and the other to the method of generating and reading the cutlines, that greatly improved the accuracy of this procedure.

The first improvement to the method for measuring the pattern matcher accuracy was

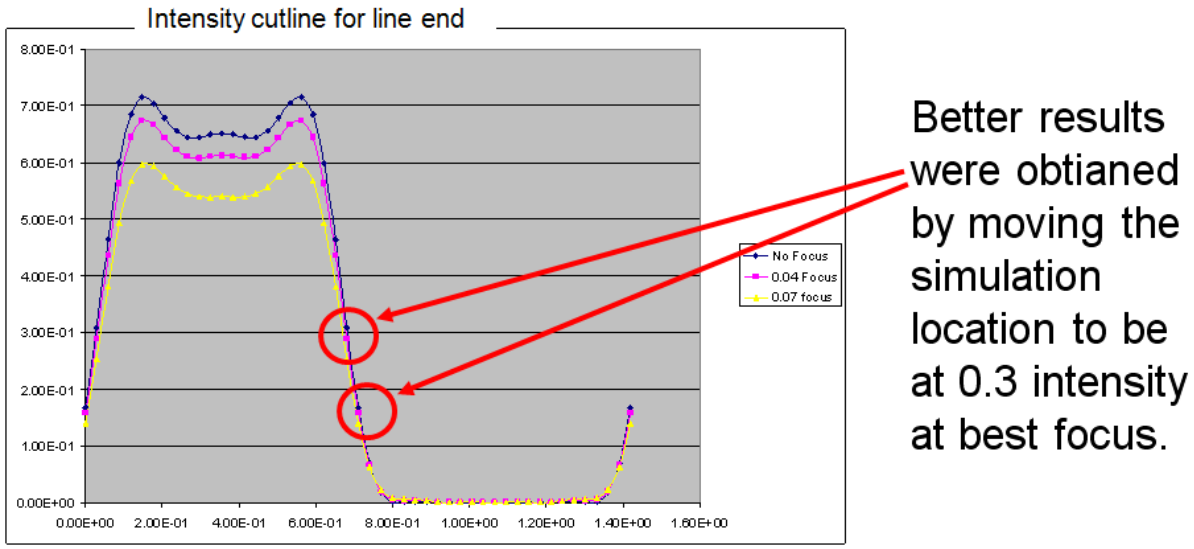

Figure 6.7: The location for measurement of intensity difference through-focus is taken at 0.3 clear field on the best focus cutline.

found through examination of the cutlines produced by the pattern matching program. It was found that cutlines on all corners were not in the correct position, and that others there were tool errors causing the cutline to not be placed over a feature. The reason that corner cutlines are not usable for this purpose is that they have been generated to be horizontal or vertical, when in fact a diagonal cutline would be preferable for modeling the pullback that the feature exhibits at corners. Figure 6.6 is one example of a corner where the cutline is placed horizontally instead of at a 45 degree angle. As a temporary solution to this problem, no match locations on corners have been accepted as valid, and lines and line ends have been studied instead.

The second improvement to the method for testing the through-focus model involves the location of the physical point where intensity change is evaluated.The midpoint of the cutline, which is the actual match location on the edge of the drawn layout, was previously taken as the location for the intensity difference measurement. However, this is not where the actual contour appears on the layout, and the change in intensity through-focus is found to be very minimal at this point. Instead of taking this point, the location was taken at 0.3 clear field intensity at best focus. See Figure 6.7 for an illustration of the choice of location.

With these improvements to the process of collecting pattern matching data, along with the new model with additional match factors, pattern matching was applied to a 130nm logic layout using conventional coherent illumination (sigma of 0.05), under best focus and 0.06λRMS, to produce the plot in Figure 6.8. This is a graph of actual intensity difference through-focus versus predicted intensity difference using match factors. Note that the coefficients for Z_0, ${Z_3}^2$ and Z_8 are determined using linear regression. It can be seen that the actual intensity differences are well predicted by the match factor formula. The R^2 value for this data is 0.92. This strong correlation implies that the pattern matcher can be

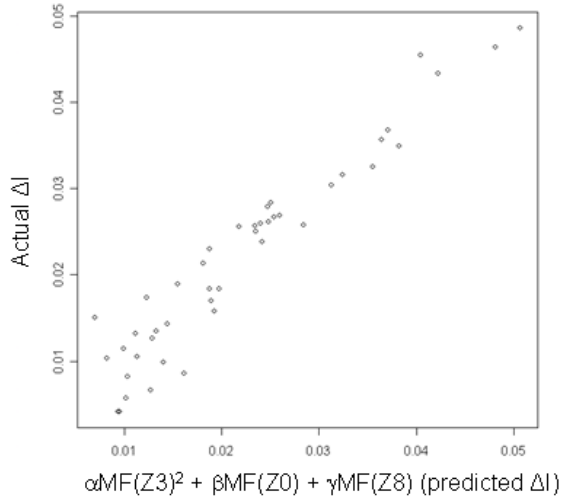

Figure 6.8: Actual intensity difference through-focus versus predicted intensity difference using match factors. The R^2 value for this data is 0.92.

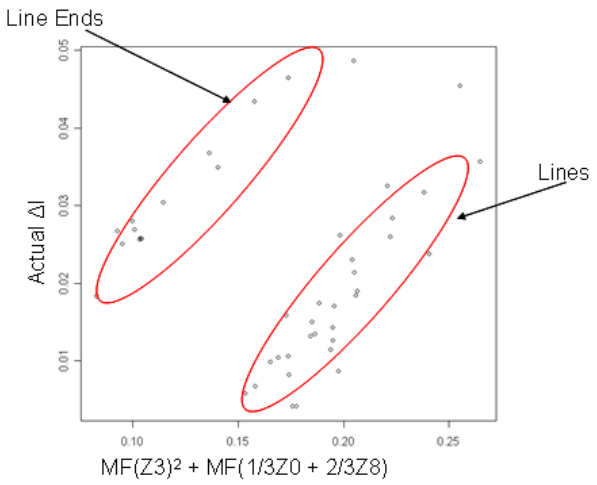

Figure 6.9: The prediction of change in intensity through-focus using a combined Z_0 and Z_8 pattern, as well as Z_3. No coefficients are used to scale the match factors of these two patterns.

	Intercept	$\mathbf{Z_3^2}$	$\mathbf{Z_0}$	$\mathbf{Z_8}$
Actual	-0.20	2.860	-0.178	-0.161
Projected	-0.0218	2.950	-0.175	-0.172

Table 6.1: Comparison of actual of projected coefficients for defocus of 0.06λRMS.

used accurately and quickly to predict the approximate sensitivity of a layout location to defocus.

Although the coefficients that multiply by match factors for Z_0, ${Z_3}^2$ and Z_8 are found through linear regression, the coefficients scale with defocus squared. In this way, once the coefficients are found for a particular defocus amount, the model easily scales for any other amount of defocus. This scaling is shown in Table 6.1 where the projected values have been found from scaling for 0.04λRMS by $(0.06/0.04)^2$.

One of the reasons that the coefficients are not known exactly ahead of time is that the pattern matcher gives each match factor a normalization based on the maximum possible value for that pattern which is the sum of the absolute values of all of its pixels, which affects the reported match factor. One way to bypass this feature of the pattern matcher is to combine Z_0 and Z_8 directly into one pattern. Our theory predicted that Z_0 and Z_8 should be in the ratio of 1/3 and 2/3, so a pattern was generated in these proportions. If we now look at the natural data without linear regression, and predict the intensity difference using Match Factor$(Z_3)^2$ + Match Factor$(1/3Z_0 + 2/3Z_8)$, the plot is shown in Figure 6.9.

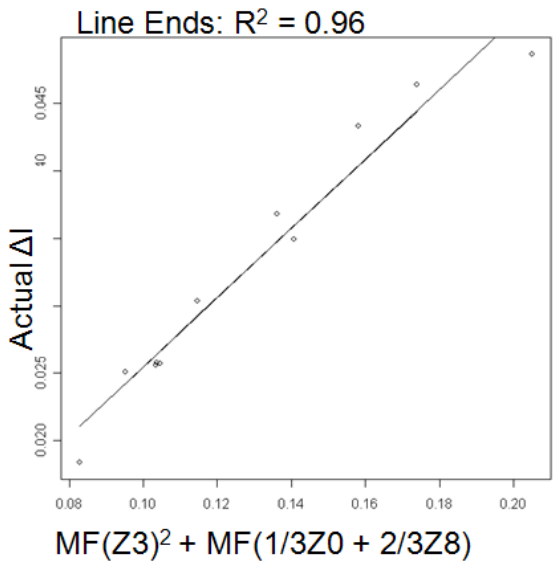

Figure 6.10: The prediction of change in intensity through-focus using a combined Z_0 and Z_8 pattern, as well as Z_3. This graph contains only data for line ends.

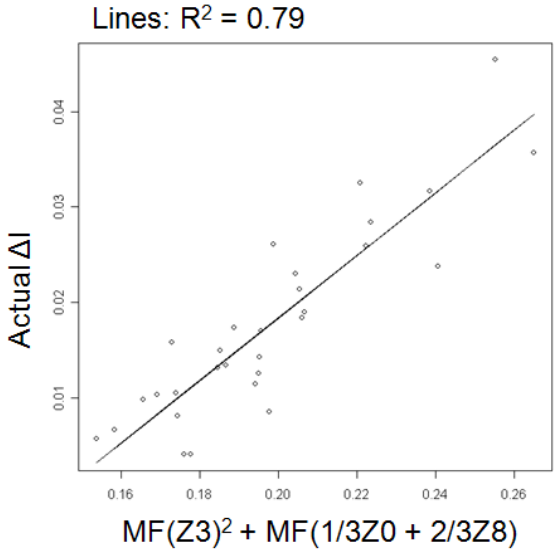

Figure 6.11: The prediction of change in intensity through-focus using a combined Z_0 and Z_8 pattern, as well as Z_3. This graph contains only data for lines.

The predicted intensities form two clusters of data – one containing all of the lines, and one containing all of the line ends. Both clusters have the same gradient, and the line ends show a higher change in intensity through-focus than the lines. While there are two clusters, clearly the weighted combination of Z_0 and Z_8 appears useful. One reason for this grouping may be that $\mathrm{MF}(Z_3)^2$ is a very small number, as it has been squared, and is about 10 times smaller than $\mathrm{MF}(1/3Z_0 + 2/3Z_8)$. This means that the Z_3 match factor is not contributing a very large weight to the final prediction. Another reason for the grouping is that internal normalizations of the match factors within the pattern matching program are affecting the coefficients and splitting the data.

The two clusters of data can be separated into individual graphs, as shown in Figure 6.10 and Figure 6.11. The R^2 value for predicting the change in intensity for line ends using these two match factors is very high at 0.96, and can be used to confidently approximate the change in intensity through-focus given that a location is known to be a line end. The graph for lines still shows a trend between predicted intensity change through-focus and actual intensity change, however with a lower R^2 of 0.79. There were a great variety of lines of varying widths and lines with pads in the layout tested that may be contributing to this variation.

The theory derived earlier gives some guidance to residual sources of inaccuracies and to a proper normalization to implement in pattern matching for the through-focus applications. With regard to residual inaccuracies, Z_0 is the only Zernike with non-zero area and thus is the only match factor that takes a measure of local feature shape within a radius of $0.4\lambda/\mathrm{NA}$.

Pattern	Area
Z_0	0.316
Z_8	0.395
$(1/3)Z_0 + (2/3)Z_8$	0.466
Z_3	-0.353

Table 6.2: The area of the match patterns, normalized to the maximum possible match factor.

Thus it is expected that the $(1/3Z_0 + 2/3Z_8)$ combined match factor will be feature type dependent.

With regard to normalization, the theory that was derived is independent of feature type and implies that the same normalization should apply for all patterns. One way to calibrate these coefficients is to evaluate an observation point in a clear field. Since this weighs all regions equally it indicates that the theoretical normalization factor is proportional to the area of the match pattern. Since the match patterns are Fourier transforms of the Zernikes, and since the area of a Fourier transform is proportional to the central value of the functions being transformed, the area of the match patterns for Z_0, Z_3 and Z_8 are proportional to their on axis values of 1, -1 and 1. Thus Z_3 and $(1/3Z_0 + 2/3Z_8)$ are expected to have identical magnitude match factor coefficients. The values of the match patterns evaluated at a point in a clear field are shown in Table 6.2.

Indeed the values are quite similar, and differences may be due to the effect of truncation of the pattern or discretization into pixels. This is promising evidence that a complete algebraic calibration of the change in the complex electric field is possible. This of course has to be combined with the pattern and observation point dependence of the in focus electric field behaviors to predict the change in intensities.

6.3.3 Limits of the Quadratic Defocus Model

We know that for small values of defocus, intensity scales with defocus squared, and that the quadratic model fits the data well for these small values of defocus. However, we would like to know how high an amount of defocus this model works for and whether or not a cubic or higher model is needed. To test how high a value of defocus we can use, a method was devised based on the theory that works for all layout patterns. When only OPD and OPD^2 are considered the intensity change with defocus should increase as $defocus^2$ for all layout shapes. A simulation of change in intensity for varying amounts of defocus was run and normalized to the changes for a small 0.02λRMS defocus in Figure 6.12.

Here for 0.048λRMS defocus, the data is linear with the changes in intensity for 0.02λRMS defocus. Each point corresponds to a different layout extraction and large changes that may need through focus compensations can be identified. As the amount of defocus is increased to 0.06λRMS the slope is still quite linear. The slope is not quite linear but it is still quite useful for finding problematic through-focus features. At 0.08λRMS defocus, the data is not as linear or neat with the change in intensity for 0.02λRMS defocus. This suggests to us

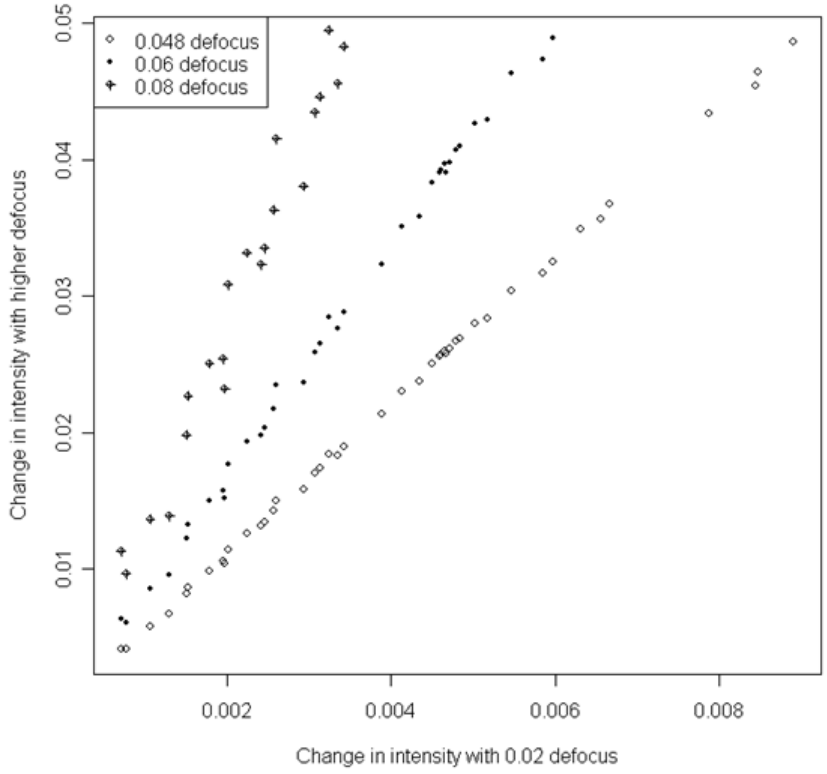

Figure 6.12: Change in intensity for varying amounts of defocus, versus the change in intensity for a small defocus of 0.02λRMS.

that the quadratic model is accurate to use for defocus less than 0.06λRMS.

Since a Rayleigh Unit corresponds to 0.072λRMS, we conclude that pattern matching for identifying problematic through focus behavior should work to a full Rayleigh Unit using only the OPD and OPD^2 terms.

6.4 Discussion

In this chapter, the accuracy of the pattern matcher was examined both for the coma pattern and the defocus pattern. First, the use of the pattern matcher was improved for prediction of edge movement under the presence of the coma aberration. The image slope was taken into account to better predict edge movement, and the R^2 for edge movement was improved from 0.73 to 0.95. One extra simulation was required at the match locations for this improvement, so a trade-off is required in speed in order to see this improvement in accuracy. However, the simulation is only required for the no-coma case, and the simulation with coma is still avoided, thus making this still a fast option for predicting coma sensitivity.

Next, the accuracy of the pattern matcher for the defocus aberration was examined. It

was found that the Z_3 pattern as the inverse Fourier transform of the Zernike polynomial, by itself, was inadequate to predict the change in intensity through defocus. The model was modified to include not only the constant and linear terms in the Taylor series expansion of the underlying theory, but to also include the quadratic term. This resulted in two more patterns being used to predict defocus, the Z_0 and Z_8 patterns. Together, these three patterns could predict the change in intensity with an R^2 value of 0.92 when the coefficients for each pattern were calibrated using a linear regression. When the coefficients were fixed, with no calibration required, the data split into two clusters, with the line end data forming a strong trend between the match factors and change in intensity and an R^2 of 0.96, and the line data having an R^2 of 0.79. If a data point was known to be a line end, such as in the case of a split polygon in a double patterning decomposed layout, the pattern matcher could be used with no calibration very accurately to predict the change in intensity through focus. All patterns showed only a focus squared change out to a Rayleigh Unit indicating that only OPD and OPD^2 are required by the pattern matcher. The potential for utilizing only two pattern matches and algebraically derived calibration weights was shown to be promising.

This improved focus model opens up applications for the pattern matcher. Since the pattern matcher is orders of magnitude faster than full simulation, it can be used to quickly scan layouts for process sensitivities. The new through-focus model allows the pattern matcher to be able to be used to test if a layout contains any focus hot-spots, or alternatively given a layout location it can predict how sensitive that location is to defocus. One application of the through-focus model is to double patterning decomposition. As outlined by Rubinstein and Neureuther (2008), the pattern matcher provides an excellent opportunity for the pattern matcher to help guide double patterning decomposition. The applications of pattern matching to double patterning design decomposition are shown in the flow diagram in Figure 7.7. This is further explored in Chapter 7.

The extended through-focus model can also be used during OPC. Since OPC simulations occur during best focus, it is possible to create a more focus sensitive layout through the layout manipulation involved in OPC. The pattern matcher could be used to check that no such hot spots are being created during the OPC algorithm.

Chapter 7

Application of Pattern Matching to Double Patterning Decomposition

7.1 Introduction

Double patterning is a process where layouts are split into two masks. One mask is exposed, followed by a treatment process, and then the second interleaving mask is exposed, thus effectively reducing the minimum possible pitch of the layout (Bailey et al., 2007). This chapter looks at how pattern matching can contribute to a better and faster double patterning layout design, either by guiding the layout decomposition itself or by scanning the post-decomposition layout for sensitivities to lithographic processes.

The first example that this chapter looks at in Section 7.2 is a layout split for complementary dipole illumination from Hendrickx et al. (2005). The post-decomposition layout is scanned by the pattern matcher for coma effects, and compared to the coma match factors from the original layout. The pattern matcher can add value to post-decomposition layouts by checking if they have any residual sensitivities to aberrations before being sent through simulation and OPC.

Next, Section 7.3 looks at how pattern matching can be used for post-decomposition assessment, using layouts from Drapeau et al. (2007) as an example. An example of a residual sensitivity to coma is found, and it is shown how by changing the layout split at this location, the sensitivity can be reduced.

Lastly, Section 7.4 looks at how the pattern matcher can be used within the double patterning decomposition process. The decomposition process is a largely heuristic based procedure for which an optimal algorithm has not yet been discovered. The method for determining how a layout is split is often automated to a large extent, followed by conflict resolution by hand. The effects of decomposition decisions on the layout across the process window can be difficult to determine without running lengthy simulations, and a fast method is required to determine the quality of the split. Split decisions can be checked for lithographic weakness using pattern matching and quantified by a cost function to dynamically guide the decision. This section shows an example flow for how to make effective use of pattern matching within the decomposition algorithm.

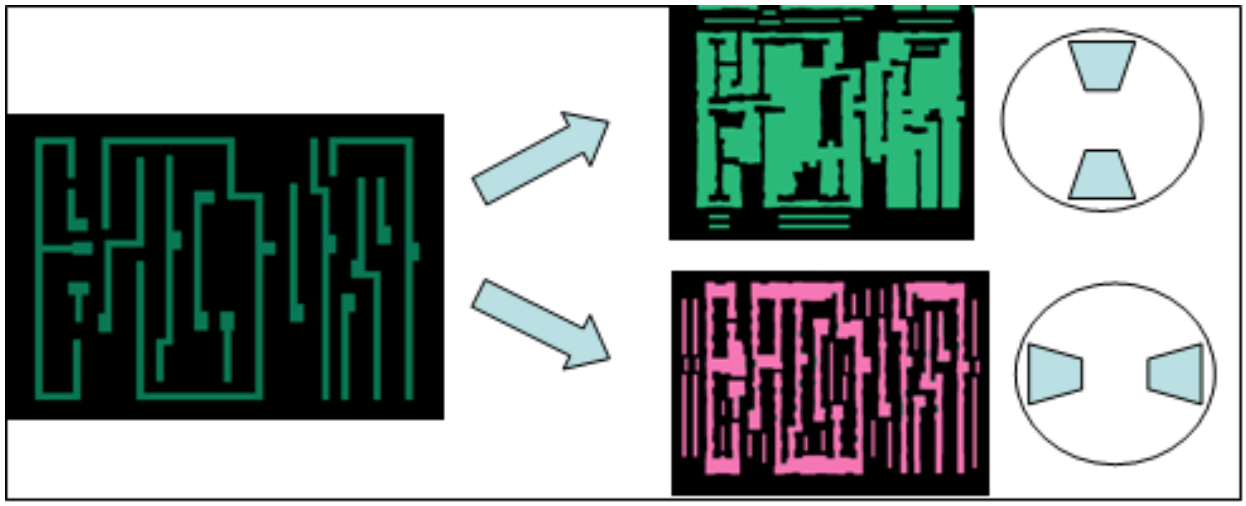

Figure 7.1: Splitting of a layout into two layers, suitable for exposure using complementary dipoles.

7.2 Pattern Matching for Double Exposure Treatments using Complementary Dipole Illumination

Double exposure or Double Patterning (DP) treatments are becoming increasingly important for printing of fine lines, where complementary dipoles are used to print features in the horizontal and vertical directions separately. In order to take advantage of the higher resolution offered by the complementary dipole exposures, the layout must first be decomposed into two layers—one in which all of the features are vertical and the horizontal features are shielded from exposure, and one in which all of the horizontal features present and the vertical features are shielded from exposure. This fragmentation process is shown in Figure 7.1. The layout used for this section is from Hendrickx et al. (2005).

Unlike the OPC treatments applied in Section 7.2, the layout changes significantly between the design layout and the post DP and OPC treatment. The area of exposed layout is increased dramatically, which could increase the number of orders of light entering the mask, and could thus alter the sensitivity of the mask to aberrations.

In order to test the changing sensitivity of the layout to aberrations across different splits of the layout, the pattern matcher was run with the coma pattern on the design intent, a constant threshold (CTR) model split (Split II) and a variable threshold (VT5) model split (Split III). On the split layouts, only the Y mask was tested, and it was tested using an off-axis coma pattern, derived as in Section 5.4. The X and Y masks can be tested for sensitivities separately, since they are exposed separately and are thus independent from each other in this respect. The resulting match factors are shown in Figure 7.2.

The match locations in the post OPC layout are not taken on the design layout as would be most optimal, but this should only make minimal differences, indicating that the results are likely still representative of a real effect. The plot in Figure 7.2 shows that the match

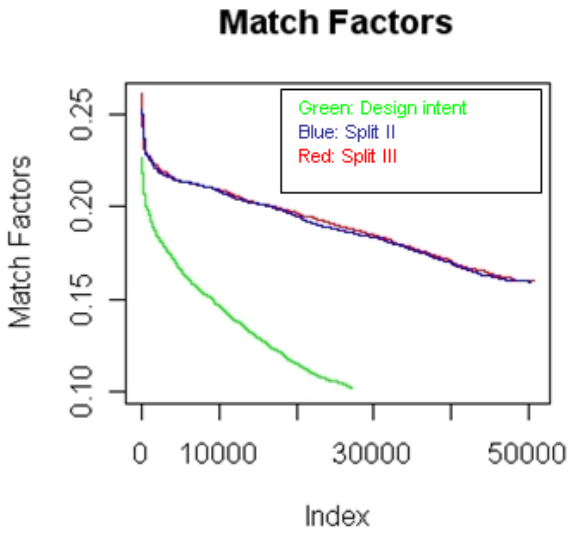

Figure 7.2: Match factors for the complementary dipole treated layout. The top 50,000 match factors higher than 0.1 are shown. The green line shows the match factors for the design intent, and the blue and red lines show the design intent for the Y mask of the decomposed layout.

factors obtained for the post OPC layouts are considerably higher than those of the design intent, even though the coma pattern used for the post OPC layouts is derived as an off axis illumination pattern having a phase ripple. OPC moves features from more being isolated to more dense but may introduce shifts in dense patterns that are affected strongly by coma. For example, if the period for which resolution enhancement with SRAFs is designed to be P, and if two SRAF modified features abut with separation $P/2$, the abutment region will be strongly affected by coma. Since pattern matching can inspect the entire layout for many causes, it can help assure manufacturability in the presence of many residual non-idealities.

When a layout is decomposed into an X mask and a Y mask, there are many ways that the features can be divided amongst the two masks. This is particularly true when there is an elbow, or horizontal and vertical features in close proximity to one another. Since the divided mask may in fact be more susceptible to aberrations such as coma, a possible strategy for minimizing risk of aberration related printing defects could be to run the pattern matcher on the layout, and then re-adjust the division of the layout amongst the X mask and Y mask to compare layout areas with high match factors.

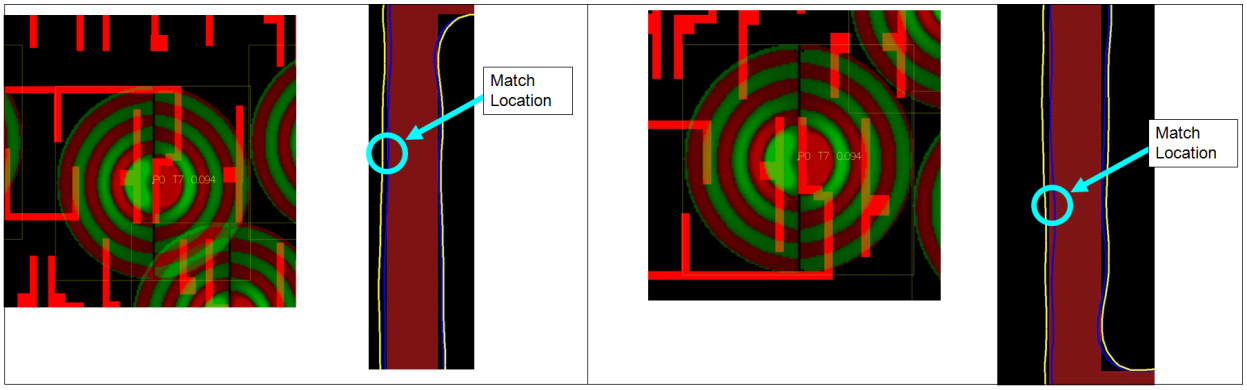

Figure 7.3: Examples of matches with coma and their corresponding aerial image simulations. The two cutlines represent the aerial image with no coma present and with 0.04λRMS coma.

7.3 Post Decomposition Assessment of Double Patterning Layouts

In this section, pattern matching methods are examined as fast-CAD tools for full-chip across process window examination of post-decomposition double patterning layouts. The post-decomposition layouts used in this section are not complementary dipole, but are rather split for annular illumination and are sourced from Drapeau et al. (2007). The split layouts in this case are not divided into their horizontal and vertical components. The goal is to demonstrate the ability to anticipate lithographic weakness due to many sources, such as the decomposition strategy, process window, illumination and aberration. This study is an intermediate step to using fast-CAD assessment tools within pattern decomposition algorithms to guide decisions based on lateral influences instead of rules. The pattern matcher is run on a post decomposition layout and locations are identified with high variability under coma, and their sensitivity is verified with aerial image simulations. For one such example, a different split is suggested and the match factor drops by 55%.

7.3.1 Simulation Conditions

The double patterning layouts used for this project were supplied by IMEC and ASML (Drapeau et al., 2007). The nominal conditions for these layouts are λ=193nm, 1.2 NA, annular illumination 0.5-0.9, with k1=0.36 and no polarization effects. SPLAT (Lee et al., 1995) and Mentor Calibre (Mentor Graphics, 2010) were used for rigorous simulation.

7.3.2 Pattern Matching Results when Applied to Post-Decomposition Layouts

The pattern matcher was used with the coma pattern on the layout supplied by IMEC (Drapeau et al., 2007). Two examples of a high match on a line adjacent to a

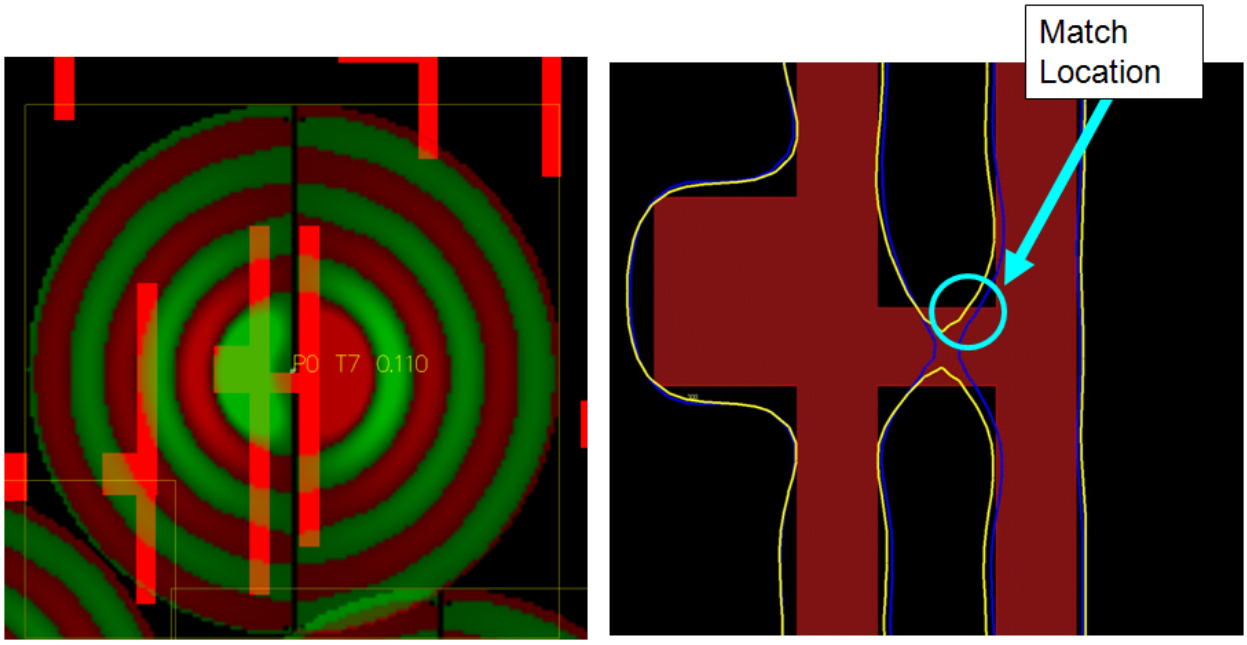

Figure 7.4: An example of an 'H' structure which performs poorly under the presence of coma.

pad are shown in Figure 7.3. Note that the aerial image contours are not close to the expected edges because the post OPC layout was designed for a clearfield mask, but instead a darkfield mask was used for simulations in this study. The reason for this mask choice in the matching and simulation is that for purposes of illustration, the MTLPs are designed for conventional illumination with a small sigma, but we assume that they can be used approximately under annular illumination with a darkfield mask due to the smaller amount of light transmittance. However, even with the larger than usual edge displacement, it can be seen that the points of high match factor correspond to points of high variation with coma.

A second type of example is shown in Figure 7.4. Here, an H structure can be seen with a high match factor of 0.11 and with poor performance in the presence of coma. A different split can be made with the feature split over two masks, as shown in Figure 7.5. If the pattern matcher is run on this structure again, the new match factor is -0.005, which is a 55% reduction in match factor. This example shows that making a different split choice can result in a much higher or lower match factor, and that the pattern matcher can be used to guide the split decision based on the match factor. This shows the value in the pattern matcher in its use for scanning post-decomposition layouts. Any sensitivities found by the pattern matcher can be re-examined and different split decisions can be made to possibly minimize these sensitivities.

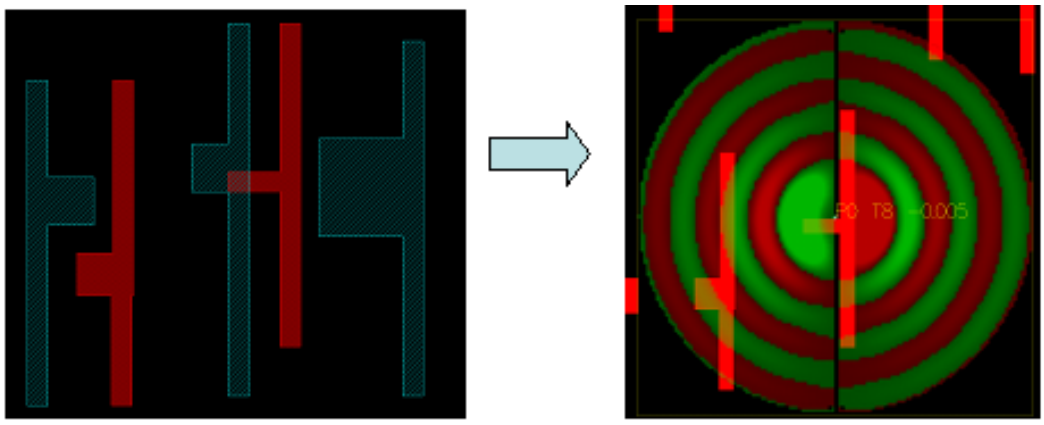

Figure 7.5: A different split for the 'H' structure which results in a lower match factor.

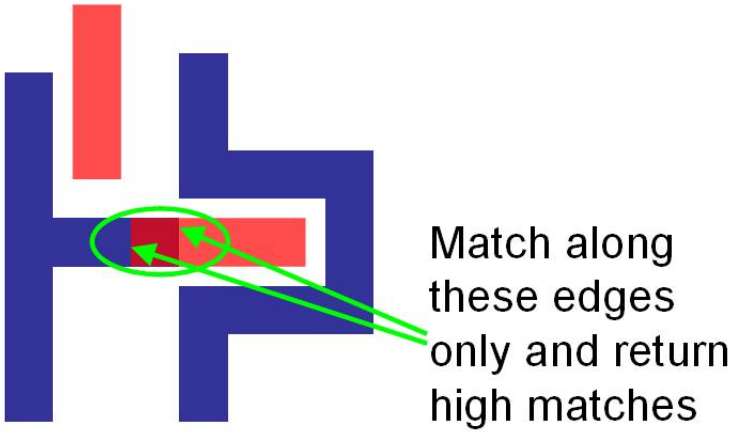

Figure 7.6: An example of a layout where a polygon must be split in order to decompose the layout into two masks. The location of the splits and the amount of overlap must be decided.

7.4 Pattern Matching Applied to Double Patterning Decomposition Guidance

This section looks at how the pattern matcher can be incorporated into a decomposition algorithm at the points in the algorithm where a split decision must be made. An example of such a decision is shown in Figure 7.6. The pattern matcher can be used at these points, and can be run very quickly to give a first estimate for any hot spots for focus or other aberrations. In this section, the defocus aberration is used for the test examples, and the new through-focus model from Chapter 6 is used. Since the pattern matcher can run on a whole chip in 17 minutes, the running time for a just a subset of layout locations such as these is very small.

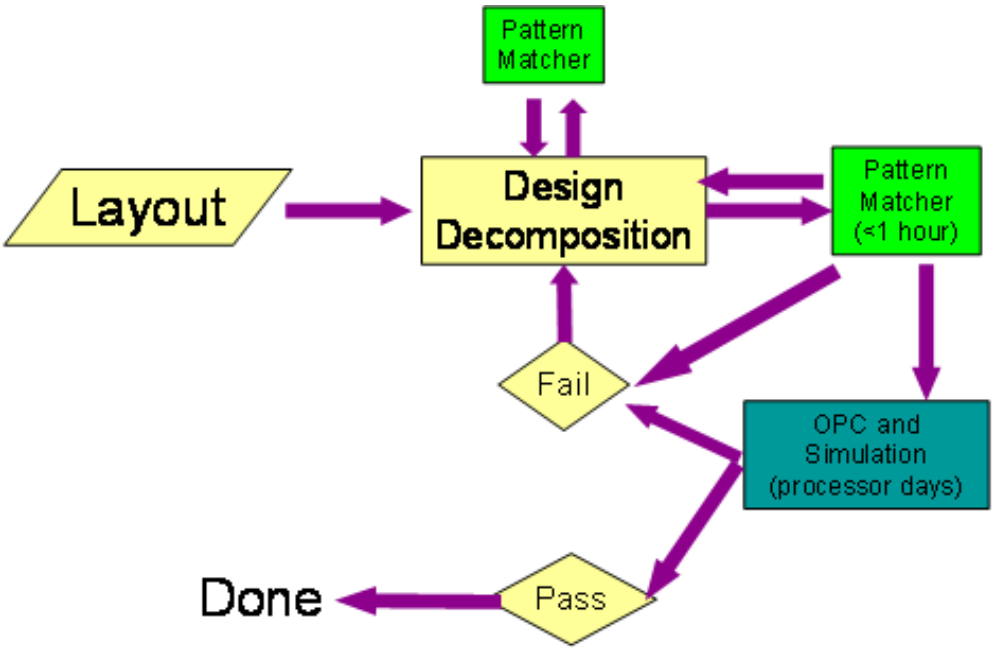

Figure 7.7: A flow diagram detailing how the pattern matcher can be used to help guide double patterning design decomposition.

An example process flow incorporating the pattern matcher is shown in Figure 7.7. The pattern matcher can be used in two places in the flow. One is within the design decomposition algorithm itself, where it is run on every possible split to check that no process sensitivities are being generated, in which case a different location for the split should be chosen. The other place in the flow that the pattern matcher can be used is once the decomposition has been made, as a last check before OPC to make sure that there are not any residual sensitivities. This process flow setup could help reduce the number of times that a layout is rejected and has to pass through OPC, which is a very time consuming aspect of the flow.

When pattern matching for defocus effects is used within the actual design decomposition algorithm, it gives a measure of how sensitive a particular split is to defocus. When a choice between different splits is to be made, the pattern matching information can be used to help decide which split should be chosen. An example of such a decision is shown in Figure 7.8 and the table of predicted and actual changes in intensity is shown in Table 7.1. Note that since the layout features are line ends, no calibration of match factor co-efficients is required. Given three different line end overlap lengths on a mask, the through-focus model correctly predicts which length has the smallest through-focus intensity change. Additionally, all actual intensity changes were approximately three times the predicted intensities, indicating that the uncalibrated change in intensity estimate from pattern matching can be used as either a cost function or acceptability threshold for decomposition. Pattern matching can also be used once decomposition is complete, to find any residual sensitivities to defocus. In these two ways, the new through-focus model of Chapter 6 can be used to help guide

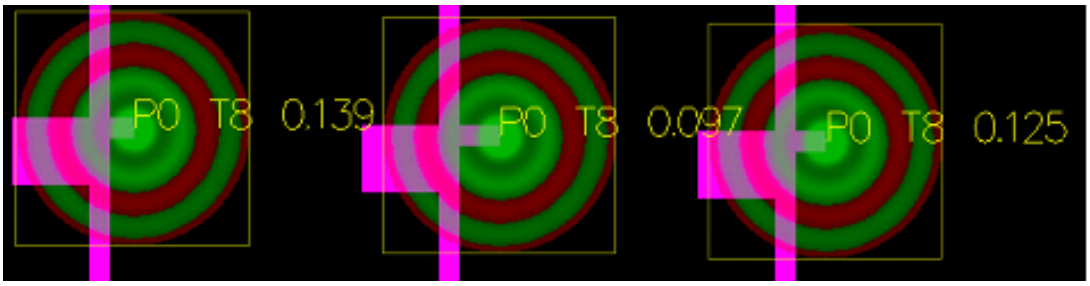

Figure 7.8: Three different split decisions with varying amounts of overlap are shown with pattern matcher overlaid at the line end.

	Pattern 1	***Pattern 2***	**Pattern 3**
$\mathbf{Z_3^2}$	0.004	*0.003*	0.003
$\mathbf{1/3Z_0 + 2/3Z_8}$	0.139	*0.097*	0.125
Predicted ΔI (uncalibrated)	0.143	*0.100*	0.128
Actual ΔI	0.051	*0.033*	0.041

Table 7.1: The match factors and predicted change in intensity through-focus, as well as the actual change in intensity through-focus.

double patterning decomposition.

7.4.1 Inclusion in an Existing Double Patterning Decomposition Flow

Kahng et al. (2008) have devised a specific double patterning decomposition flow. In order to demonstrate the feasibility of the pattern matcher for guiding double pattern decomposition in a collaborator study with an agreed upon modified flow was devised. The modifications that are necessary in order to integrate the pattern matcher into the existing flow have been discussed. The flow shown in Figure 7.9, where pattern matching fits in between node splitting and the graph update is suggested.

The way that the flow from (Kahng et al., 2008) currently works is to fracture a layout, construct a graph representation of the fractured layout, color the graph until there is a conflict cycle identified, choose a place to split the layout with an overlap length that is within the acceptable overlap margins (without simulation), and then iterate until the graph is complete. The acceptable polygon overlap margins are determined ahead of time, so that the margin is not too small so as to create pinching, or too large so as the split node interferes with the original polygon that it was too close to. The proposed modification is to refine the overlap length and split location using information provided by the pattern matcher.

To test the principles of this idea, a dry-lab study is being made. After a node is split with an acceptable overlap margin, a snippet of the layout is taken and placed in a new layout file. A grid of such snippets are placed on the layout, each with the split node having

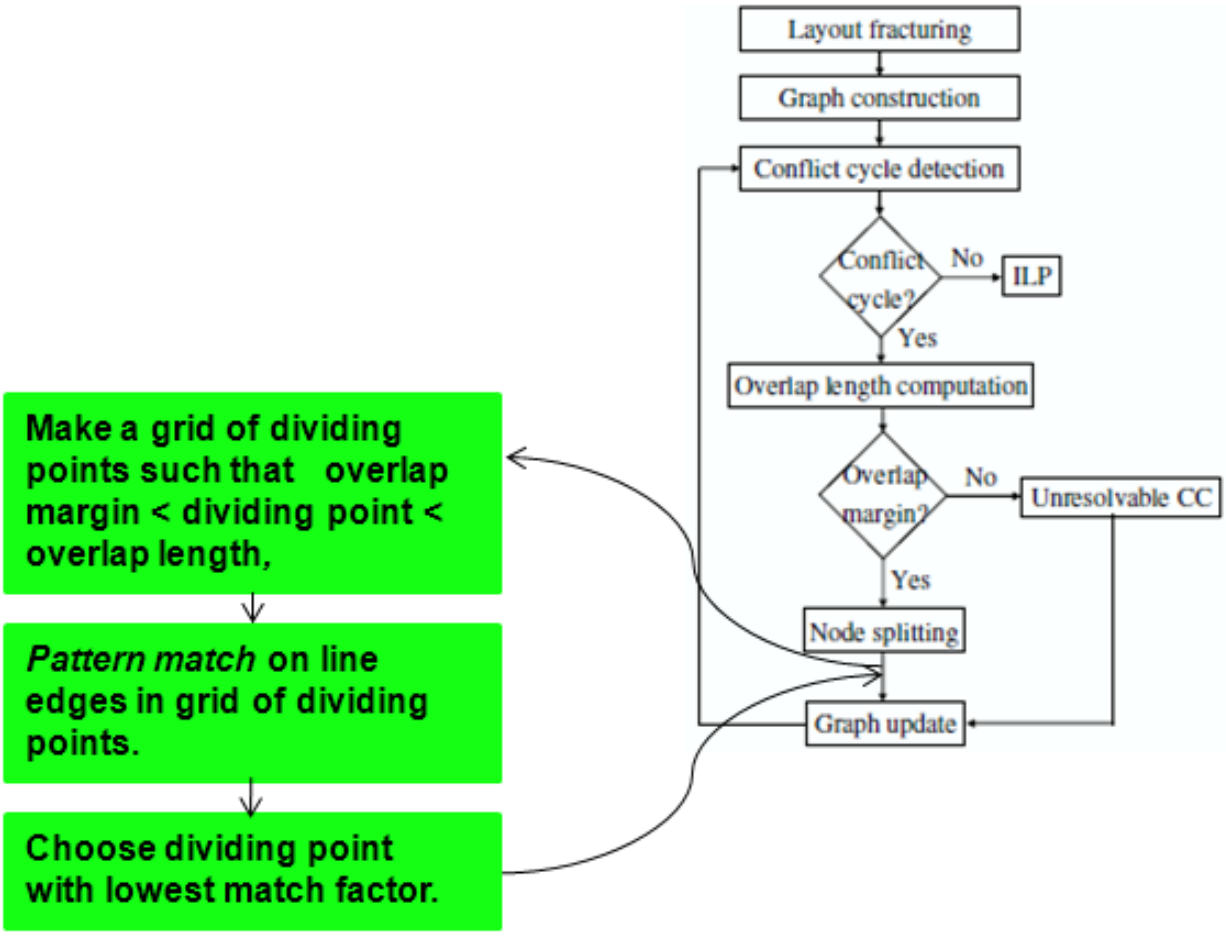

Figure 7.9: The double patterning decomposition flow from Kahng et al. (2008), with additions in the green boxes to generate a grid of splits and return pattern matching results on them.

a slightly smaller or larger overlap margins, with the dividing points moving by a designated amount in each snippet. An example of such a grid of snippets is shown in Figure 7.10. The number of snippets to include in the grid can be a customizable feature, depending on the amount of granularity desired in evaluating the dividing points. The pattern matcher is matched with the defocus patterns, for example, at each of the dividing points, and the match factors are returned to the original flow to give extra guidance. Then, the snippet with the lowest match factor can be chosen, or if there are other metrics that are also to be taken into account, the match factor can be used to help weight the goodness of the split decision.

This evaluation by the pattern matcher during decomposition would help to improve yield, because any split decisions that give an unacceptable variation through the process window can be eliminated ahead of time.

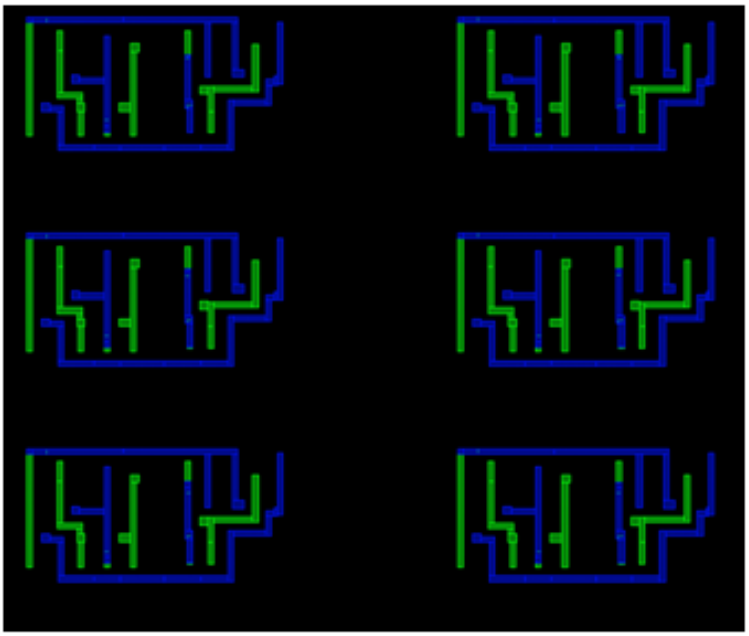

Figure 7.10: A grid of snippets with varying split choices.

7.5 Summary

Pattern matching was investigated for its use during and after a layout is decomposed for double patterning. In the first study, a layout that was split for exposure under complementary dipoles was evaluated. The split layouts and the original, unsplit layout were scanned with the pattern matcher for sensitivities to coma. It was found that the match factors for the split layouts were much higher than the match factors for the original layout in this case. A hypothesis for this was that with more of the mask opened up in the split layouts, more orders of light would enter the mask, thus altering the sensitivity of the layout to aberrations. Also, the pitch of the features may be increased in such a way as to increase coma sensitivity.

Another post-decomposition layout, which was split for annular illumination rather than complementary dipoles, was scanned with the pattern matcher to find sensitivities to coma. Locations with a high match factor were simulated to show that there were in fact sensitivities to coma at those locations. One such example was further split, and with the new split the match factor was reduced by 55%.

An example flow for layout decomposition incorporating the pattern matcher to be used for guiding split decisions was shown. In this flow, the pattern matcher is to be used as in the cases above for identifying locations with a high variance under aberrations. An example situation of an H-structure that needed to be split was shown with different split decisions, and the split decisions were evaluated for defocus effects using the pattern matcher. In this case, it was found that the pattern matcher could quantitatively predict which of the split decisions reduced the variation by 30% through defocus, and thus which would make a good split location.

The example flow for layout decomposition using pattern matcher was applied to the existing flow of Kahng et al. (2008). It was suggested that a grid of layout splits could be saved to a layout file, to be scanned by the pattern matcher only at the split decision locations.

These studies and flows show the potential for the pattern matcher to improve the largely heuristic based process of double patterning decomposition. Examples have been shown where the pattern matcher has been able to predict which split would have the least variability through focus, and the flows have shown exactly how the pattern matcher can be incorporated into existing flows, in order to increase yield and reduce the number of iterations that the layout is required to go through OPC and simulation.

Chapter 8

Conclusion

The main contributions of this thesis have been the extension of the pattern matcher to advancing lithographic technologies, and the identification of an emerging application which is a good fit to take advantage of the pattern matcher's features. Extensions have been shown for technologies such as OPC treated layouts, polarization and high-NA effects. The accuracy of the pattern matcher was examined and improved for edge movement through coma, and for defocus. A new, quadratic model for defocus was introduced and shown to improve the model to a usable accuracy. Pattern matching, with the addition of these improvements, was shown to be a useful aid for double patterning lithography.

The pattern matcher is a fast-CAD tool that takes as its input a Maximum Lateral Test Pattern (MLTP) and scans a layout for any locations that are geometrically similar. The MLTPs, taken as the inverse Fourier transform to the Zernike polynomials, are the theoretically most sensitive patterns to aberrations. Therefore, any layout locations that are similar in geometry to the MLTP are likely to also have a sensitivity to the aberration. The challenges in extending the pattern matcher to new technologies is that often new MLTPs need to be derived, and that its accuracy must be verified and improved via new models, new patterns and new technical solutions until it reaches an acceptable level.

As motivation for why pattern matching is important and interesting, Chapter 3 presented the modeling of a gate CD distribution. This chapter provided an in-depth study on how to take a joint-probability distribution for focus and exposure and a CD response curve, and produce a probability distribution of gate CDs. The CD response curve was found using only points at the $+3\sigma$, -3σ and nominal values, and the rest of the values on the response surface were interpolated using a model by Mack and Byers (2003). This made the whole process of producing the CD distribution relatively fast. The advantage of allowing the input of a distribution of focus and exposure values, rather than just fixed values, is that this more closely models what is actually present in a system, and the resulting CD distribution was shown to produce a number of useful metrics that allow valuable analysis of the layout variability. The high variation transistors, the low yield transistors, the spread of variation of transistors, the goodness of the biasing and Optical Proximity Correction (OPC) and other characteristics of the design were all shown to be easily identified once the CD probability distribution was generated. All of these metrics allow a better analysis

and thus tighter control of the variability and yield of a layout. This work was completed during an industry summer internship at AMD, and highlights the high importance that industry places on being able to predict and control variability. The pattern matching work in this thesis was shown to assist in the prediction of variability and yield in the presence of aberrations, and is thus of high importance to the field of lithography and circuit design.

A variety of mask issues of relevance to pattern matching were presented in Chapter 4. The ability to write a MLTP to a mask was addressed, and it was found that the MLTPs were inherently very costly and unfriendly for mask manufacturing, with their round edges and touching phases. An automatic method for the modification of patterns in order to pass Design Rule Checks (DRC) was presented, resulting in minimally modified patterns that passed DRC. Additionally, it was shown that a hand-made pattern which resembled the defocus pattern retained 68% of its sensitivity to the aberration, and remained orthogonal to the spherical aberration. The ability to modify patterns to be more mask manufacture friendly has the impact on industry that the monitors can be used to test the aberration levels of lithographic systems, as has been shown by Robins and Neureuther (2004); Holwill and Neureuther (2006); Rubinstein and Neureuther (2007), but with a lower cost due to the removal of expensive small jogs and other geometries.

The effects on pattern matching of Optical Proximity Correction (OPC), typically performed on a layout as the last step before tape-out, were examined. The effects of OPC of varying levels of aggressiveness on coma match factors were examined, and it was found that in many cases OPC did not significantly alter the pre-OPC match factors. This allowed us to conclude that in most cases, the pre-OPC match factors could still be used as a guide to the expected sensitivities in the post-OPC layout. It was noted that in some cases, especially when Sub Resolution Assist Features (SRAFs) were present in the OPC treatment, the match factors could vary more significantly. This, in addition to the fact that it was shown that proximity and defocus sensitivities occur in distinct location on a layout, allowed us to conclude that it is possible for OPC to increase or decrease the sensitivity of a layout location to an aberration. The pattern matcher can be run again on a post-OPC layout as another check for any residual sensitivities to non-idealities.

Extensions of pattern matching for detection of vulnerabilities to high-NA and polarization vector effects were shown. Three to five patterns were required for the calculation of the vulnerability score, depending on whether the illumination was on-axis or off-axis. Being able to screen for these effects is of importance to the area, as the effects were shown to range from 8% to 40% in the experiments that were run. All layout regions act differently, and the vulnerabilities are non-intuitive and hard to capture with design rules. The pattern matcher was shown to be of use here for quickly finding sensitivities, and examples were shown for both the on and off axis illumination cases, demonstrating the accuracy of the method.

The accuracy of the pattern matcher was investigated and improved for both edge-movement prediction and through-focus behavior. While the pattern matcher had already been shown to be accurate in predicting the change in intensity through coma, the edge-movement prediction was less accurate. An improved method for predicting edge-movement was demonstrated, which used the image slope information as well as the match factors. This

is important because it is the final edges that are printed on the wafer that will determine the circuit's performance. The speed advantage of the pattern matcher is still present when image slopes are used in this way, as only one simulation is required and only at selected, filtered locations as determined by the pattern matcher.

A new, quadratic through-focus model was devised, which used three patterns rather than the original one pattern. Using only one pattern was found to be insufficient for predicting defocus due to the fact that defocus is an even aberration, producing an imaginary spillover, and also the fact that defocus is not a small aberration. The new model is based on using the Optical Path Difference (OPD) as well as OPD^2, whereas the original model used only OPD. The three patterns can likely be reduced to two patterns, representing the contributions of the above two terms, and some promising results were presented with the use of the two patterns. It was shown that the new model with the three patterns is accurate for defocus for up to one Rayleigh Unit. Previously, the linear model with one pattern for defocus could not predict the change in intensity through focus any better than random. The new quadratic model, along with a few technical improvements to the way the experiments were run, was shown to predict the through focus change in intensity with an R^2 of 0.92.

Pattern matching was shown to be of use for guidance during the double patterning decomposition process, by offering a quantitative metric for the expected change in intensity through focus of a suggested polygon split. Additionally, the pattern matcher was also shown to be useful for checking post-decomposition layouts for sensitivities to aberrations before they go through OPC and simulation, potentially saving time consuming iterations through the design flow. A variety of split choices were tested using the pattern matcher to show that the change in intensity could be quantitatively predicted, and post-decomposition algorithms were scanned using the pattern matcher to find hot spots due to aberrations. One such sensitivity was shown to be mitigated by introducing a new split.

In summary, pattern matching has been extended and improved in accuracy for a number of technologies that are relevant to the field today. These allow the pattern matcher to find sensitivities in layouts to lithographic effects due to complex 2-D geometries that would be difficult to capture in design rules. The pattern matcher is 10^4 to 10^5 times faster than rigorous simulation, and has its niche as an approximate tool for finding possible sensitivities further up in the design flow, saving time and money by reducing the number of iterations through the much slower OPC and simulation phases. This thesis has introduced a number of additional technology configurations which the pattern matcher can now handle, allowing the pattern matcher to be used for emerging applications such as double patterning.

Bibliography

K. Adam and W. Maurer. Polarization effects in immersion lithography. In *Proceedings of the SPIE*, volume 5377, pages 329–343, 2004.

George E. Bailey, Alexander Tritchkov, Jea-Woo Park, and Le Hong. Double pattern EDA solutions for 32nm HP and beyond. In *Proceedings of the SPIE*, volume 6521, page 65211K, 2007.

Edward Charrier, Chris A. Mack, Q. Zuo, and M. Maslow. Methodology for utilizing cd distributions for optimization of lithographic processes. In *Proceedings of the SPIE*, volume 3051, pages 541–551, 1997.

E. Y. Chin, J. A. Holwill, and A. R. Neureuther. Prediction of interconnect delay variations using pattern matching. In *Proceedings of the SPIE*, volume 6521, pages 65210I.1–65210I.6, 2007.

Tsann-Bim Chiou, Robert Socha, Hong Chen, Luoqi Chen, Stephen Hsu, Peter Nikolsky, Anton van Oosten, and Alek C. Chen. Development of layout split algorithms and printability evaluation for double patterning technology. In *Proceedings of the SPIE*, volume 6924, pages 69243M–69243M–10, 2008.

N. Cobb, A. Zakhor, and E. Miloslavsky. Mathematical and cad framework for proximity correction. In *Proceedings of the SPIE*, volume 2726, pages 208–222, 1996.

M. Drapeau, V. Wiaux, E. Hendrickx, S Verhaegen, and T Macida. Double patterning design split implementation and validation for the 32nm node. In *Proceedings of the SPIE*, volume 6521, page 652109, 2007.

F. Gennari. *Linking TCAD and EDA through Pattern Matching.* Ph.d. dissertation, University of California, Berkeley, 2004.

F. Gennari and A. R. Neureuther. A pattern matching system for linking TCAD and EDA. In *IDQED 2004*, pages 165–170, 2004.

F. Gennari, G. Robins, and A. R. Neureuther. Validation of the aberration-pattern-matching OPC strategy. In *Proceedings of the SPIE*, volume 4692, pages 444–453, 2002.

E. Hendrickx, A. Torres, N.V. Lafferty, S. Johnson, L. Le Cam, C. Reita, G. Vandenberghe, and W. Maurer. Complementary double-exposure solutions at 0.29k1. In *Proceedings of the SPIE*, volume 5754, pages 327–338, 2005.

J. Holwill, G. McIntyre, W. Poppe, and A. R. Neureuther. Layout 'hot spots' for advancing optical technologies. In *Proceedings of the SPIE*, volume 6154, pages 1212–1220, 2006.

Juliet Holwill and Andrew R. Neureuther. Self-interferometric electrical image monitors. In *Proceedings of the SPIE*, volume 6152, pages 408–415, 2006.

Juliet Holwill, Jongwook Kye, and Yi Zou. Statisitical analysis of gate cd variation for yield optimization. In *Proceedings of the SPIE*, volume 6521, page 65211P, 2007.

JMP, 2010. `http://www.jmp.com/`; accessed April 19, 2010.

A. B. Kahng, C. Park, X. Xu, and H. Yao. Layout decomposition for double patterning lithography. In *Proceedings of the 2008 IEEE/ACM International Conference on Computer-Aided Design*, pages 465–472, 2008.

J. Kirk. Review of photoresist-based lens evaluation methods. In *Proc. SPIE*, volume 4000, pages 2–8, 2000.

I. Lalovic, O. Kritsun, S. McGowan, J. Bendik, M. Smith, and N.Farrar. Defining a physically accurate laser bandwidth input for optical proximity correction (OPC) and modeling. In *Proceedings of the SPIE*, volume 7122, pages 71221R–71221R–12, 2008.

D. Lee, D. Newmark, K. Toh, P. Flanner, and Andrew R. Neureuther. SPLAT v5.0 user's guide. Technical Report UCB/ERL M95/13, EECS Department, University of California, Berkeley, 1995.

B. J. Lin. The exposure defocus forest. *Japanese Journal of Applied Physics*, 33(12B): 6756–6764, 1994.

Chris A. Mack and Jeffrey D. Byers. Improved model for focus-exposure data analysis. In *Proceedings of the SPIE*, volume 5038, pages 396–405, 2003.

Mathworks. Matlab, 2010. `http://www.mathworks.com/`; accessed April 19, 2010.

G. McIntyre and A. Neureuther. Monitoring polarization and high-na at 193nm and immersion with phase shifting masks. In *Proceedings of the SPIE*, volume 5754, pages 80–91, 2005a.

G. McIntyre, J. Holwill, A. R. Neureuther, L. Capodieci, Y. Zou, H. Levinson, and J. Kye. Screening layouts for high-na polarization effects using pattern matching. *Journal of Vacuum Science & Technology B: Microelectronics and Nanometer Structures*, 23(6):2646–2652, November 2005.

Gregory McIntyre and Andrew R. Neureuther. Monitoring polarization and high-numerical aperture with phase shifting masks: Radial phase grating. *Journal of Vacuum Science & Technology B: Microelectronics and Nanometer Structures*, 23(1):302–306, January 2005b.

Mentor Graphics, 2010. `http://www.mentor.com/`; accessed April 18, 2010.

H. Nishinaga, N. Tokuda, S. Owa, S. Hirukawa, O. Tanitsu, T. Kudo, and H. Tanaka. Development of polarized-light illuminator and its impact. In *Proceedings of the SPIE*, volume 5754, pages 669–680, 2004.

R Development Core Team. *R: A Language and Environment for Statistical Computing*. R Foundation for Statistical Computing, Vienna, Austria, 2009. URL `http://www.R-project.org`. ISBN 3-900051-07-0.

G. Robins. *Interferometric Pattern and Probe-Based Aberration Monitors*. Ph.d. dissertation, University of California, Berkeley, 2005.

G. Robins and A. R. Neureuther. Are pattern and probe aberration monitors ready for prime time? In *Proceedings of the SPIE*, volume 5754, pages 1704–1715, 2004.

Garth Robins, Konstantinos Adam, and Andrew R. Neureuther. Measuring optical image aberrations with pattern and probe based targets. *Journal of Vacuum Science & Technology B: Microelectronics and Nanometer Structures*, 20:338–343, January 2002.

Garth C. Robins, Mircea Dusa, Bernd Geh, and Andrew R. Neureuther. Interferometric-probe aberration monitors: aerial image and in-resist performance. In *Proc. SPIE*, volume 5256, pages 309–317, 2003.

Rian Rubingh, Marco Moers, Manfred Suddendorf, Peter Vanoppen, Aernout Kisteman, Michael Thier, Vladan Blahnik, and Eckhard Piper. Lithographic performance of a dual-stage 0.93na arf step and scan system. In *Proceedings of the SPIE*, volume 5754, pages 681–692, 2005.

J. Rubinstein and A. Neureuther. Images in photoresist for self-interferometric electrical image monitors. In *Proceedings of the SPIE*, volume 6730, page 673039, 2007.

J. Rubinstein and A. R. Neureuther. Post decomposition assessment of double patterning layout. In *Proceedings of the SPIE*, volume 6924, pages 69240O–69240O–12, 2008.

B. W. Smith and J. Cashmore. Challenges in high na, polarization, and photoresists. In *Proceedings of the SPIE*, volume 4691, pages 11–24, 2002.

Panoramic Technology, 2010. `http://panoramictech.com`; accessed Apr 10, 2010.

O. Toublan, K. Lucas, J. Entradas, A. Borjon, K. Patterson, C. Miramond, Y. Trouiller, and J. Belledent. Verification requirements for 45nm and 65nm optical proximity correction. In *Proceedings of the Interface Microlithography Symposium*, 2005.

L.T. Wang, W. J. Poppe, L. Pang, A. R. Neureuther, E. Alon, and B. Nikolic. Hypersensitive parameter-identifying ring oscillators for lithography process monitoring. In *Proceedings of the SPIE*, volume 6925, pages 69250P–69250P–10, 2008.

Lynn T.-N. Wang, Anthony Yeh, Lilly Kem, and Andrew R. Neureuther. Illustration of illumination effects on proximity, focus spillover, and design rules. In *Proceedings of the SPIE*, volume 7275, page 72750B, 2009.